PREDICTION OF AERODYNAMIC CHARACTERISTICS OF SAVONIUS WIND TURBINE USING ARTIFICIAL NEURAL NETWORK AND FOURIER SERIES

A THESIS SUBMITTED TO THE GRADUATE SCHOOL OF APPLIED SCIENCES OF NEAR EAST UNIVERSITY

By
Tijjani Murtala Ahmed

In Partial Fulfillment of the Requirements for the Degree of Master of Science in Mechanical Engineering

NICOSIA, 2016

TIJJANI MURTALA AHMED
PREDICTION OF AERODYNAMIC CHARACTERISTICS OF SAVONIUS WIND TURBINE USING ARTIFICIAL NEURAL NETWORK AND FOURIER SERIES
NEU 2016

PREDICTION OF AERODYNAMIC CHARACTERISTICS OF SAVONIUS WIND TURBINE USING ARTIFICIAL NEURAL NETWORK AND FOURIER SERIES

A THESIS SUBMITTED TO THE GRADUATE SCHOOL OF APPLIED SCIENCES OF NEAR EAST UNIVERSITY

By
Tijjani Murtala Ahmed

In Partial Fulfillment of the Requirements for the Degree of Master of Science in Mechanical Engineering

NICOSIA, 2016

I hereby declare that all information in this document has been obtained and presented in accordance with academic rules and ethical conduct. I also declare that, as required by these rules and conduct, I have fully cited and referenced all material and results that are not original to this work.

Name, Last Name:
Signature:
Date:

ACKNOWLEDGEMENTS

I wish to extend my profound gratitude to my supervisor Assist. Prof. Dr. Huseyin Camur and my co-supervisor Asst. Prof. Dr. Elbrus Bashir Imanov for their time, guidance, courage, advice and corrections which contributed vastly to the completion of this work.

I wish to also express my gratitude to all staff of Mechanical Engineering Department of Near East University for their advice, support and the vast knowledge I have acquired from them. Their excitement and willingness to provide feedback made the completion of this research an enjoyable experience.

I am indeed grateful to my parents whose constant prayers, love, support and guidance have been my source of strength and inspiration throughout these years.

I cannot forget to acknowledge the support I received from my sponsor and also a Father Engr. Dr. Rabiu Musa Kwankwaso: who stood by me throughout the stormy years and gave me the courage that I very much needed to pursue my studies.

I also wish to acknowledge all my friends and relatives whose names are too numerous to mention.

To all sickle cell patients globally….

ABSTRACT

Vertical axis wind turbines are of different types and Savonius wind turbine is of them. It is characterized as cheaper, simple in construction and low speed turbine. It is basically used in applications where high torque low speeds are required such as water pumping although it is also used in electricity generation for residential purpose and small commercial use. This research is done to create model to predict the aerodynamic performance of Savonius wind turbine such as the torque, torque coefficient and power coefficient. In this research, artificial neural network and trigonometric Fourier series modeling has been used to predict the aerodynamic characteristics based on four past experimental data's with various geometries.

A trigonometric Fourier series and back propagation neural network architecture are used in the prediction of various performance terms of different Savonius wind turbine geometries. The torque coefficient, torque and power coefficient are the performance terms predicted as a function of rotor angle. Different percentage training data's are used in training the back propagation neural network after which the network is tested with new data to evaluate its performance and generalization ability. The mean square error and coefficient of determination also called R-square (R^2) are used in evaluating the network performance for both training and testing as the case maybe. Both the trigonometric Fourier series and back propagation models gives a good result within an acceptable error limit.

Keywords: Artificial intelligence; artificial neural network; Fourier series; R-squared; Savonius wind turbine

ÖZET

Dikey eksenli rüzgar türbinleri farklı türlerde mevcuttur ve Savonius rüzgar türbini bunlardan biridir. Bu, inşaat ve düşük hız türbinleri arasında daha ucuz ve basit olarak nitelendirilmektedir. Bu temelde su pompalama gibi yüksek tork ve düşük hızın gerekli olduğu uygulamalarda kullanılır, buna rağmen yerleşim amaçlı ve küçük ticari kullanım için elektrik enerjisi üretiminde kullanılmaktadır. Bu araştırma, tork, tork katsayısı ve güç katsayısı gibi Savonius rüzgar türbininin aerodinamik performansını tahmin modeli oluşturmak için yapılmıştır. Bu araştırmada, yapay sinir ağı ve trigonometrik Fourier serileri modelleme çeşitli geometrilere sahip dört geçmiş deneysel verilere dayalı aerodinamik özelliklerini tahmin etmek için yapay sinir ağı ve trigonometrik Fourier serileri modelleme kullanılmıştır.

Trigonometrik Fourier serileri ve arka yayılım sinir ağı mimarisi farklı Savonius rüzgar türbini geometrilerin çeşitli performanslarının tahmininde kullanılmaktadır. Tork katsayısı, tork ve güç katsayısı rotor açısının bir işlevi olarak tahmin edilen performans terimlerdir. Farklı yüzdelik eğitim verileri ağın performansı ve genelleme yeteneğini değerlendirmek için yeni verilerle test edildiktne sonra geri yayılım sinir ağı eğitiminde kullanılmaktadır. Ortalama karesel hata ve determinasyon katsayısı R-kare olarak adlandırılır ve hem eğitim hem de test etme için ağın performansını değerlendirmede kullanılmaktadır. Hem trigonometrik Fourier serileri hem de arka yayılım modelleri kabul edilebilir bir hata sınırı içerisinde iyi bir sonuç vermektedir.

Anahtar Kelimeler: Yapay zeka; Yapay sinir ağları; Fourier serileri; R-kare; Savonius rüzgar türbini

TABLE OF CONTENTS

CHAPTER 3: ARTIFICIAL NEURAL NETWORKS

CHAPTER 4: FOURIER SERIES THEORY

CHAPTER 5: METHODS AND PUBLISHED EXPERIMENTAL RESULTS

CHAPTER 6: RESULTS AND DISCUSSIONS

CHAPTER 7: CONCLUSION

LIST OF TABLES

LIST OF FIGURES

ABBREVIATIONS AND SYMBOLS

AI:	Artificial intelligence
ANFIS:	Adaptive neuro-fuzzy inference system
ANN:	Artificial neural network
BPNN:	Back propagation neural network
CCS:	Carbon capture and storage
CFD:	Computational fluid dynamics
CSP:	Concentrated solar power
C_p:	Power coefficient
C_t:	Torque coefficient
C_{ts}:	Static torque coefficient
D:	Rotor diameter
d:	Blade diameter
DFT:	Discrete Fourier transform
FFT:	Fast Fourier transform
FIS:	Fuzzy inference system
FS:	Fourier series
H:	Rotor height
HAWT:	Horizontal axis wind turbine
LOGSIG:	LOGSIGMOID function
MATLAB:	Matrix laboratory
MSE:	Mean square error
P_a:	Available power in wind
P_w:	Extracted power from wind
PURELIN:	Linear function
R:	Rotor radius

R^2:	Regression coefficient
RBF:	Radial basis function
T:	Fundamental time period
TANSIG:	TANSIGMOID function
TRAINLM:	Levenberg-Marquadt training function
T_r:	Rotor torque
T_s:	Static torque
T_w:	Wind available torque
V:	Wind speed
VAWT:	Vertical axis wind turbine
ω_0:	Fundamental frequency
ρ:	Air density
Ω:	Angular velocity of Savonius rotor

CHAPTER 1
INTRODUCTION

1.1 Study Background

Wind energy refers to the process by which wind is used to generate mechanical power that can be harnessed to produce electricity. They are used to transform energy of wind to mechanical energy as in the case of wind mill and produce electricity.

Horizontal axis and vertical axis also written as HAWT and VAWT respectively are the two main categories of wind turbines. HAWT has axis of rotation parallel to the ground while VAWT has axis of rotation perpendicular to the ground. VAWT has simple structure and easy to install than HAWT.

VAWT rotors are of different types and Savonius rotor is one of them. The Savonius wind turbine rotor has shape of letter S in cross-section and is made from two or more blades also called buckets fixed between two end plates. It is used in applications such as pumping water, milling, sawing, driving an electrical generator and providing ventilation.

In recent times, many researchers are making effort towards the use of artificial intelligence in predicting the performance of wind turbine rotor which would complement for the time and cost involved in testing the wind rotors for the variety of input parameters. Artificial neural network (ANN) modelling is one of such techniques.

In this research, feed forward back propagation network architecture, ANN, and Fourier series, FS, are used to create a model between various performance parameters (such as the torque, torque coefficient, power coefficient and rotor angle) of Savonius wind turbine.

Several data were obtained from published experimental data on the Savonius wind turbine rotors and a comparison is made between ANN and FS models with published experimental data to ensure the accuracy of the models. Additionally, ANN and FS models are compared with RBF models (Published models).

1.2 Aims of the Research

The aims of this research work are as folows:

I. To create a model using ANN and FS to predict the aerodynamic characteristics of Savonius wind turbines with various geometries.

II. To make comparison between results of the above models with published experimental results obtained of previous works by various researchers.

1.3 Outline of the Research

This research work is outlined in the following order:

i. A summary of wind turbine theory, artificial intelligence, Fourier series and a brief study of various experimental and numerical work carried out on Savonius wind turbine

ii. The result and discussion on different methodology used in the present study and finally the conclusion.

CHAPTER 2
WIND TURBINE THEORY

2.1 Wind Concept

Winds are motion of air masses in the atmosphere and an indirect action of solar radiation unevenly hitting the earth as they are generated mainly by temperature variation within air layers due to differential solar heating. It is a form of renewable energy generated from solar energy unevenly heating the earth. This non uniform heating generates pressure changes in the atmosphere resulting to wind which can be harnessed using wind turbines. As the wind pushes the turbine blades, a generator attached to the shaft axis and when spun creates electricity that can be sent to grid for usage (Adaramola, 2014).

It is an environmental friendly energy supply that possess immense potential to meet the energy desires of individuals and additionally to ease the global climate change from gasses such as CO_2 and SO_2 emitted by burning fossil fuels. Ten million megawatt of energy are presence in earth's available wind according to rough estimation by researchers (Wenehenubun et al., 2015).

2.2 Wind Turbines

Wind turbines generate electricity by turning kinetic energy of wind into torque (force) which causes the turbines to turn and drives an electrical generator. In other words, wind turbines works the opposite of a fan, they use wind to generate electricity rather than using electricity to make wind like a fan. They basically consist of aerodynamically blades that are rotating and fixed on shaft which transfers the created power into the individual energy utilizing device (such as milling, sawing, generator and pump) (Ali, 2013).

The wind moves past the wind generator blades or rotors resulting to low pressure system on the trailing edge of the blades similar to airplane wing. The efficiency of wind turbine is greatly affected by the size and shape of rotors, turbine location which includes the geography and height and other mechanics that either increase or decrease drag force on the system. Many believe the old style windmill with many blades is more efficient as a result of many rotors. But, the number of rotors can actually increase the drag, add extra weight and get in the way of wind flow through the blade area. Now days, two or three

bladed turbines are most popular because of more thrust and less wind resistance (Tummala et al., 2016).

Wind turbines are a clean way to generate electricity, but there are many significant problems associated with them as well. One major shortcoming is that they are highly expensive to design and install, and in order to generate sufficient wind energy for locals and cities a space is required for wind farms. Another issue is that they have to be created in locations with sufficient wind energy to produce enough electricity to justify the cost of the machine.

In history, they were more frequently used as mechanical device that turned machinery but today wind turbines can be used to generate large amount of electrical energy both onshore and offshore (Jin et al., 2016).

According to Menet (2004), the procedure of converting wind into mechanical energy starts with the blades of the wind turbine. That is the lift and drag type blade designs:

- Lift type: This is the most common type of modern horizontal axis wind turbine blade located in big wind farms. The blade design is similar to airplane wing. As the wind blows on both side of the blade, it takes the wind long to travel across the leading edge resulting to lower and higher air pressure on the trailing edge. The pressure difference 'pulls' and 'pushes' the blade around. This blade type have higher rotational speeds than the drag type which make them well suited for electricity generation.
- Drag type: The first set of wind turbines created used the drag design. This design normally uses the wind force to push the blade. Savonius wind turbine is a typical example of this design. The wind is resisted by the blade and the wind's force on it pushes it around. Turbines in this category have slow rotational speed with higher torque than the lift type. The design has been used for centuries in milling, sawing, pumping and rarely used for large scale energy generation.

2.3 Horizontal Axis Wind Turbine (HAWT)

In HAWT the rotors rotation axis is parallel to wind stream and the ground. Both the electrical generator and rotor shaft are positioned at the top of the tower. Most HAWTs now are two or three bladed, though some may have fewer or more blades (Al-Shemmeri, 2010).

HAWT blades operate to extract wind energy by generating lift/ resulting to a net torque about the axis of rotation. To perform such task effectively, especially for large HAWTs,

active pitch controllers are employed to ensure that each blade is adjusted to maintain the required angle of attack for maximum power extraction at a given speed (Bai & Wang, 2016).

Figure 2.1: HAWT

The turbine blades are constrained to move in plane with a hub at its center, as such the lift force induces rotation about the hub. In addition to lifting force the drag force which is vertical to the lift force retards rotor rotation. HAWT must be pointed to the wind direction for optimum efficiency. The smaller scale turbines use a wind vane (tail fan) while the utility scale use sensor and servo motor to keep pointed in the right direction. This type of wind turbines are have higher efficiency than VAWT as such been used for generation of electricity (Tummala et al., 2016).

HAWT can be classified into two groups depending on the different relative position of the rotor and tower as:

2.3.1 Upwind wind turbine

In this type of HAWT the rotor rotates before the tower facing the wind. It is designed to have to have a certain type of steering installation to make sure the rotor is directed toward the wind during work.

2.3.2 Downwind wind turbine

In this case the rotor is installed on the tower following the wind. This does not require any steering installation as the turbine will automatically face the wind.

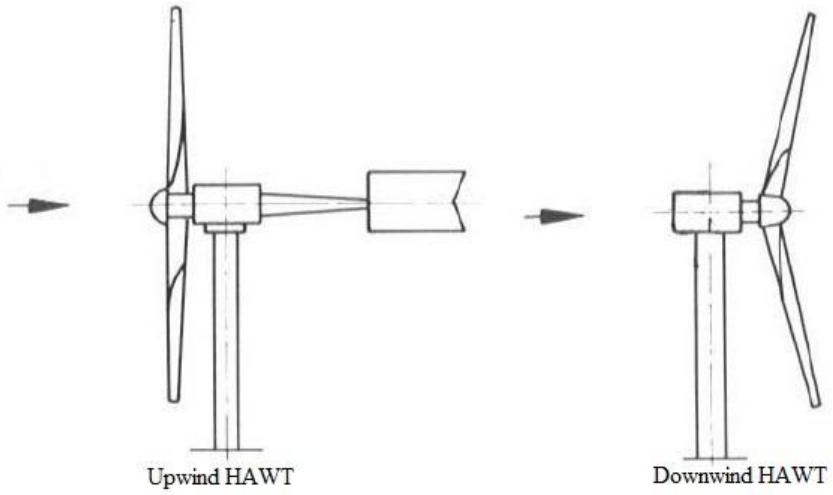

Figure 2.2: Upwind and Downwind HAWT

Horizontal axis wind turbines can also be categorized into the lift and the resistance type. The lift type has a high rotational speed while the resistance type has a low rotational speed. The lift type is more frequently used to generate power. Most of HAWTs has the steering device and can rotate with the wind. A tail vane is used as steering device for small sized wind turbine while sensors and servo motor are used for large sized type (Bai & Wang, 2016).

HAWT has advantages over VAWT such as:

- Most of HAWTs are self-starting
- Can be cheaper due to high production volume
- HAWTs gets maximum amount of wind energy because the angle of attack can be remotely adjusted
- The turbine is stable because the blades are to the side of its center of gravity
- Tall tower allow access to stronger wind
- It has the ability to pitch rotor blades in a storm so as to minimize damage

However, the disadvantages of HAWT compared to VAWT include:

- May cause navigation problems when offshore
- Difficulties operating near the ground

- Long blades and tall tower are difficult to transport from one place to another and require a distinct installation procedure.
- Mainly employed for electricity generation
- Mainly used in areas with permanent and high speed wind

2.4 Vertical Axis Wind Turbine (VAWT)

VAWT has axis of rotation perpendicular to the ground. The generator, gearbox and vertical rotor shaft are placed on the ground and specially designed rotor blade to capture wind energy irrespective of which direction it is blowing (Al-Shemmeri, 2010).

Though less efficient than HAWT, it offers solution in low wind speed areas wherein HAWTs have a high time operating. It is easier and safer to fabricate, it can be installed near the ground and can handle turbulence better than HAWT and this makes VAWT more suited to residential areas where obstacles such as other houses, buildings and trees generally disturb the airflow (Wenehenubun et al., 2015).

2.4.1 Darrieus wind turbine

French engineer G.J.M Darrieus first proposed the Darrieus wind turbine in 1931.The turbine consist of thin curved blades placed vertically on a rotating shaft or framework. They are commonly called “Eggbeater” turbines because they resemble a giant eggbeater (Jin et al., 2016).

The turbine blades rolled into chain lines joined to the shaft at the upstream and downstream side. The wind energy is taken by the lift force component operating in the direction of rotation in the way as HAWT. However, a Darrieus rotor with straight blades (H-Darrieus) has been developed with large hubs provided with spokes. When it has enough speed, the wind moving through the airfoils generates torque thus, the rotor is moved by the wind. The blades allow the turbine to attain speeds higher than the actual wind speed which makes the Darrieus rotor well suited to electricity generation when there is wind turbulence (Jin et al., 2016).

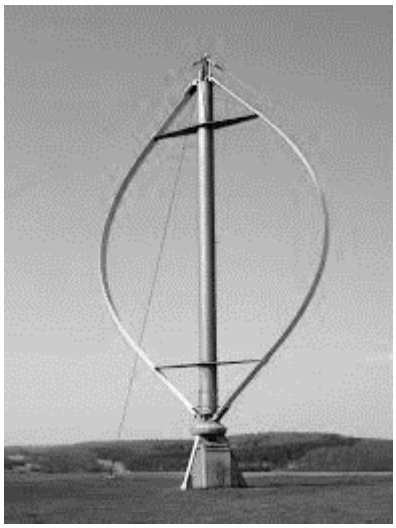

Figure 2.3: Darrieus wind turbine

2.4.2 Savonius Wind Turbine

This is one of the categories of VAWT invented and patented by Savonius J. Sigurd in 1922, a Finnish Engineer. It comprises of two or more semicircular blades also called buckets fixed between two end plates. A two blade look like the letter “S” shape in cross section. The bucket will make the flow within the rotor regular and it is based on drag concept (Rosmin et al., 2015).

Savonius rotor is used for pumping water, driving electrical generator, ventilation and many more. It also has excellent initial torque and good peak power return for particular rotor size, cost and weight which makes it less efficient. In aerodynamic efficiency view, the Savonius rotor cannot compete with Darrieus type wind turbines and high speed propellers (Saha & Rajkumar, 2006).

Providing a certain overlap between drums increases the torque because the wind blowing on the concave side turns around and pushes the inner surface of the other drum, which partly cancels the wind thrust on the convex side. An overlap of one- third of the drum diameter gives the best results (Singh, 2008).

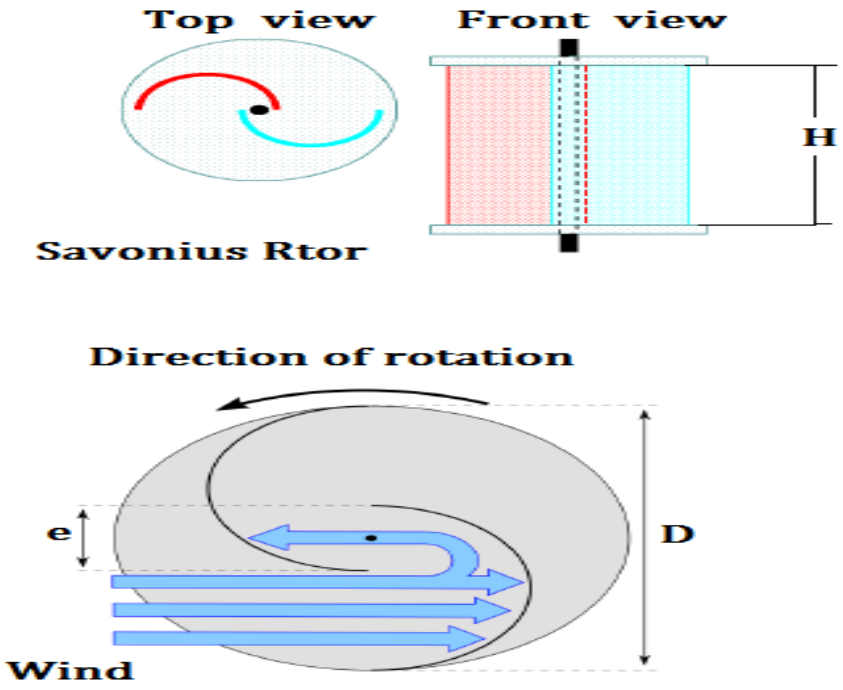

Figure 2.4: Savonius rotor

Menet (2004) outlined some advantages and disadvantages of Savonius wind turbines as follows:

- They are simple machines as such easy to construct with low cost
- Can be designed with different rotor configurations
- Easy to maintain
- They are able to start and run at whatever wind velocity because of their high starting torque.
- Little noise and angular velocity operation
- They are supposed to be running even in case of "strong" winds when most of the fast running wind turbines must be stopped.
- Ability to capture wind from any direction

The main shortcomings of Savonius wind turbines include:

- Low efficiency
- Slow running behavior

Advantages of VAWTs

- Good for places with extreme weather conditions like mountains

- Turbine blades spin at lower velocity thus reducing the chances of birds injury
- Easy access to maintenance because VAWT parts are placed near the ground
- Little production, transportation and installation cost
- VAWT does not need to be pointed towards wind direction in order to be efficient
- Suitable for places such as hilltops, ridgelines and passes

On the other hand VAWT has some shortcomings such as:

- Most of VAWTs are only as half as efficient as HAWTs due to drag force
- Airflow near the ground and other objects can create turbulent flow thus resulting to vibration
- Guy wires may be needed to hold VAWTs up (guy wires are heavy and impractical in farm areas)

Table 2.1: Comparative parameters between VAWT and HAWT

Serial number	**Performance**	**VAWT**	**HAWT**
1	Power generation efficiency	Above 70%	50%-60%
2	Noise	0.1Db	5.6Db
3	Starting wind speed	Low (1.5-3m/s)	High (2.5-5m/s)
4	Failure rate	Low	High
5	Maintenance	Simple	Complicated
6	Rotating speed	Low	High
7	Power curve	Full	Depressed
8	Effect on birds	Small	High
9	Cable standing problem	No	Yes
10	Wind resistance capacity	Strong (can resist typhoon up to 12-14 class)	Weak
11	Blade rotation space	Small	Large
12	Gear box	No	Yes Above 10KW
13	Wind steering mechanism	No	Yes
14	Electromagnetic interference	No	Yes
15	Ground projection effects on human beings	No	Dizziness

2.4.3 Theory of Savonius wind turbine

Savonius wind turbine operates because of the variation of forces exerted on its blade. The concave side to wind direction captures the wind and causes the blade to rotate within its middle perpendicular shaft. On other hand, the convex section hits the air wind and causes the blade deflect sideways inbetwen the shaft. Curvature of the blade has less drag when moving against wind at F_{convex} than blades moving with wind at $F_{concave}$ as shown in Figure 2.5. Therefore, the concave blades that has more drag force than the convex side will cause the rotor rotation (Ali, 2013).

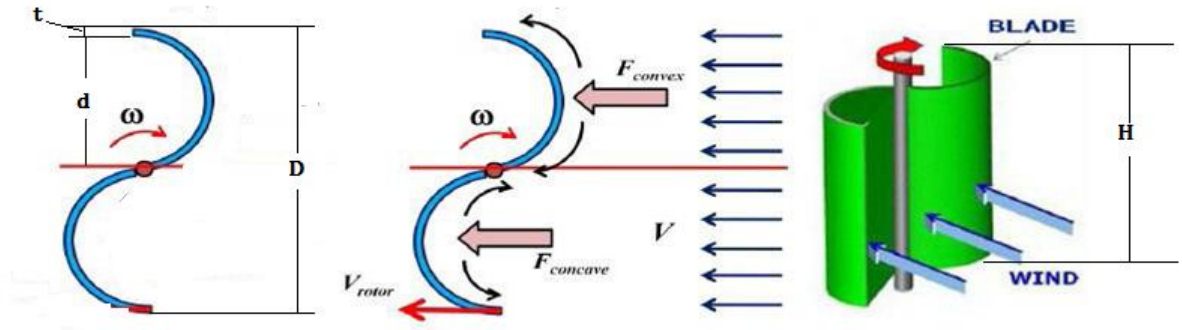

Figure 2.5: Two blades conventional Savonius wind turbine (Ali, 2013)

The rotor torque (T_r), torque coefficient (C_t) and power coefficient (C_p) of Savonius wind turbine rotor are used to express its performance characteristics in comparison with the rotor angle.

The torque is a twisting force that tends to cause rotation. It is the force tangentially acting on blade of the rotor at a radius (r) to the center. The point where the rotor rotates is called the center of rotation. It is expressed as:

$$T_r = F \times r \ (Nm) \tag{2.1}$$

The torque coefficient is expressed as ratio of the torque develop by the rotor (T_r) to the torque present in the wind (T_w) as:

$$C_t = \frac{Rotor\ Torque}{wind\ Torque} = \frac{T_r}{T_w} = \frac{T_r}{\frac{1}{4} \times \rho \times H \times D \times d \times V^2} \tag{2.2}$$

T_r= rotor torque (Nm), ω= rotor rotational speed (rad/s), D=diameter of rotor (m), ρ= Air density (kg/m^3), H= rotor height (m), V= wind speed (m/s) and d= blade diameter (m).

The power coefficient (C_p) is the ratio of maximum power from the wind (P_t) to the total power available in the wind (P_a) as:

$$C_p = \frac{Power\ output\ from\ wind\ machine}{Power\ contained\ in\ the\ wind} = \frac{P_w}{P_a} = \frac{T_r \times \omega}{\frac{1}{2} \times \rho \times H \times D \times V^3} \quad (2.3)$$

Another term called the static torque (C_{ts}) can be used to evaluate wind turbine performance. The static torque coefficient is expressed as:

$$C_{ts} = \frac{T_s}{T_w} = \frac{T_s}{\frac{1}{4} \times \rho \times H \times D \times V^2} \quad (2.4)$$

2.5 Reviews on Wind Turbines

Many researchers have been working to enhance and better the aerodynamic characteristics of Savonius wind turbine. This research work ranges from laboratory experiment, full scale simulation to numerical and theoretical prediction for flow around Savonius wind turbine. A lot of work has been done on HAWT and Darrieus VAWT, because of their high prospect of wind energy efficiency. Presently, an extensive research work has been carried out on Savonius wind turbine by several researchers around the globe so as to improve its performance and make it suitable for small scale power production. A brief literature of experimental and numerical work on Savonius wind turbine will be presented in this chapter.

2.5.1 Related research on experimental investigation

Ali (2015) conducted an experiment to study the performance and make comparison between two and three bladed Savonius wind turbine at low wind speed. Two models of two and three blades were fabricated from Aluminum sheet for this work. The two models were assembled with zero overlap ratio and separation gap. Observation from the measured and calculated result indicates that the two bladed Savonius wind turbine is more efficient and has higher power coefficient under the same test condition than the three bladed Savonius wind turbine. This is because increasing the blade number will increase the drag surfaces against wind airflow and lead to increase in the reverse torque and causes the decrease of the net torque working on the Savonius wind turbine blade.

McWilliam et al. (2008) investigated different Savonius wind turbine models to observe the vortex formation and the effect of the scale of downstream wake using particle image velocimetry (PIV) in a close loop wind tunnel. In that experiment, they used standard Savonius design (diameter = 30.18 mm) with two semicircular blades overlapping. The

design of these blades include deep blade design (diameter = 31.20 mm), shallow blade design (diameter =28.04mm), outside J blade design (diameter = 32.97 mm) and inside J blade design (diameter = 31.18mm).They executed the experiment at a constant 3 m/s wind velocity. They observed that vortex shedding from the following blade was common to all five designs they tested, which had an effect on the scale of the downstream wake of the rotor. They found that the forward curved blade was the critical area for external flow and the overlap ratio of Savonius wind turbine blades allows flow from the top blade to enter the bottom blade that reduces the negative pressure region behind the blades.

Gupta et al. (1988) combined Savonius wind rotor and Darrieus type in their experiment. The results obtained were compared with the conventional Savonius rotors. They found an improvement in power coefficient with the combined Savonius-Darrieus rotor.

The aerodynamic performance of Savonius wind turbine by measuring the distribution of pressure on the blade surfaces at various rotor angles and tip speed ratios were studied by Fujisawa et al. (1994) torque and power performance were evaluated by integrating pressure were in close agreement with the experimental torque measurement.

Aldoss et al. (1987) used the discrete vortex method to measure the performance of two Savonius rotors operating side by side at various separations. The computational and experimental results on torque and power coefficient were compared and are compatible with each other.

Sawada et al. (1986) examined the rotational mechanism of Savonius wind turbine with two semi-cylindrical blades and found that a rotor with a gap ratio of 0.21 yields positive static torque at all angles. They also observed that the lift force contributes significantly to dynamic torque at rotor angles between 240^0 and 330^0.

2.5.2 Related research on numerical investigation

Akwa et al. (2012) examined numerically the influence of overlap ratio of Savonius wind turbine on power and torque coefficient. Results obtained show a maximum rotor performance at overlap ratio close to 0.15.

Sargolzaei et al. (2009) carried out a modeling and simulation of wind turbine Savonius rotor using artificial neural networks for estimation of torque and power ratio based on experimental data collected from prototype tested in wind tunnel. The torque and rotors power factor were simulated at various tip speed ratio and blade angles. Based on the

artificial neural network and experimental results, the tip speed ratio is directly proportional to power ratio and torque. The maximum and minimum torque occurs at an angle of 60^0 and 120^0 respectively for all the tested rotors.

Altan et al. (2008) simulated their experimental work numerically using FLUENT 6.0 and GAMBIT 2.0. They used two dimensional and standard k-ε turbulence model. Semi implicit method for pressure linked equation (SIMPLE) analysis algorithm was employed to calculate pressure and velocity distribution. After comparing the numerical with the experimental results, it was concluded that curtain improved the Savonius wind turbines performance.

Rahman et al. (2009) conducted both experimental and work and computational fluid dynamics (CFD) simulations to establish the possibility of improving the performance of three bladed, simple Savonius vertical axis wind turbine. The torque coefficient, tangential drag coefficient and normal drag coefficient were evaluated both experimentally and numerically. The results were compared and are in good agreement. The numerical results were more accurate and gave positive values for the combined drag coefficients and total static torque coefficient.

CHAPTER 3
ARTIFICIAL NEURAL NETWORKS

3.1 Artificial Intelligence (AI)

This is a specialization in computer science devoted in software packages capable of performing intelligent and complex computations analogous to what brain of humans performs habitually. It involves ways, equipment and programs dedicated to imitate human ways of logical information processing and reasoning of human brain for problems solution (Kustrin & Beresford, 2000).

Artificial intelligence developments are of two types:

3.1.1 Expert systems

Expert systems include process and networks that imitate the experience of humans and make deductions using some set of rules. They are knowledge oriented systems, a continuation of traditional computation also known as the 5^{th} generation computing. Recognition base allow experts to specify set of rules which imitate thinking process and leads to an easiest route to draw conclusions and provide solution to problems by taking the guide lines set into consideration. Using expert systems logical reasoning can be modeled by composing sets of logical prepositions and carrying out intelligent modifications upon them. They are very important in medicine and many other medical diagnostic problems solution (Kustrin & Beresford, 2000).

3.1.2 Artificial neural networks

ANNs are computer programs that are inspired biologically to imitate some basic tasks of the human brain by various training algorithms that can comprehend from experience. They are structures composed of highly integrated flexible simple processing elements (known as artificial neurons or nodes) that are have the ability of performing massively parallel computations for processing data and knowledge representation. ANNs learn through experience with the proper training examples as humans do and not from conventional computer programs. ANNs have information processing characteristics of human brains like nonlinearity, learning, failure and tolerance of fault, robustness, high parallelism and ability to generalize. Therefore, ANNs are used in solving complex real

life problems like optimization, function approximation and pattern classification. Table 3.1 below shows a comparison between ANN and conventional computing (Sun et al, 2003).

Table 3.1: Comparison between ANNs and conventional computing

Characteristics	**Conventional computing (including expert systems)**	**Artificial neural networks**
Learning rule	Rules	By experience
Functions	Logically	Perceptual pattern
Method of processing	Sequential	Parallel

Various ANN models was developed for numerous different applications. ANN models can be supervised or unsupervised based on the learning (training) algorithm. The input and output data sets are presented to the ANN model for supervised learning while only the input data set is presented to the ANN model in unsupervised learning which learns to recognize the pattern in the data. ANN can also be classified according to topology as feed forward and feedback. The connection between neurons does not form circles in feed forward architecture. The model does not have a connection back from the output to input neurons and thus the record of previous output values are not available. In Feedback ANN models the connection between nodes consists of circles. The output of one layer routes back to the input of same layer or previous layer. Feedback models are normally very difficult to train than the feed forward (Sun et al., 2003).

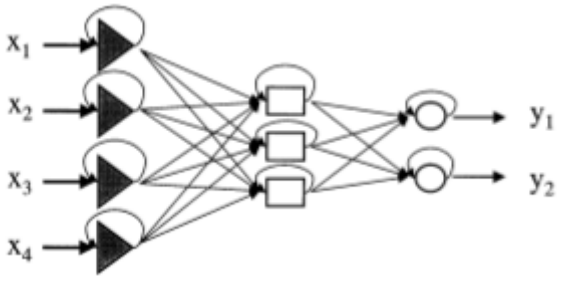

Figure 3.1: Feedback network (Kustrin and Beresford, 2000)

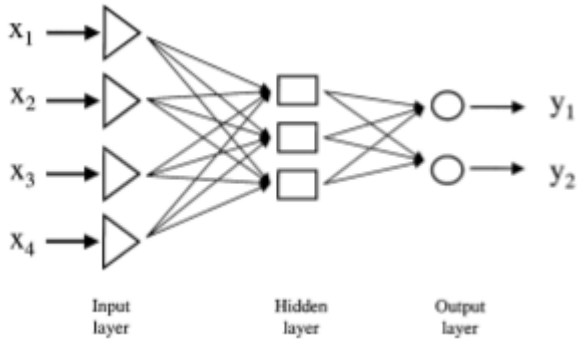

Figure 3.2: Feed forward network (Kustrin & Beresford, 2000)

3.2 Artificial Neuron

Artificial neuron is the main element of artificial neural network designed to imitate the functions of biological neuron. Inputs signal times the connection weight are first combined (summed) and then passed the transfer function to produce desired output of that particular neuron. The activation function is the weighted combination of neuron's inputs and sigmoid function is mostly used (Kustrin & Beresford, 2000).

Artificial neurons or nodes are the building block of ANN which process information based on weighted inputs using transfer functions and send outputs. Adjacent layers neurons are fully or partially connected with weighted links. Net input into a neuron is given as:

$$\text{Net input to a neuron} = \sum_{i} x_i \, w_i \qquad (3.1)$$

where w_i = the weight factor

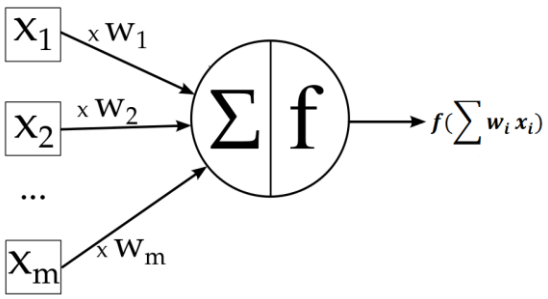

Figure 3.3: Artificial neuron model (Kustrin & Beresford, 2000)

3.3 Components of Artificial Neuron

3.3.1 Bias

A bias increases the neural network performance. It functions as a weight on a connection from unit that always has activation function of 1. The same way to initialization of weights, bias should be initialized to either 0 or any other specific value based on neural net. The net input if bias is present is given as:

$$Net = b + \sum x_i w_i \tag{3.2}$$

Where: Net=net input, b=bias, x_i=input from neuron i and w_i=weight of neuron i to the output neuron

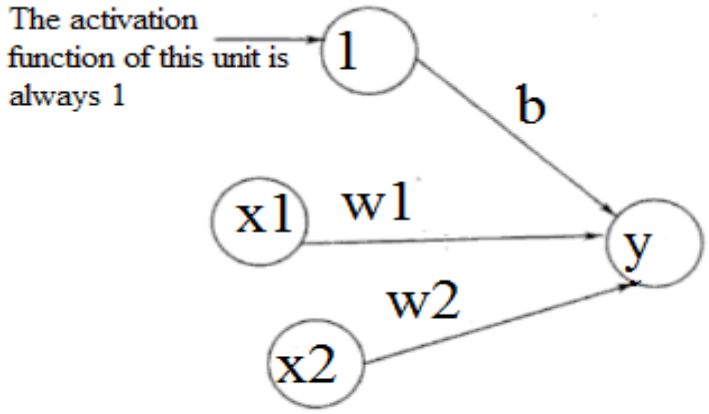

Figure 3.4: A simple network with bias included

3.3.2 Weighting factors

Artificial neuron normally receives many input variables at same time. A Particular input possesses its own weight that gives it the impact it requires on the summation function. Some inputs are designed to be more essential than others so as to have high impact on the neuron as they join together to give a neural output. The weights used on the different layers exert more influence in the function of neural network. Steps below are taken when choosing the weights:

- Run the network with one set of weights
- Run the network again with new sets of weights after modifying some or all the weights
- The process is repeated until some predetermined goal is achieved

3.3.3 Summation Function

The initial step in neural network processing elements function is computing the weighted sum of all inputs to neuron. Mathematically, the inputs data and the equivalent weights are like vectors that can be expressed as (I_1, I_2... I_N) and (W_1, W_2… W_N) respectively. Each component of I vector is multiplied by the respective component of W vector and then summing up all the products to find the summation function.

Example

$\text{Input1} = I_1 \times W_1$

$\text{Input2} = I_2 \times W_2$ etc. are added as

$\text{Input1} + \text{Input2} + \cdots + \text{InputN}$

Single number not multi-element vector is the result.

3.3.4 Transfer function

Each neuron is assigned a transfer function which determines the output values. Summation function output value is converted to working output using a logarithmic process called the transfer function. The summation total can be compared with some threshold to find neural output. There are many transfer functions used in ANN such as LOGSIG, TANSIG and PURELIN functions. LOGSIG transfer function is widely used for non-linear relations between input and output values. The LOGSIG is expressed as:

$$Y^{sigmoid} = \frac{1}{1 + e^{-X}} \tag{3.3}$$

3.3.5 Output function

Each neuron normally has one output signal that it may forward to hundreds of other neurons which is similar to biological neuron in which there are several inputs but only single output. The output value is equivalent to the result of transfer function.

3.3.6 Error function and back propagated value

Variations between expected and predicted values are calculated in most learning architectures. This value is transformed by target error function to be a replica of a particular architecture. This error is used directly by most networks but some square it, others cube it while the raw error is modified by other paradigms based on their purposes (Anderson & McNeill, 1992).

3.4 Basic Back Propagation ANN Model Architecture

This architecture was developed early 1970's by several non-aligned authors (Werbor, Parker, Rumelhat, Hinton and Williams). It is presently known most, efficient and easy to train for complicated, multi-layered networks. It is used more than all other networks together combined. It is greatest advantage is non-linear solutions to inexplicit problems.

Levenberg-Marquardt optimization (TRAINLM) is used as training function in this work. TRAINLM determines the weight and bias values in back propagation algorithm which was found to be useful in networks training.

It is made of three layers as seen in Figure 3.5 below:

- The input is the first layer which does not have computing capability. The independent parameters are fed to the first hidden layer through the input layer.
- The output is the last layer used to process output of dependent variables.
- The hidden layer lies at the middle between input and output layers that provides interconnection between layers. Connection between layers can be fully or partial. Each neuron in the first layer is connected to all neurons in the second layer for fully connected ANN model. For partially, each neuron on first layer does not have to be joined to all neurons on the next layer.

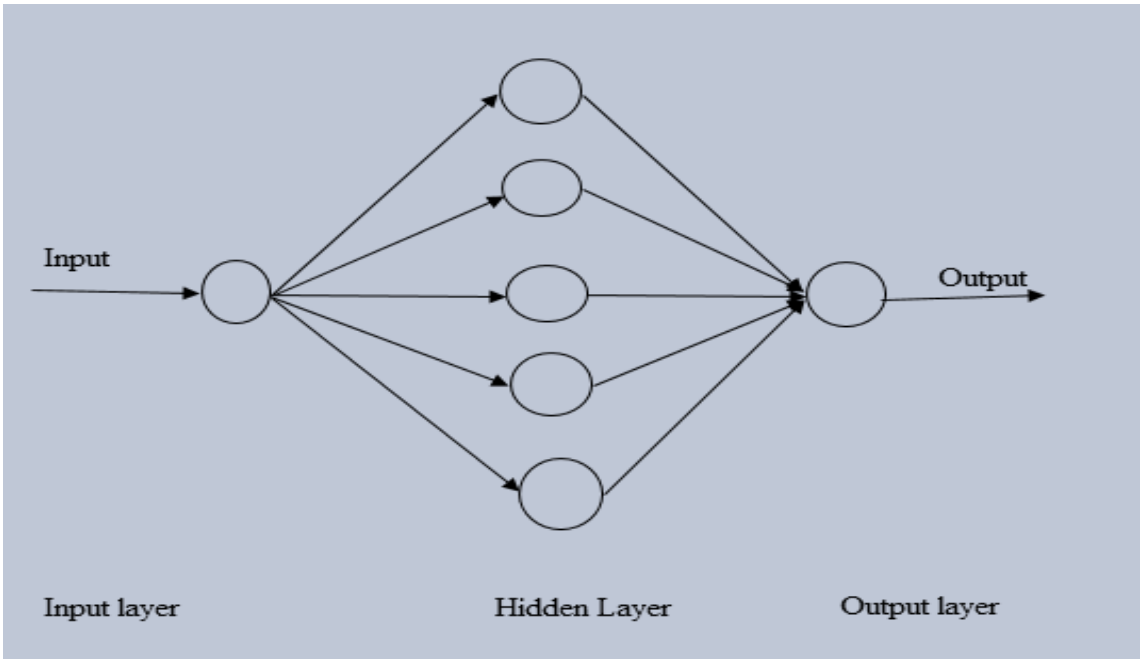

Figure 3.5: Back propagation ANN model architecture

Complexity of a problem normally determined the number of hidden layers. One hidden layer is used by most ANN models since it is enough to provide good prediction. Modeling complex problems can be done with more than one hidden layer.

3.6 How ANN Model Learn

Artificial neural network models learn from experience gained through training procedure. The training includes fitting data to ANN models. Supervised learning involves presenting input/output data sets. It is used to predict one or more output values from one or more input values. Majority of ANN solutions use supervised learning. The neural network output is compared with the desired or target output. The weights, which are usually randomly set to begin with, are adjusted by the network so that subsequent cycle or iteration will yield a closer match between the network output and desired output. The training procedure tries to minimize present errors of all neurons. This universal reduction is created with time by continuously changing the input weights until acceptable network accuracy is reached (Anderson & McNeill, 1992).

When supervised ANN performs perfectly on training data, it is necessary to view its performance with data that it has not seen prior to learning. The training period is not over if a poor performance is obtained for the testing data. Thus, the testing is crucial to ensure that the model has not just memorized a given data set but learn the overall pattern involved (Anderson & McNeill, 1992).

CHAPTER 4
FOURIER SERIES THEORY

A French physicist and mathematician; Jean Baptiste Joseph Fourier initialized Fourier series, Fourier transform and their application to heat transfer and vibrtations. Born on 21st march 1768 in Auxerre, France. The Fourier series, Fourier transform and Fourier's Law were all named in his honour.

4.1 Fourier Series

Fourier developed an expression named Fourier series which can be used to represent any periodic signal f(t) interms of infinite sum of sines and cosines or exponentials which uses condition of orthogonality.

- Fourier series representation of continuous time periodic signals/functions

A function or signal is said to be periodic if it satisfies the condition:

$$f(t) = f(t+T) \; or \; x(n) = f(n+N) \tag{4.1}$$

Where T=Fundamental time period

$$\omega_o = \frac{2\pi}{T} = Fundamental \; frequency$$

There are two main periodic signals or functions, namely:

$$f(t) = cos\omega_o t \;\; (sinusoidal \; function) \tag{4.2}$$

$$f(t) = e^{jw_o t} \;\; (complex \; exponential) \tag{4.3}$$

A harmonically related complex exponential can be expressed as:

$$\varphi_k(t) = \{e^{j\omega_o t}\} = \left\{e^{jk\left(\frac{2\pi}{T}\right)t}\right\} \tag{4.4}$$

Where $k = 0 \pm 1, \pm 2 \ldots . n$

Based on orthogonal signal space approximation of a function f(t) with n mutually exclusive orthogonal functions is given as:

$$f(t) = \sum_{-\infty}^{\infty} a_k \, e^{jkw_o t} \tag{4.5}$$

$$= \sum_{-\infty}^{\infty} a_k \, k e^{jkw_o t}$$

Where $a_k = \text{fourier coefficient} = \text{coefficient of approximation}$

The equation above represents Fourier series representation of a periodic signal f(t).

The term $k = 0$ is constant

$k = \pm 1$ with fundamental frequency w_o, is referred to as 1^{st} harmonic

$k = \pm 2$ with fundamental frequency $2w_o$, is referred to as 2^{nd} harmonic

$k = \pm n$ with fundamental frequency nw_o, is referred to as n^{th} harmonic

The Fourier series coefficient a_k is given as:

$$a_k = \frac{1}{T}\int_0^T e^{-jkw_o t}\, dt \tag{4.6}$$

4.2 Types of Fourier Series

4.2.1 Trigonometric Fourier series (TFS)

$\sin k\omega_0 t$ and $\sin m\omega_0 t$ are orthogonal over the interval $(t_0, t_0 + \frac{2\pi}{T})$. Thus, $\sin\omega_0 t$ and $\sin 2\omega_0 t$ forms an orthogonal set but this set is not complete without the $\cos k\omega_0 t$ because cosine set is also orthogonal to sine set. Therefore, complete this set both the cosine and sine terms are included. So, the complete orthogonal set contains all cosine and sine terms i.e ($\cos k\omega_0 t$ and $\sin k\omega_0 t$) wher k=0,1,2,3,…….

Therefore, any function f(t) within the range $(t_0, t_0 + \frac{2\pi}{T})$ can be expressed as

$$\begin{aligned} f(t) &= a_0 cos0\omega_0 t + a_1 cos1\omega_0 t + a_2 cos2\omega_0 t + \cdots + a_k cosk\omega_0 t + \cdots \\ &\quad + b_0 sin0\omega_0 t + b_1 sin1\omega_0 t + b_2 sin2\omega_0 t + \cdots + b_k sink\omega_0 t + \cdots \\ &= a_0 + a_1 cos1\omega_0 t + a_2 cos2\omega_0 t + \cdots + a_k cosk\omega_0 t + \cdots + b_1 sin1\omega_0 t \\ &\quad + b_2 sin2\omega_0 t + \cdots + b_k sink\omega_0 t + \cdots \end{aligned}$$

$$f(t) = \frac{a_0}{2} + \sum_{k=1}^{\infty}(a_k cosk\omega_0 t + b_k\, sink\omega_0 t)\;\; t_0 < t < t_0 + T \tag{4.7}$$

The above equation expressess the trigonometric Fourier series representation of f(t).

Where

$$a_0 = \frac{1}{T}\int_{t_0}^{t_0+T} f(t)dt \tag{4.8}$$

$$a_k = \frac{2}{T}\int_{t_o}^{t_0+T} f(t)cosk\omega_0\, tdt \tag{4.9}$$

$$b_k = \frac{2}{T}\int_{t_0}^{t_0+T} f(t)sink\omega_0 tdt \tag{4.10}$$

If the interval $t_0 < t < t_0 + T$ is (-Y, Y) (thus T=2Y), then the Fourier series coefficients a_0, a_k and b_k are:

$$a_0 = \frac{1}{2Y}\int_{-Y}^{Y} f(t)dt \tag{4.11}$$

$$a_k = \frac{1}{Y}\int_{-Y}^{Y} f(t)cosk\omega_0 tdt \tag{4.12}$$

$$b_k = \frac{1}{Y}\int_{-Y}^{Y} f(t)sink\omega_0 tdt \tag{4.13}$$

For a periodic function on [-π, π], above equations changes to:

$$a_0 = \frac{1}{2\pi}\int_{-\pi}^{\pi} f(t)dt \tag{4.14}$$

$$a_k = \frac{1}{\pi}\int_{-\pi}^{\pi} f(t)cosktdt \tag{4.15}$$

$$b_k = \frac{1}{\pi}\int_{-\pi}^{\pi} f(t)sinktdt \tag{4.16}$$

- Symmetrical considerations

If f(t) is even that is f(-t)=f(t), then $b_k = 0$

Therefore,

$$a_k = \frac{2}{L}\int_{0}^{L} f(t)cosk\omega_0 tdt \tag{4.17}$$

$$f(t) = \frac{a_0}{2} + \sum_{k=1}^{\infty}(a_k\, cosk\omega_0 t) \tag{4.18}$$

Also, if f(t) is odd that is f(-t)=-f(t), then $a_k = 0$

Therefore,

$$b_k = \frac{2}{L}\int_{0}^{L} f(t)sink\omega_0 tdt \tag{4.19}$$

$$f(t) = \frac{a_0}{2} + \sum_{k=1}^{\infty}(b_k\, sink\omega_0 t) \tag{4.20}$$

4.2.2 Exponential Fourier series (EFS)

Given set of complex exponential functions ($e^{jk\omega_0 t}$) for $k = 0, \pm 1, \pm 2 \ldots\ldots$ which is orthogonal over the interval $(t_0, t_0 + T)$. Where $T = \frac{2\pi}{\omega_0}$. This is a complete set, so it is possible to express any function f(t) as follows:

$$f(t) = F_0 + F_1 e^{J\omega_0 t} + F_2 e^{J2\omega_0 t} + \cdots + F_k e^{Jk\omega_0 t} + \cdots + F_{-1} e^{-J\omega_0 t} + F_{-2} e^{-J2\omega_0 t} + \cdots + F_{-k} e^{-Jk\omega_0 t} + \cdots$$

$$f(t) = \sum_{k=-\infty}^{\infty} F_k e^{jk\omega_0 t} \quad (t_0 < t < t_0 + T) \tag{4.21}$$

The above equation expressess the exponential Fourier series representation of signal f(t) over the interval $t_0 < t < t_0 + T$. The Fourier coefficient F_k is given as

$$F_k = \frac{1}{T} \int_{t_0}^{t_0+T} f(t) e^{-jk\omega_0 t} dt \tag{4.22}$$

4.3 Fourier Transforms

Although Fourier series is a useful tool for investigating the spectrum of a periodic functions or signals, there are many waveforms that do not repeat themselves regularly.The main shortcomings of Fourier series is that, it is only applicable to periodic signals. There are many naturally produced signals such as non periodic or aperiodic, which cannot be expressed using Fourier series. To overcome this drawback, Fourier developed a mathematical model to convert signals between time (or spatial) domain to frequency domain and vice versa which is called Fourier transform. It has different applications in engineering and physics such as RADAR, astronomy, signal processing, analysis of LTI systems etc. (Chapra & Canale, 1990).

$$f(t) = \sum_{k=-\infty}^{\infty} \tilde{c_k}\, e^{jk\omega_0 t} \tag{4.23}$$

Where

$$\tilde{c_k} = \frac{1}{T} \int_{-T/2}^{T/2} f(t) e^{-jk\omega_0 t} dt \tag{4.24}$$

The change from a periodic to nonperiodic function can be done by letting the period to approach infinity. Thus, as T approaches infinity, the function never repeat itself and therefore becomes aperiodic.

The Fourier transform of a function is given as

$$F(i\omega_0) = \int_{-\infty}^{\infty} f(t)e^{-j\omega_0 t}dt \tag{4.25}$$

The inverse Fourier transform is given by

$$f(t) = \frac{1}{2\pi}\int_{-\infty}^{\infty} F(i\omega_0)e^{j\omega_0 t}d\omega_0 \tag{4.26}$$

The main difference between the Fourier series and Fourier transform is that the series applies to periodic function while the transform to nonperiodic waveforms. Also, the Fourier series converts a continuous, periodic time domain function to frequency domain magnitudes at discrete frequencies while the Fourier transform converts a continuous time domain function to a continuous frequency domain function. Therefore, the discrete frequency spectrum generated by Fourier series is analogous to continuous frequency spectrum generated by Fourier transform.

4.4 Discrete Fourier Transform

In engineering applications, functions and signals are normally represented by a finite sets of discrete values. Moreover, data is often gathered in or converted to such a discrete format. Figure 4.1 shows an interval from 0 to T which can be divided into N equispaced subintervals with widths of $\Delta t = T/N$. The subscript n is used to depicts the discrete times at which samples are collected. Therefore, f_n indicates a value of the continous function f(t) taken at t_n.

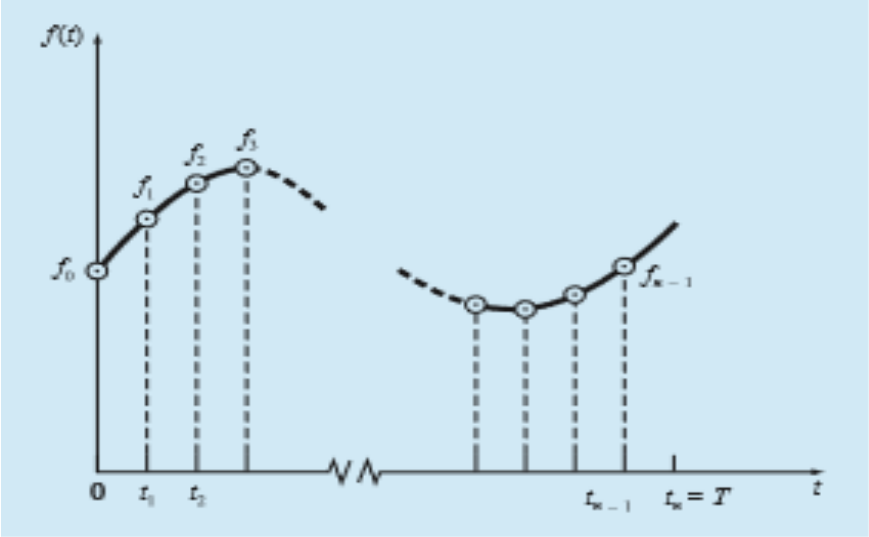

Figure 4.1: Points sampling of discrete Fourier transform

The data points are specified at n=0, 1, 2,…,N-1. For the system shown in below, a discrete Fourier transform can be written as

$$F_k = \sum_{n=0}^{N-1} f_n e^{-jk\omega_0 n} \; for\; k = 0\; to\; N-1 \tag{4.27}$$

And the inverse Fourier transform as

$$f_n = \frac{1}{N}\sum_{k=0}^{N-1} F_k\, e^{jk\omega_0 n}\; for\; n = 0\; to\; N-1 \tag{4.28}$$

$$where\; \omega_0 = \frac{2\pi}{T}$$

Equations (4.19) and (4.18) represent the discrete analogs of (4.17) and (4.16) respectively. Thus, they can be used to compute both the direct and inverse Fourier transform of a discrete data. Though such computations can be done by hand, they are extremely difficult.

4.5 The Fast Fourier Transform

For data samples of big and even moderate size, the direct determination of the DFT can be extremely time consuming. The fast Fourier transform (FFT) is an algorithm developed to calculate DFT in an extremely economical fashion. Its speed results from the fact that it uses the results of previous computations to minimize the number of operations. It uses the symmetry and periodicity of trigonometric functions to find the transform with approximately $N\log_2 N$ operations. For N=50 data samples, the FFT is about ten times faster than the standard DFT. For N=1000, the FFT is about 100 times faster.

The first FFT algorithm was developed by Gauss in the early nineteenth century (Heideman et al., 1984). Other main contributions were made by Runge, Danielson, Lanczos and others in the early twentieth century. Fortunately, because DFT often took days to weeks to compute by hand, they did not attract much interest prior to the development of modern digital computers. J.W. Cooley and J.W. Tukey in 1965 published a key paper which they designed an algorithm for calculating FFT (Chapra & Canale, 1990).

CHAPTER 5
METHODS AND PUBLISHED EXPERIMENTAL RESULTS

5.1 Published Experimental Results

Published experimental results were obtained from previous studies related to vertical axis Savonius wind turbine. In total, eight rotors, with two or three blades, but different blade geometry were collected from Published experimental results and they were subjected to power coefficient, torque coefficient and torque as function of rotor angle.

5.1.1 Mechanical torque

Ali (2013), carried out an experimental study for Savonius Wind Turbine using subsonic wind tunnel under low wind speed. Two and three blades performance was also investigated and compared. The blade has diameter of 100 mm, height of 200 mm and thickness of 0.079 mm as depicted in Figure 5.1. The torque variation with rotor angle at 5.3 m/s speed and 458rpm rotational speed is shown in Figure 5.2.

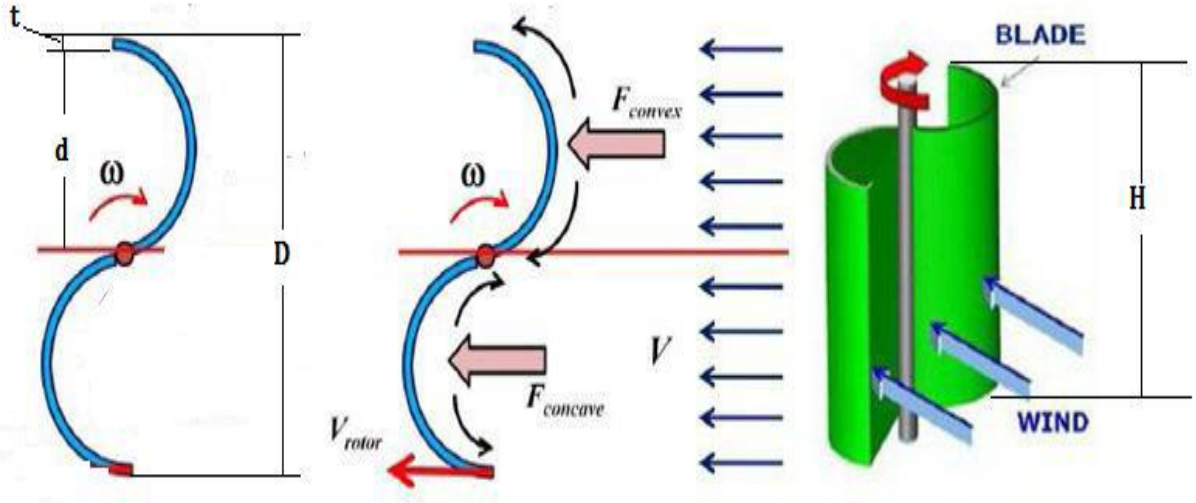

Figure 5.1: Two blades conventional Savonius wind turbine

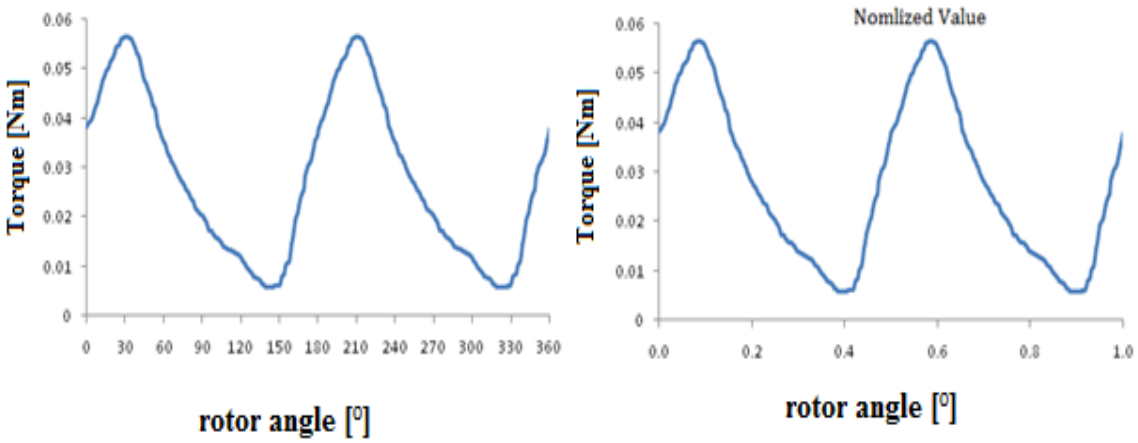

Figure 5.2: Torque of Savonius turbine various rotor angle

Sargolzaei and Kianifar (2009), predicted the torque of three Savonius rotor using ANNs according to experimental data collected for various prototype vertical Savonius rotors tested in a wind tunnel. Radial basis function (RBF) network was the proposed model. The Savonius rotor has blades nominal diameter (D) and height (H) as in Figure 5.3. The distance gap changes the amount of drag force on the rear and front of blade for various angles with respect to the wind direction. 30 cm was the height (H) in all produced models and the thickness of blade 1 mm, which was made of aluminum (Figure 5.3).

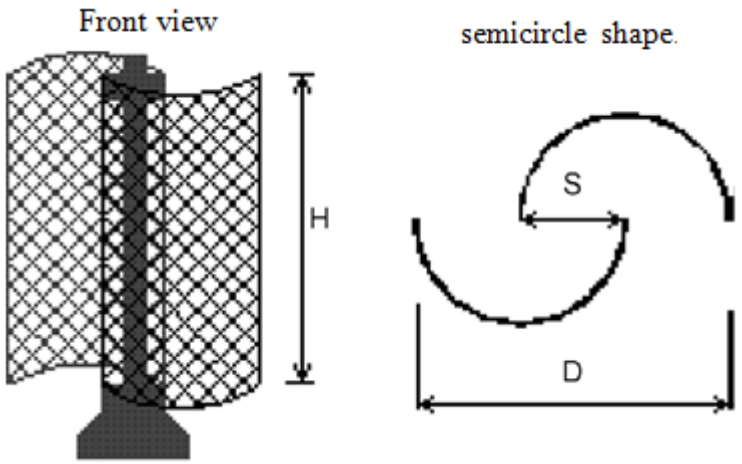

(a) front view (b) semicircle shape

Figure 5.3: Schematic of Savonius rotor

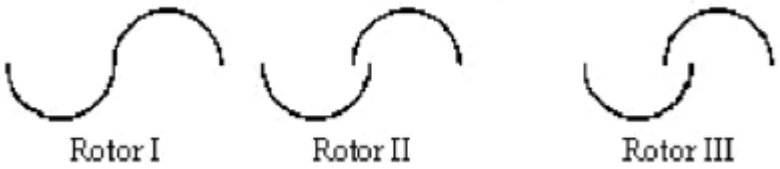

Figure 5.4: Experimented rotor's blade shapes

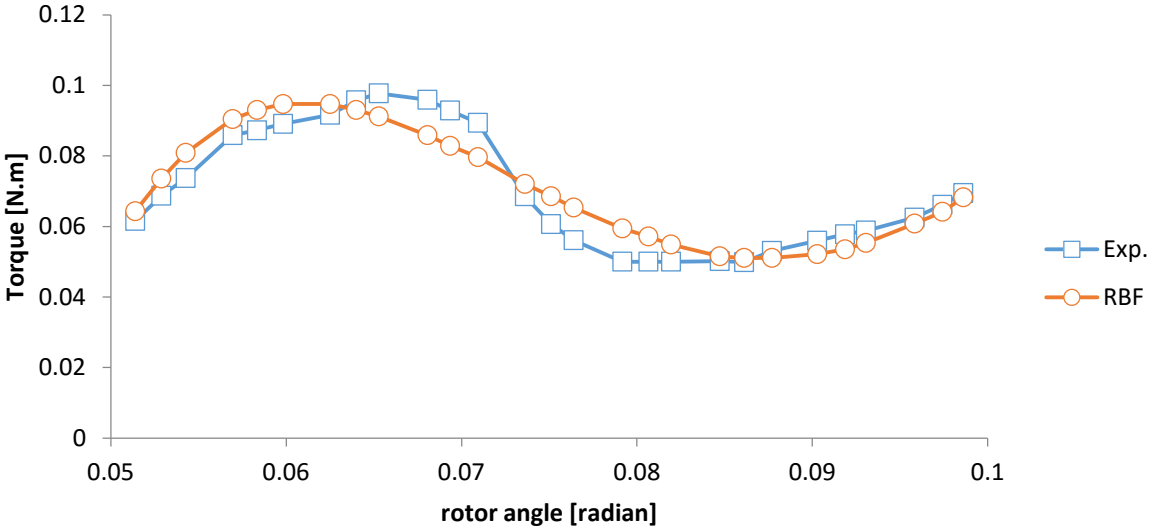

Figure 5.5: Torque of Savonius rotor I various rotor angle

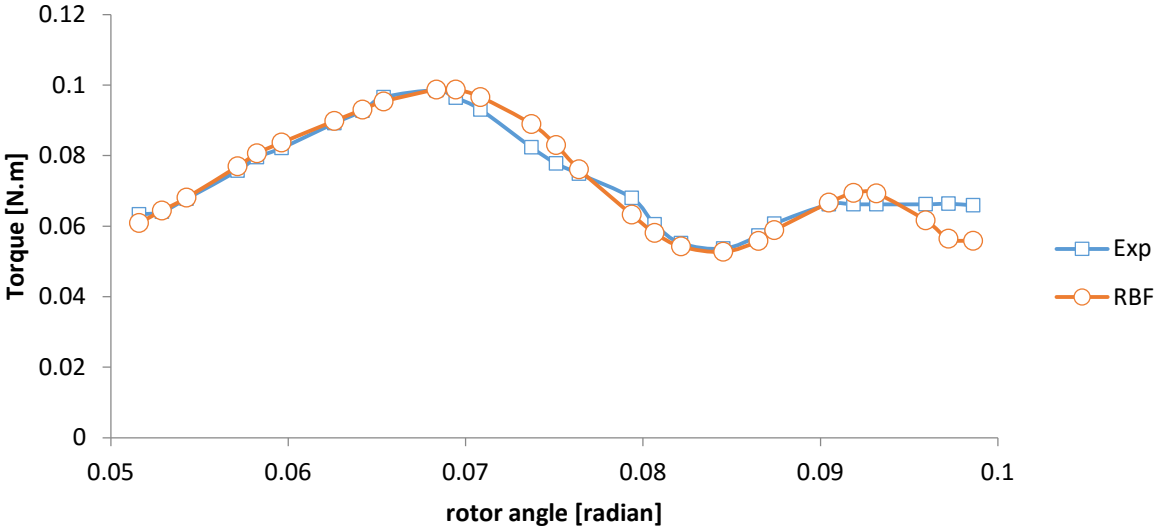

Figure 5.6: Torque of Savonius rotor II various rotor angles

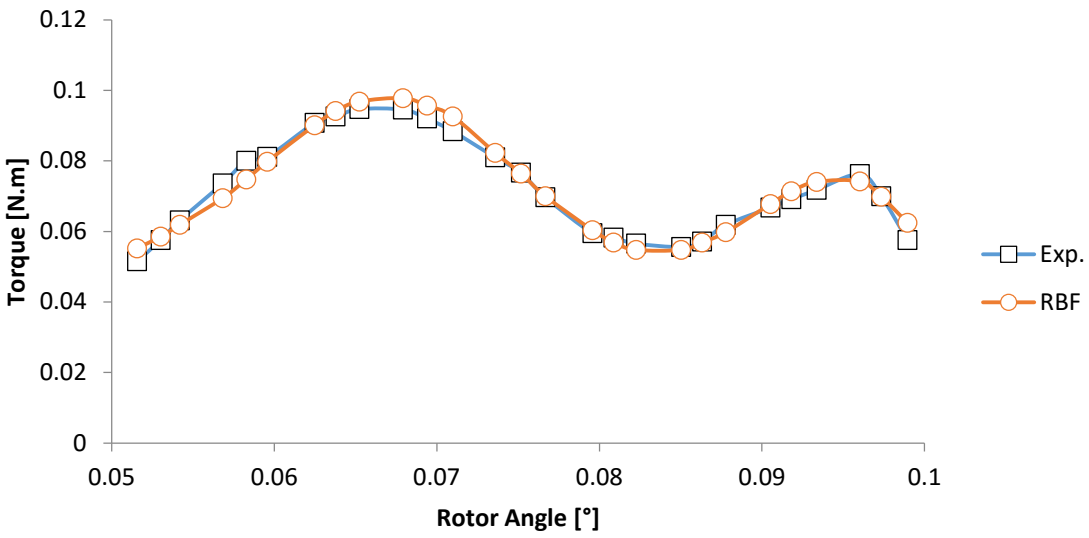

Figure 5.7: Torque of Savonius rotor III various rotor angle

5.1.2 Power coefficient (C_p), torque coefficient (C_t) and static torque coefficient

Debnath et al. (2014), experimentally measured the torque and power coefficients of helical Savonius wind turbine rotor. Savonius rotor with shaft of 40 cm in height and 24 cm in diameter (see Figure 5.7). The representation of the power coefficient and torque coefficient are shown in Figure 5.8 and 5.9 at different blade number and in one revolution (360°) of the rotor angle.

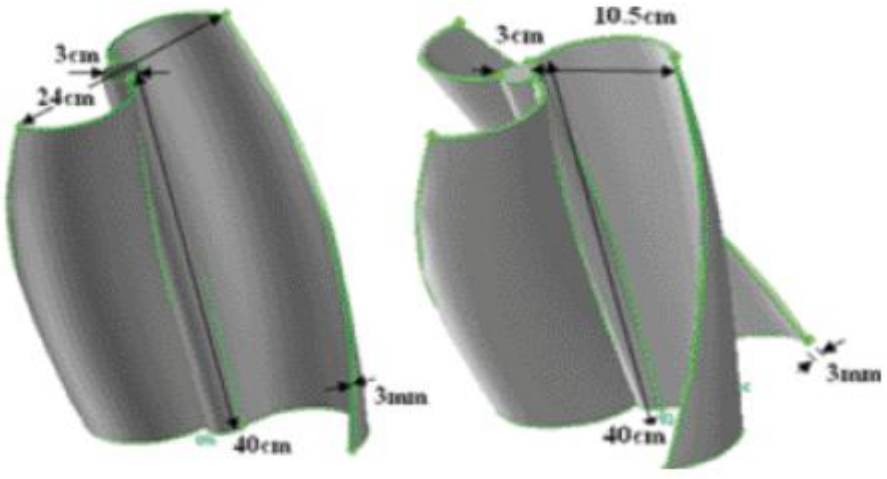

Figure 5.8: Helical Savonius rotor two and three blades at 90° angle of twist

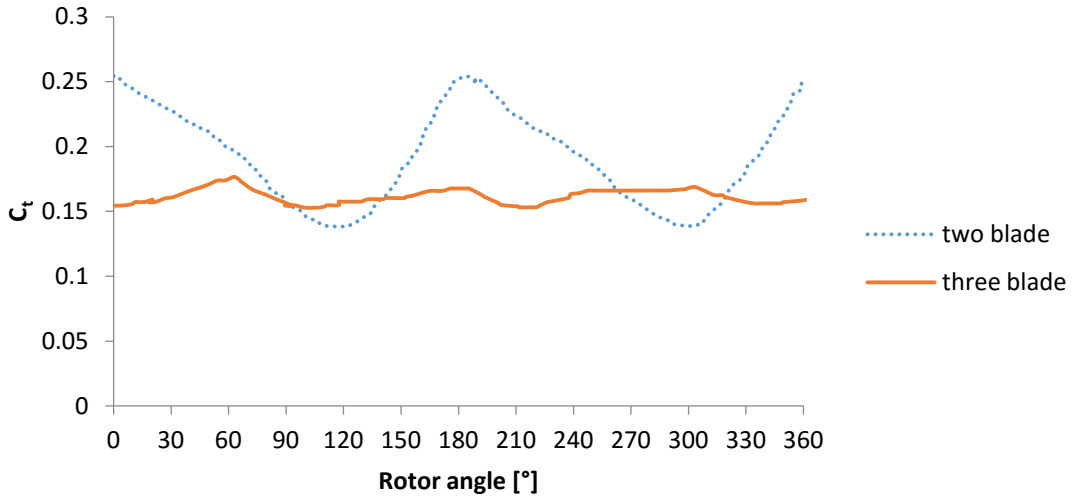

Figure 5.9: Variation of torque coefficient at one revolution (360°).

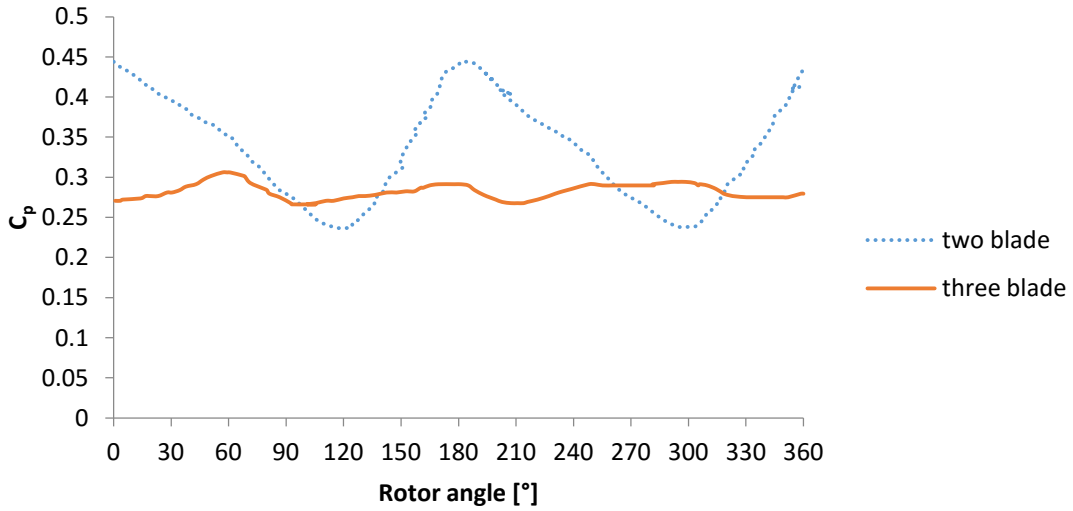

Figure 5.10: Power coefficient variation plot

Kamoji et al. (2009), measured the torque coefficient for helical Savonius wind turbine rotor in one cycle of 360°. Experiment on helical Savonius rotors were carried out in an open jet wind tunnel. The helical rotors (with and without shaft in between end plates) with a twist of 90° were manufactured in a rapid prototyping machine as shown in Figure 5.10. Figures 5.11 shows torque coefficient without shaft at various rotor angle with overlap ratio 0.88 and 0.1, respectively. The torque coefficient with shaft at various rotor angle with overlap ratio 0 is shown in Figure 5.12.

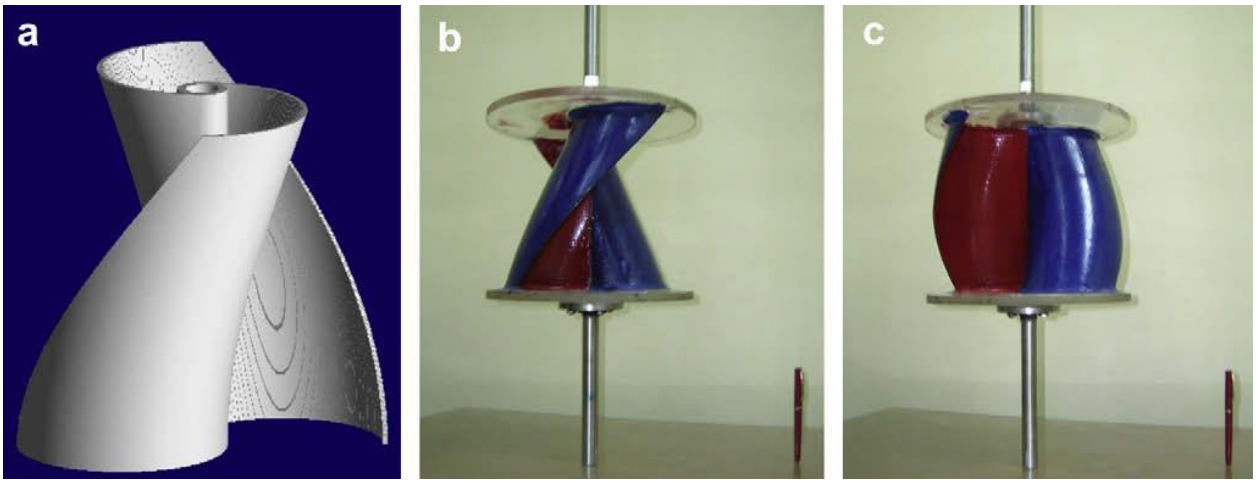

Figure 5.11: (a) Helical Savonius rotor with shaft between the end plates (b) and (c) two views of helical rotor without shaft between the end plates

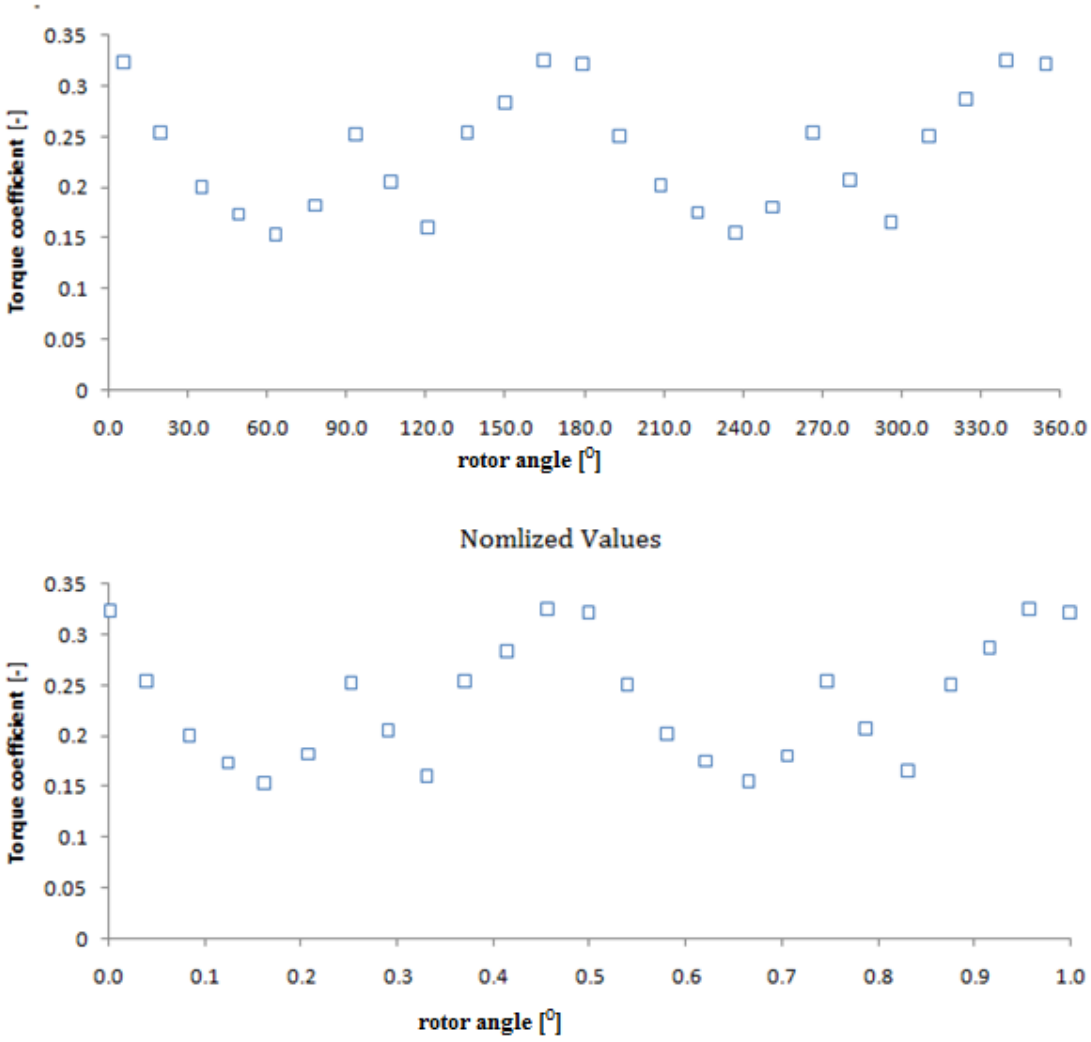

Figure 5.12: Ct without shaft; overlap ratio = 0.1 at one revolution (360°)

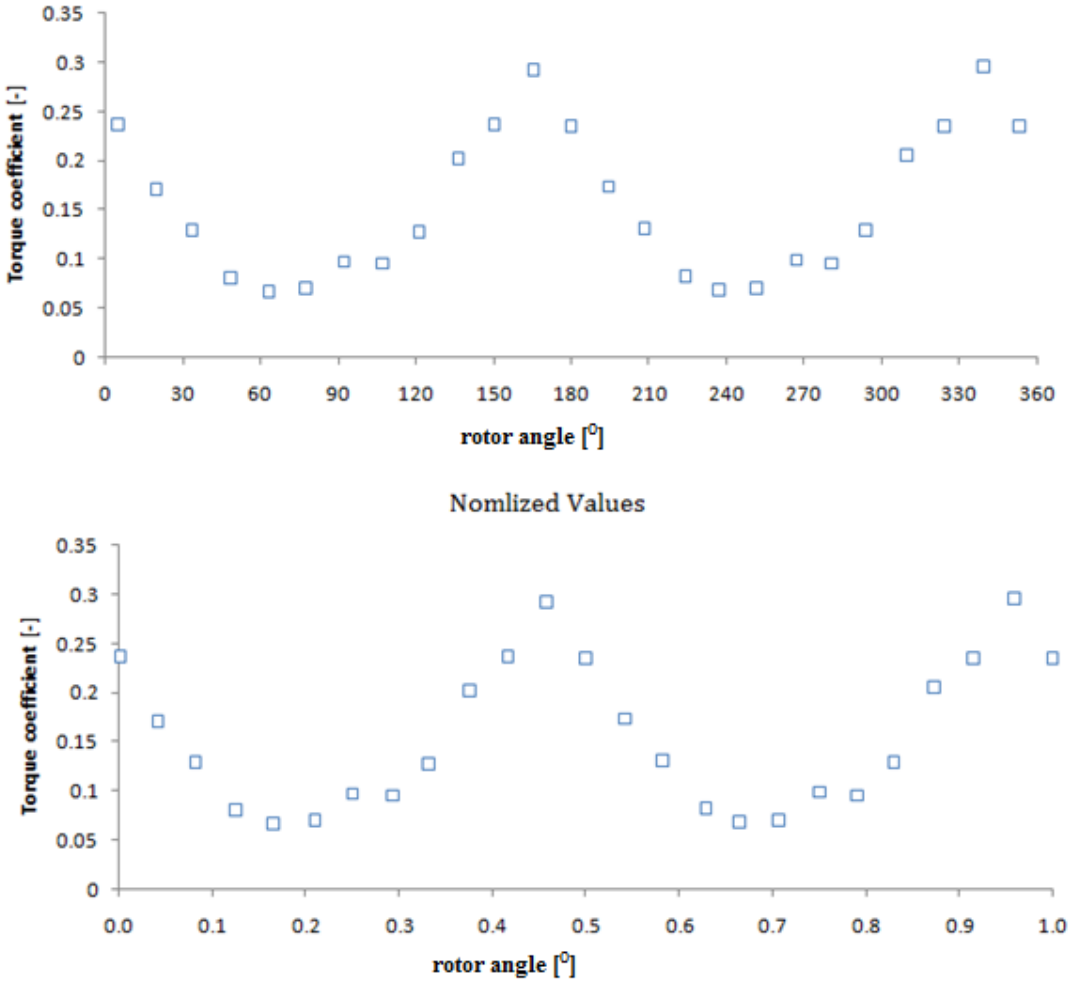

Figure 5.13: Ct with central shaft; overlap ratio = 0.0 at one revolution (360°)

5.2 Statistical Terms and Definitions

Statistical terms used in the regression analysis are defined as follows:

5.2.1 R-squared or the coefficient of determination

The *R*-squared value is an indicator of how well the model fits the data (e.g., an *R*-square value close to 1.0 indicates that almost all the variables variability have been accounted in the model) and an R value of zero means a random relationship. However, *R*-squared increases with increase in a number of predictors in the model, even when the role of the individual predictor is not significant.

$$R^2 = 1 - \frac{\sum(y_{exp} - y_{pred})^2}{\sum(y_{exp} - \bar{y})^2} \tag{5.1}$$

$$where\ \bar{y} = \frac{\sum y_{exp}}{N}$$

5.2.2 Mean square error (MSE)

This is defined as the average squared difference between the expected and predicted values. Small values are preferred and zero suggests no error. It is expressed as:

$$MSE = \frac{1}{N}\sum_{i=1}^{N}(y_{exp} - Y_{pred})^2 \tag{5.2}$$

Where, N number of data set.

5.2.3 Input data normalization

The initial step is the data normalization. This step is done by transforming the actual input data Y into a normalized value Yn (with zero mean and unit variance):

$$Y_n = \frac{Y - Y_{min}}{Y_{max} - Y_{min}} \tag{5.3}$$

Where Y_n is value of Y after normalization, Ymin is the minimum Y value and Y_{max} is the maximum Y value of the data to be normalized.

CHAPTER SIX
RESULTS AND DISCUSSION

6.1 Hidden Layers, Transfer Function and Hidden Neurons

6.1.1 Selection of transfer function

Table 6.1 shows the R-squared of trained and simulated torque of various experimental result (target) for different types of transfer functions with 15 hidden neurons and one hidden layer. It can be observed from the table and figures that LOGSIG transfer function gives the best fitting regression line with R^2 of 0.9981 for training and simulation.

Table 6.1: *R*-squared for the transfer functions type on published experimental data (Ali, 2013)

Transfer function	R^2	
	Training	**Simulation**
LOGSIG	0.9981	0.9981
TANSING	0.9979	0.9978
PURELIN	0.0989	0.1996

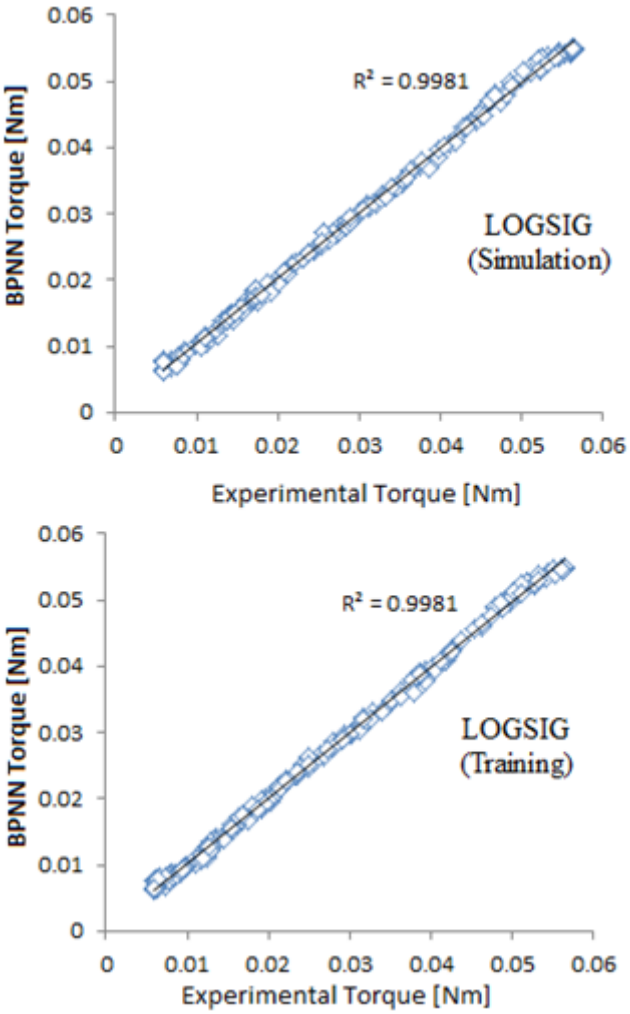

Figure 6.1: Simulated and trained torque vs. experimental torque for LOGSIG transfer function

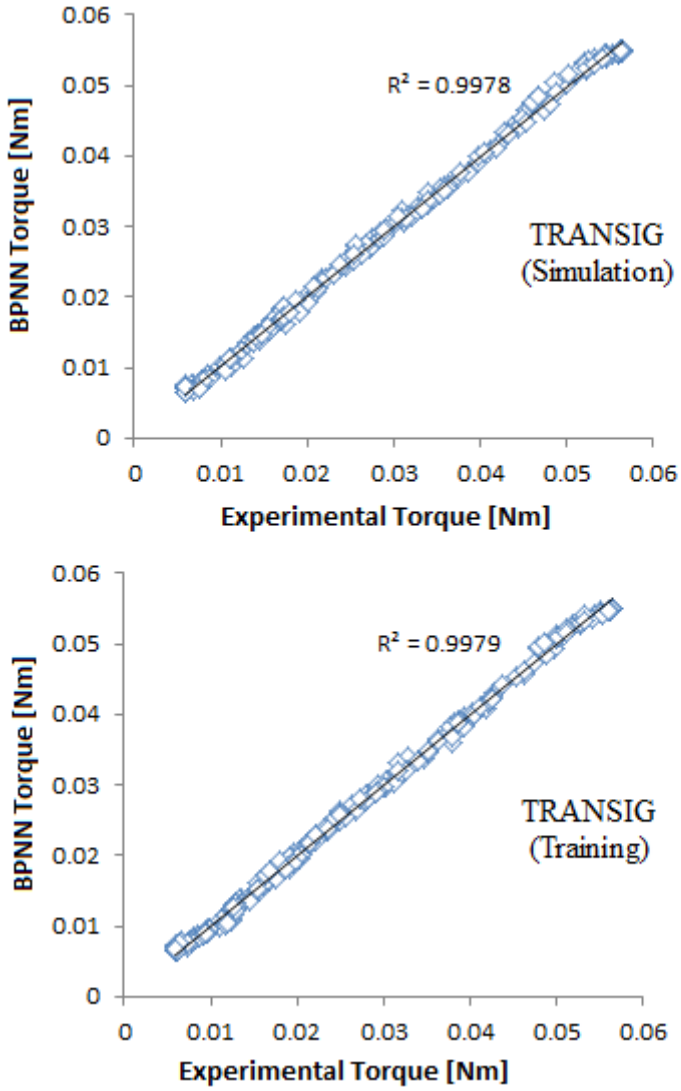

Figure 6.2: Simulated and trained torque vs. experimental torque for TANSIG transfer function

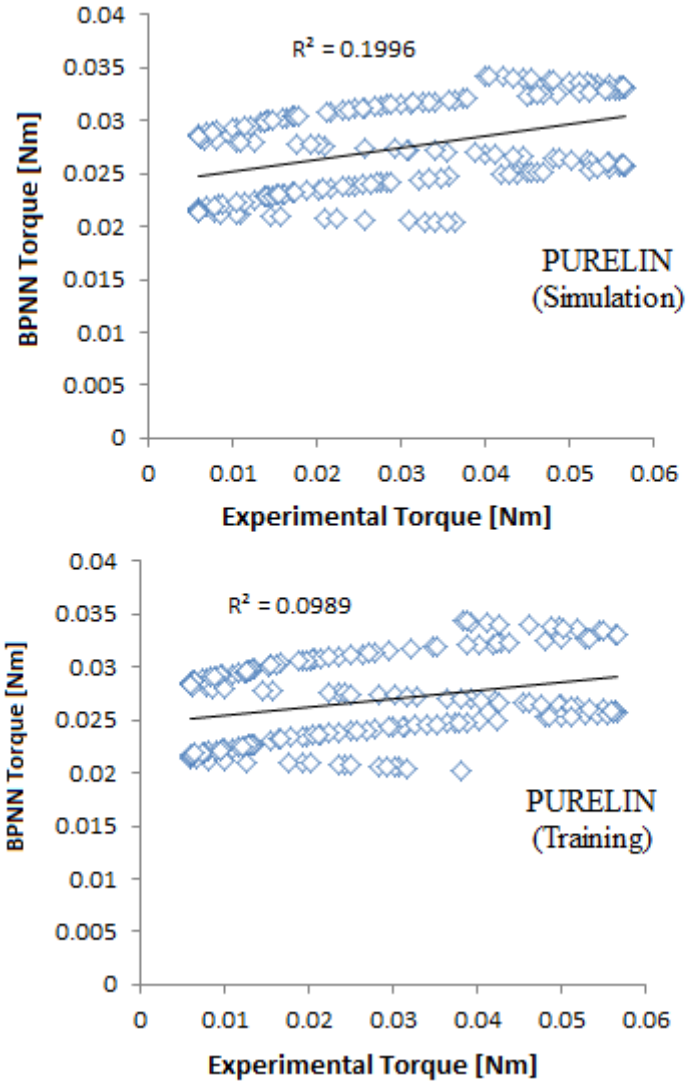

Figure 6.3: Simulated and trained torque vs. experimental torque for PURELIN transfer function

6.1.2 Number of layers

Artificial neural network consist of three different of layers:

- Input
- Hidden and
- Output

Most of models used only one hidden layer since it is sufficient for good prediction. In modeling complex problems, many hidden layers are used. Therefore, a single hidden layer is used throughout this work.

6.1.3 Hidden layer neurons

Many networks with various hidden neurons number are used and estimate the generalization error for each. Then the best network with the best performance was chosen. The R^2 values for case of LOGISG transfer function and one hidden layer with different neurons number of 5, 10, 15 and 20 neurons are shown in Table 6.2 and Figures 6.4 to 6.7. It can be observed that the high R^2 value show that 15 neurons can be used to predict torque of wind turbine. Therefore, 15 neurons are choosen to ensure the best generalization.

Table 6.2: *R*-squared for hidden layer neurons of published experimental data (Ali, 2013)

Hidden layer neurons	R^2	
	Training	**Simulation**
5	0.9947	0.9948
10	0.9981	0.9981
15	0.9989	0.9991
20	0.9934	0.9968

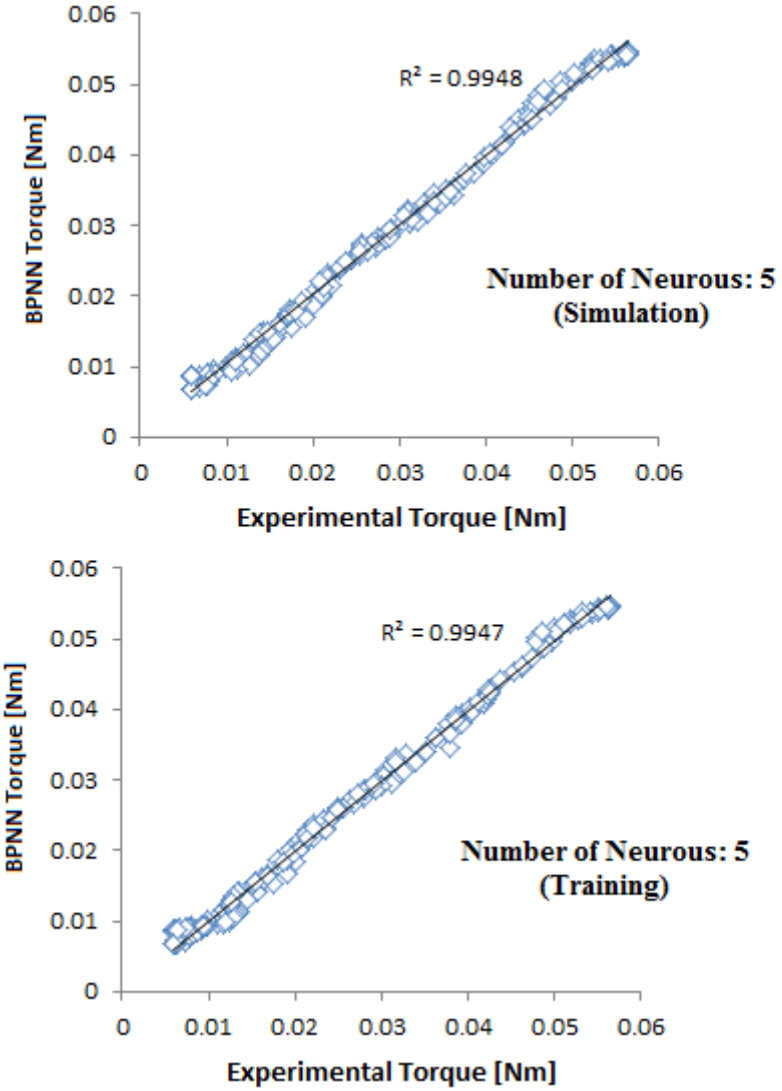

Figure 6.4: Simulated and trained torque vs. experimental torque (number of neurons: 5)

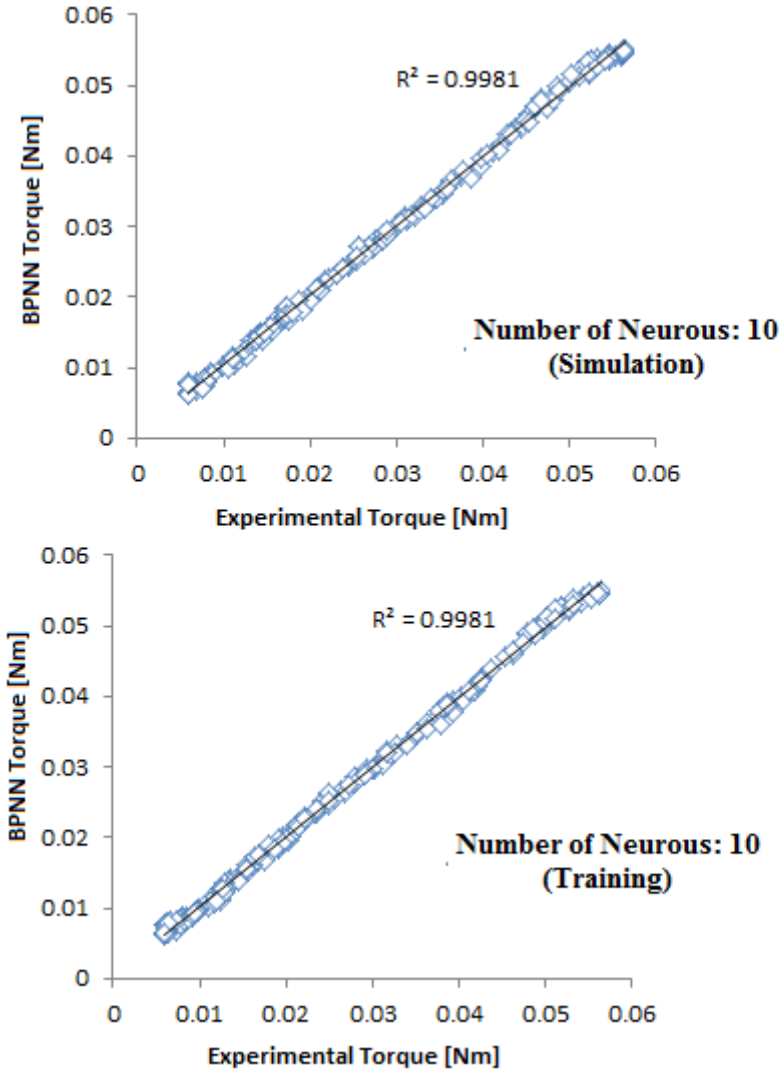

Figure 6.5: Simulated and trained torque vs. experimental torque (number of neurons: 10)

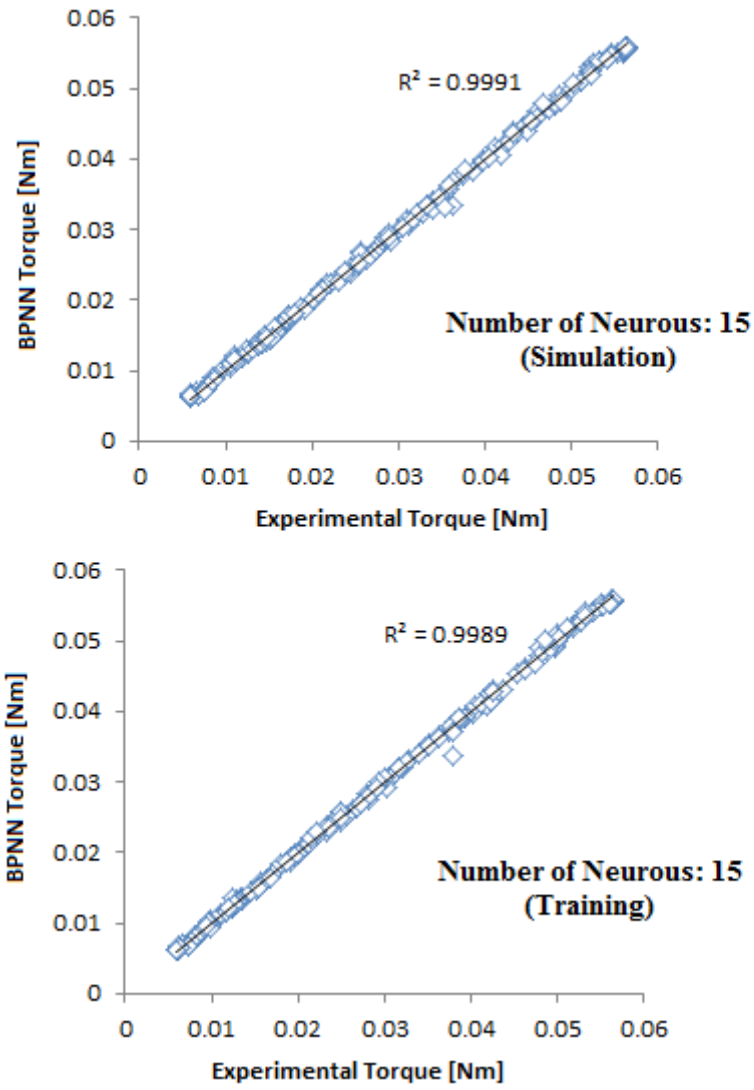

Figure 6.6: Simulated and trained torque vs. experimental torque (number of neurons: 15)

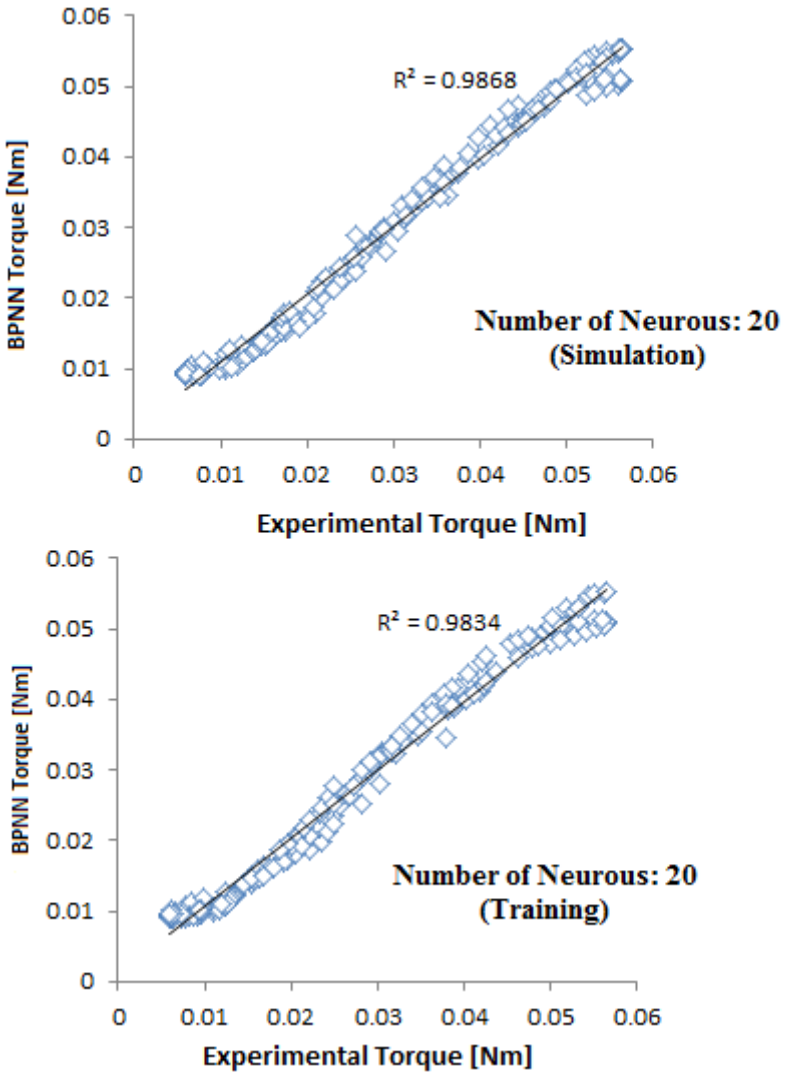

Figure 6.7: Simulated and trained torque vs. experimental torque (number of neurons: 20)

6.2 Published Experimental Data (Ali, 2013)

To perform this task, the experimental data is randomly divided into a set of training/testing sets. In this work, the experimental data is divided into three groups as follows:

1. Group 1: 50% for training data and 50% for similulation (randomly chosen)
2. Group 2: 60% for training data and 40% for similulation (randomly chosen)
3. Group 3: 70% for training data and 30% for similulation (randomly chosen)

Figures 6.8, 6.9, 6.10 and 6.11 shows the plot between the experimental data and the predicted data 50% 50%, 50% for training data and 50% for simulation, 60% 40%, 60% for training data and 40% for simulation, 70% 30%, 70% for training data and 30% for

simulation, and FS, Fourier series, respectively. These figures shows that the models are very accurate to estimate the torque of the Savonius rotor.

As observed in Table 6.3 and Figures 6.13 to 6.14, all groups could be used to predict the torque of Savonius rotor. It was noticed that the predicted mechanical torque using these models is close to the measured mechanical torque. The highest R^2 between measured and predicted torque is 0.9981 for FS showing that this model is very accurate, likewise to 70% 30%, the minimum R^2 is 0.9951 which also shows that the predicted and measured results are very close to each other (Figure 6.13 and 6.14). Hence suggests that these models should be used with caution when predicting the mechanical torque of the Savonius wind turbine.

Table 6.3: Percentage division of experimental data for BPNN

Group 1					
Training		50%			
Simulation		50%			
Epoch		20			
MSE		5.684E-7			
Equations of Training					
$Output = A\,Target + B$					
Training		R^2	**Test**		R^2
A	0.98	0.998	A	1	0.998
B	0.005		B	8E-5	
Validation		R^2	**All**		R^2
A	1	0.998	A	0.99	0.998
B	6.1E-5		B	0.00037	
Group 2					
Training		60%			
Simulation		40%			
Epoch		15			
MSE		5.33E-7			
Equations of Training					
$Output = A\,Target + B$					
Training		R^2	**Test**		R^2
A	0.99	0.998	A	0.99	0.998
B	0.00019		B	0.00020	
Validation		R^2	**All**		R^2
A	0.99	0.998	A	0.99	0.998
B	0.00017		B	0.00019	
Group 3					
Training		70%			
Simulation		30%			
Epoch		16			
MSE		8.456E-7			
Equations of Training					
$Output = A\,Target + B$					
Training		R^2	**Test**		R^2
A	0.99	0.997	A	0.98	0.988
B	0.00027		B	0.00047	
Validation		R^2	**All**		R^2
A	0.99	0.996	A	0.99	0.996
B	0.00041		B	0.00031	

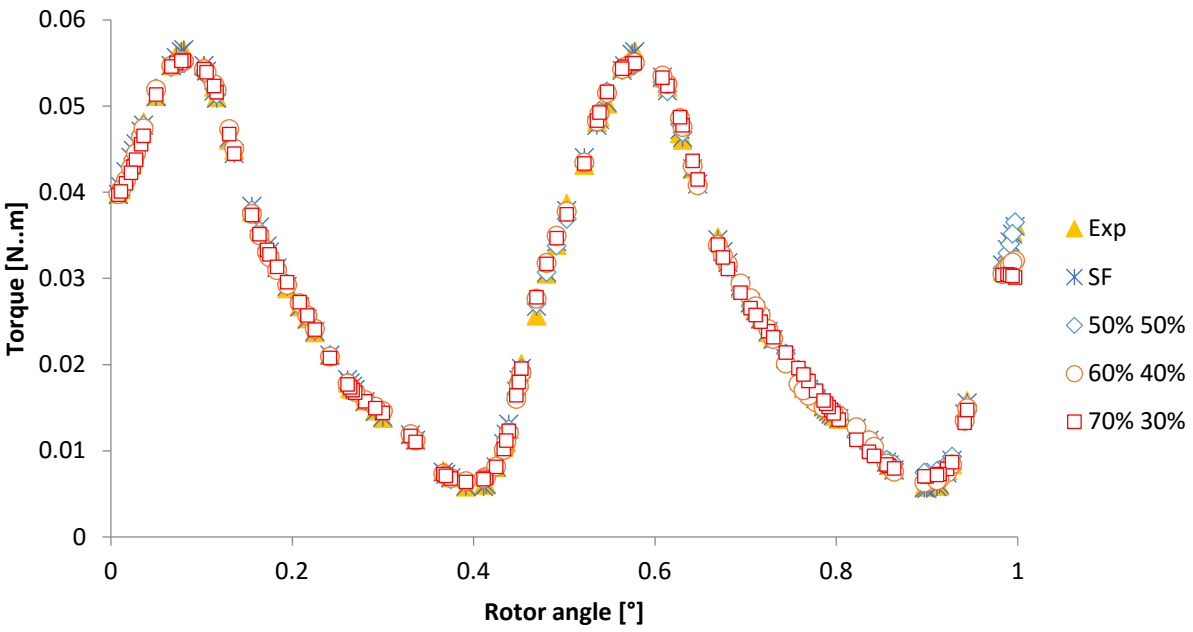

Figure 6.8: Comparison of Proposed Models with experimental data

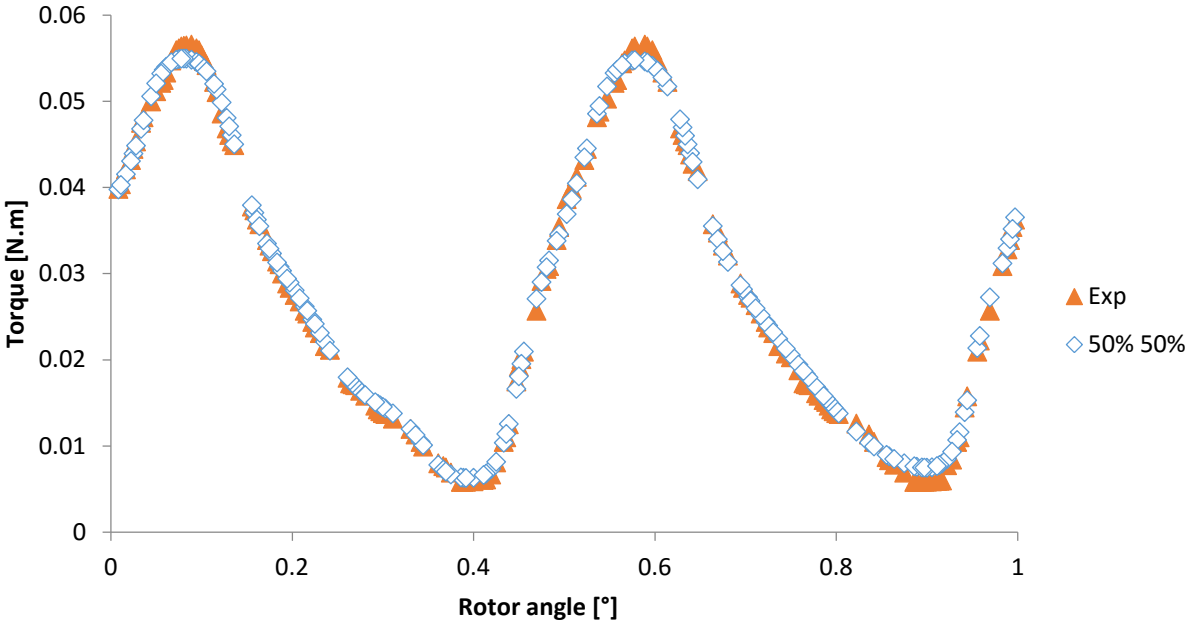

Figure 6.9: Comparison of 50% simulated BPNN with experimental data

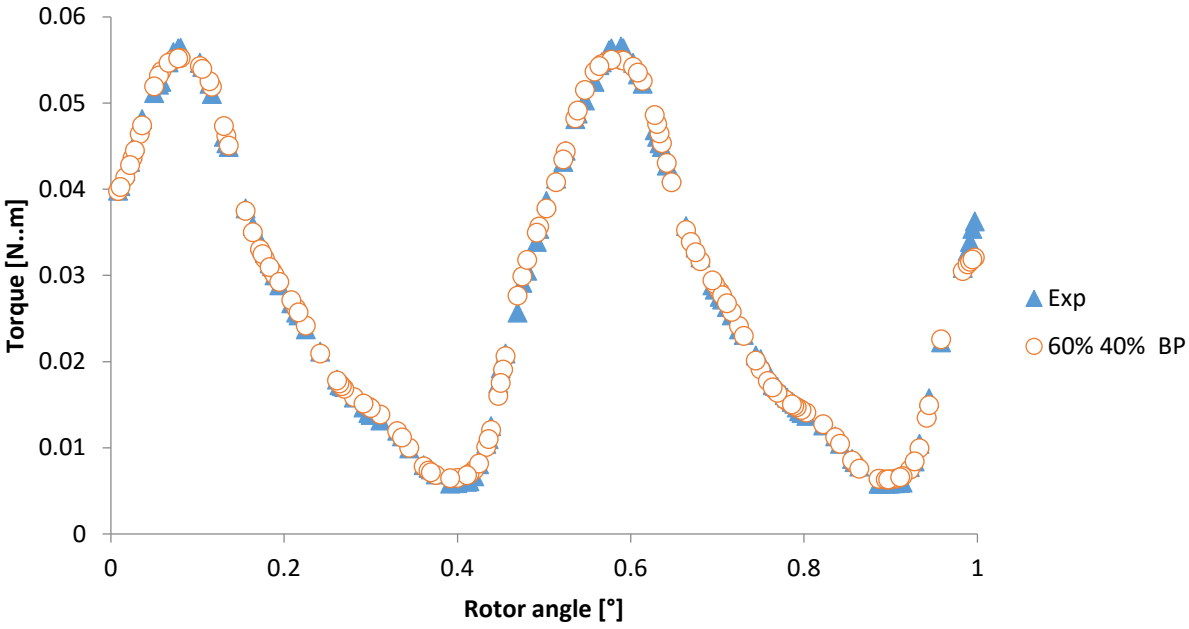

Figure 6.10: Comparison of 40% simulated BPNN with experimental data

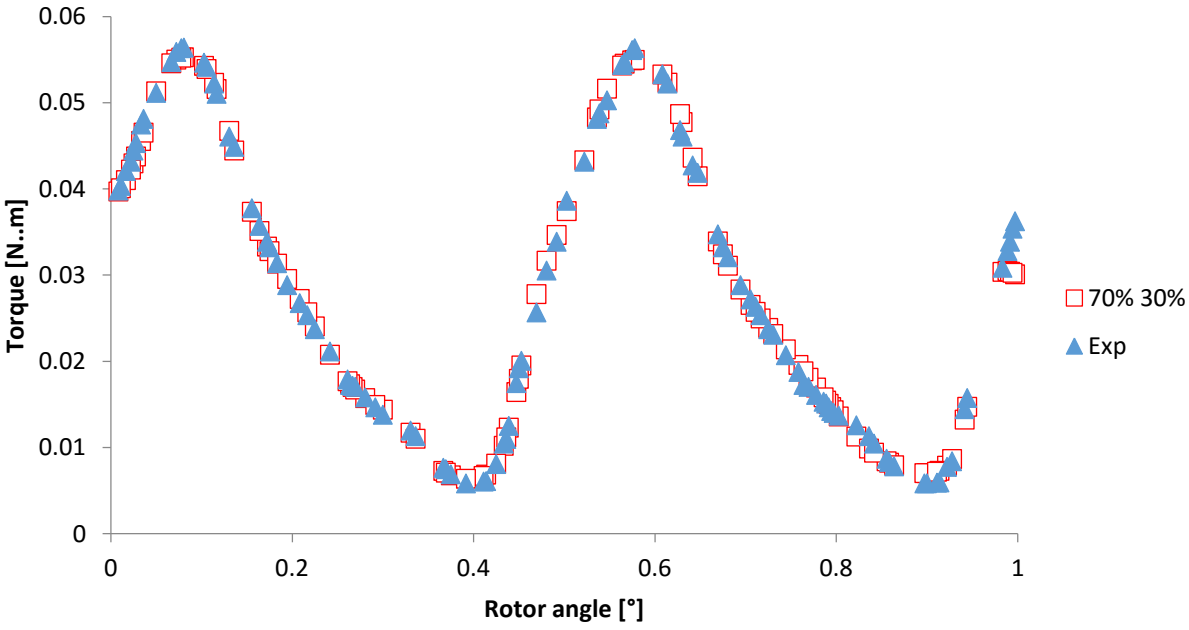

Figure 6.11: Comparison of 30% simulated BPNN with experimental data

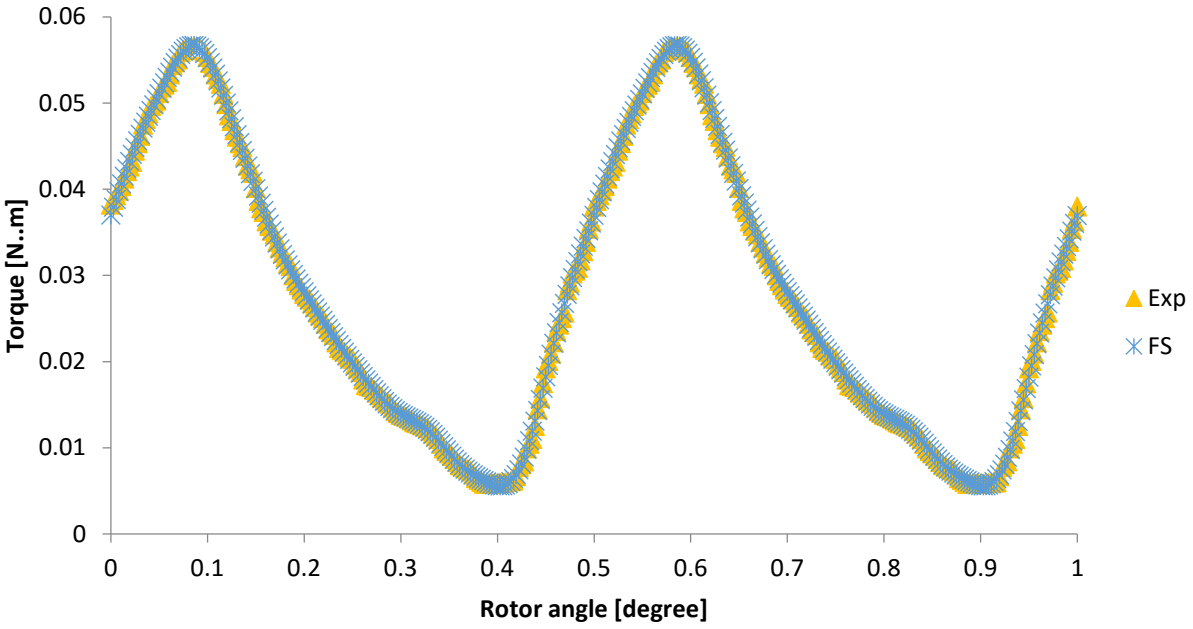

Figure 6.12: Comparison of FS with experimental data

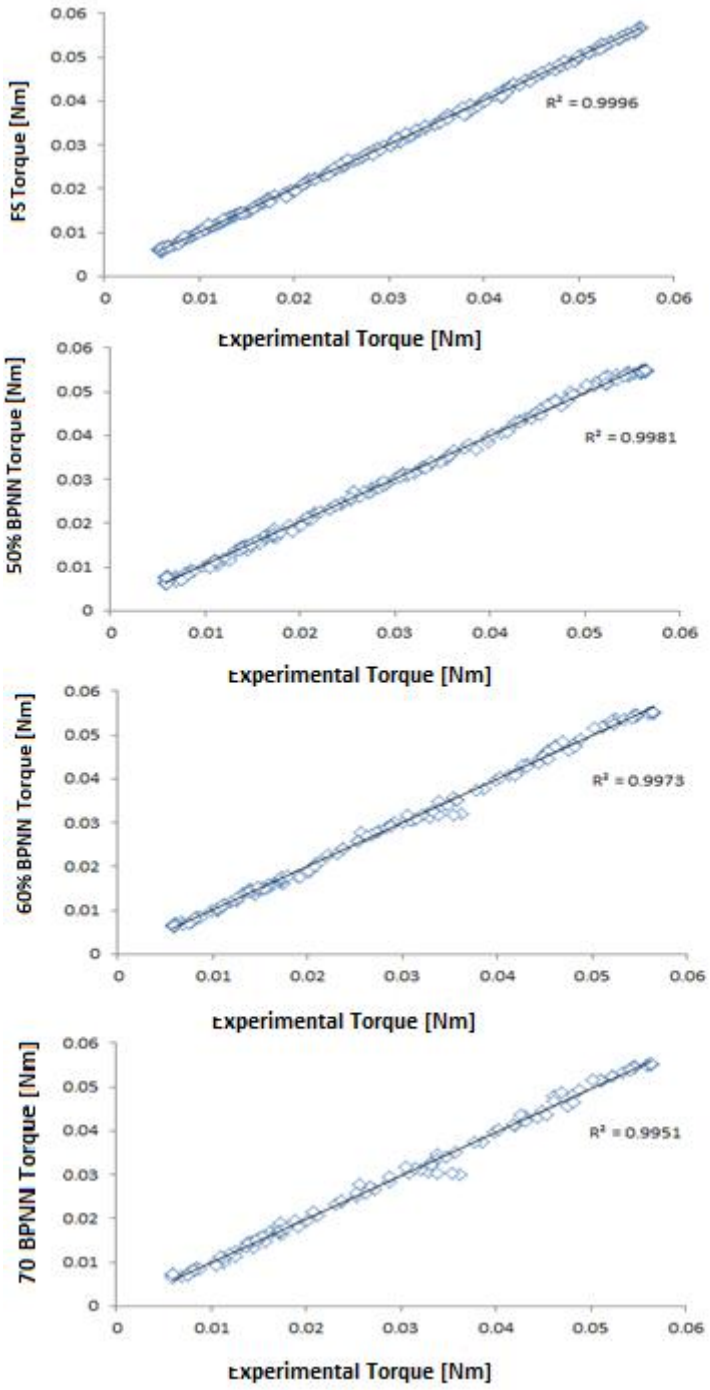

Figure 6.13: Simulated torque vs. experimental torque for all models

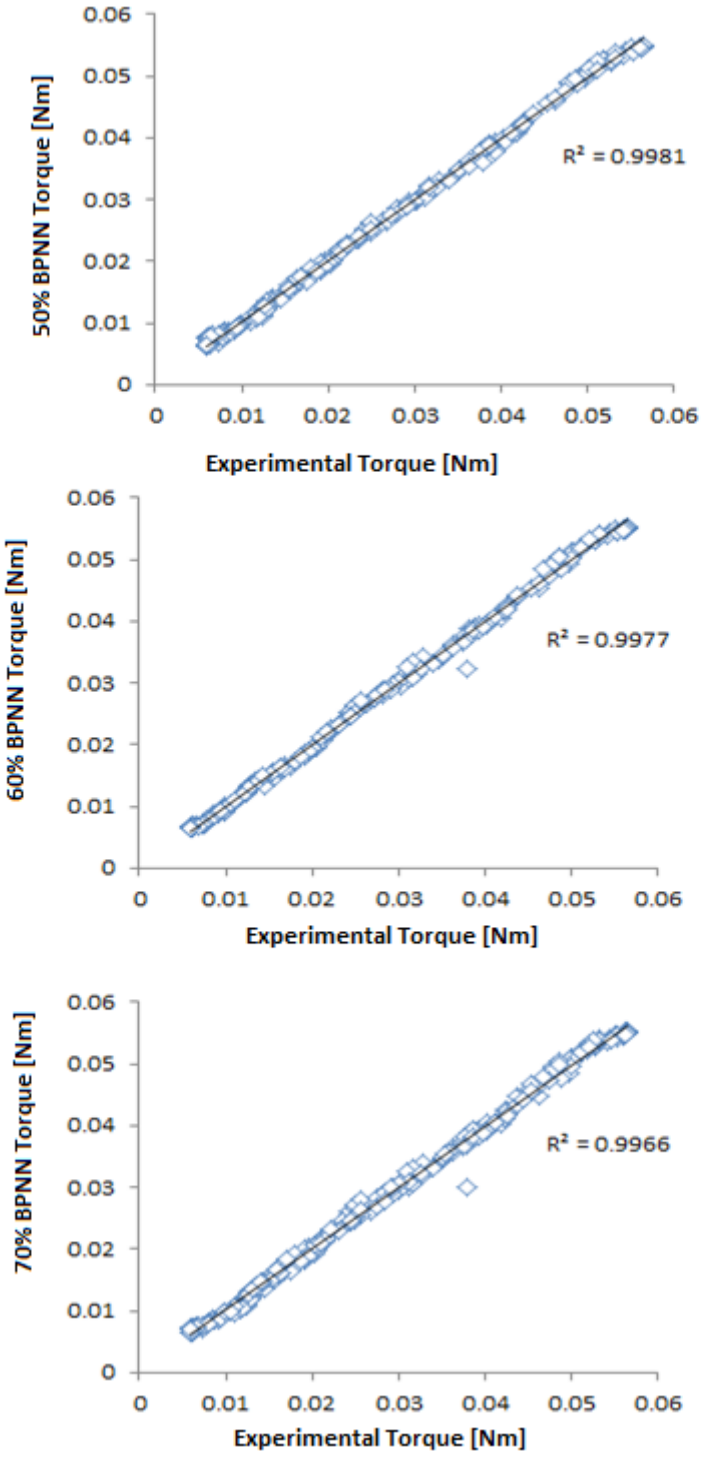

Figure 6.14: Trained torque vs. experimental torque for all models

6.3 Published Experimental Data (Debnath et al., 2014)

6.3.1 C_p for two blades

Similar to the pervious section, the experimental data is divided into two groups as mentioned before (see Table 6.4).

The predicted data are too close to experimental data as shown in Figures 6.15 to 6.19. Simulated and trained and experimental values for C_p were fitted with linear regression equations as shown in Figures 6.20 and 6.21 respectively. It shows that these models are very accurate to predict the power C_p of helix Savonius wind turbine.

Figure 6.18 shows that group 3 is best model for predicting the value of power coefficient of the turbine, rather than using group 1 and group 2.

Table 6.4: Percentage division of experimental data for BPNN (C_p for two blade of helix Savonius turbine)

Group 1					
Training		50%			
Simulation		50%			
Epoch		24			
MSE		3.346E-5			
Equations of Training					
$Output = A\,Target + B$					
Training		R^2	**Test**		R^2
A	0.99	0.996	A	1	
B	0.0028		B	0.0024	0.998
Validation		R^2	**All**		R^2
A	1	0.992	A	1	0.994
B	0.01		B	0.0013	
Group 2					
Training		60%			
Simulation		40%			
Epoch		33			
MSE		1.67E-5			
Equations of Training					
$Output = A\,Target + B$					
Training		R^2	**Test**		R^2
A	0.99	0.996	A	0.98	0.990
B	0.0023		B	0.0085	
Validation		R^2	**All**		R^2
A	0.98	0.994	A	0.99	0.996
B	0.006		B	0.0037	
Group 3					
Training		70%			
Simulation		30%			
Epoch		12			
MSE		3.337E-5			
Equations of Training					
$Output = A\,Target + B$					
Training		R^2	**Test**		R^2
A	0.99	0.996	A	0.99	0.994
B	0.0036		B	0.0046	
Validation		R^2	**All**		R^2
A	0.95	0.992	A	0.98	0.994
B	0.0018		B	0.0057	

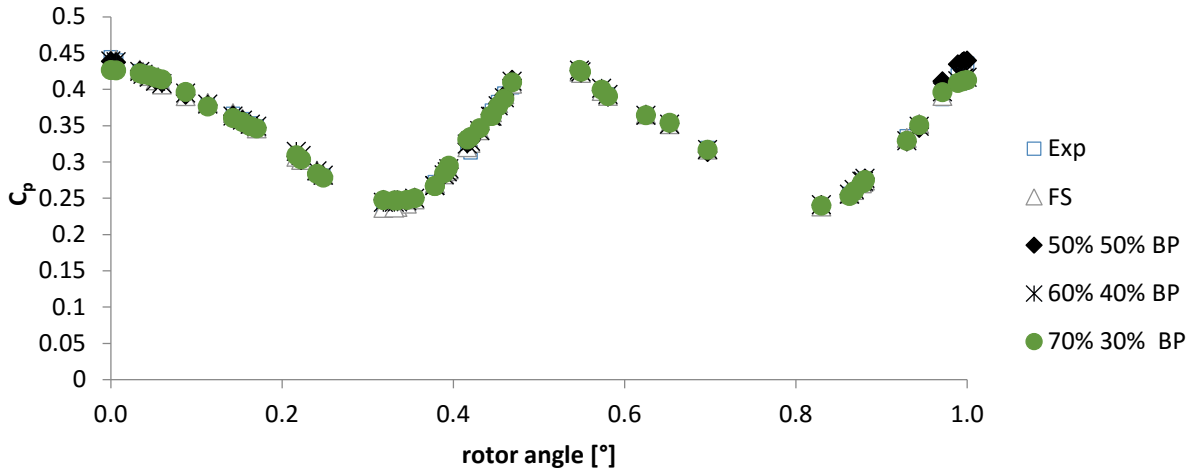

Figure 6.15: Plot of all models with experimental data

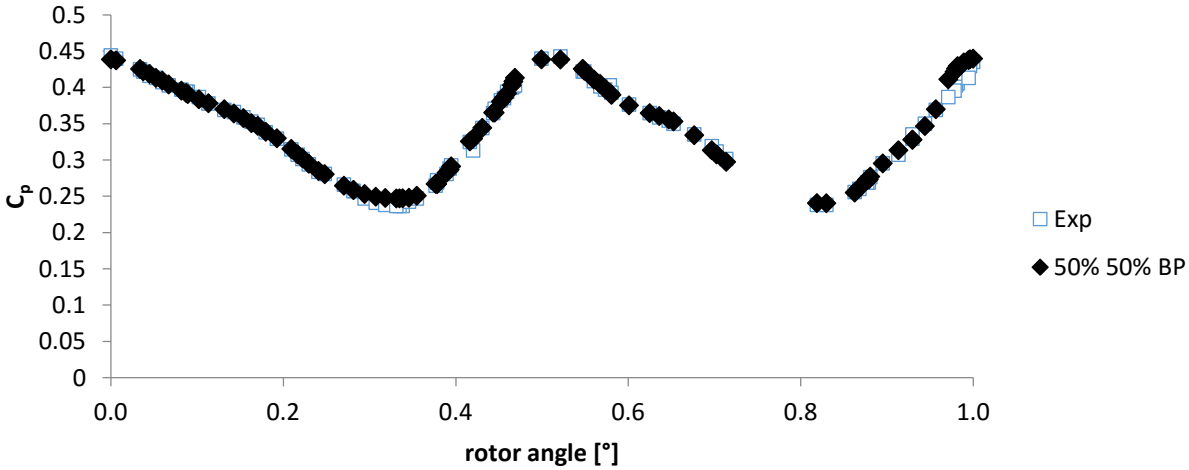

Figure 6.16: 50% simulated BPNN with experimental data

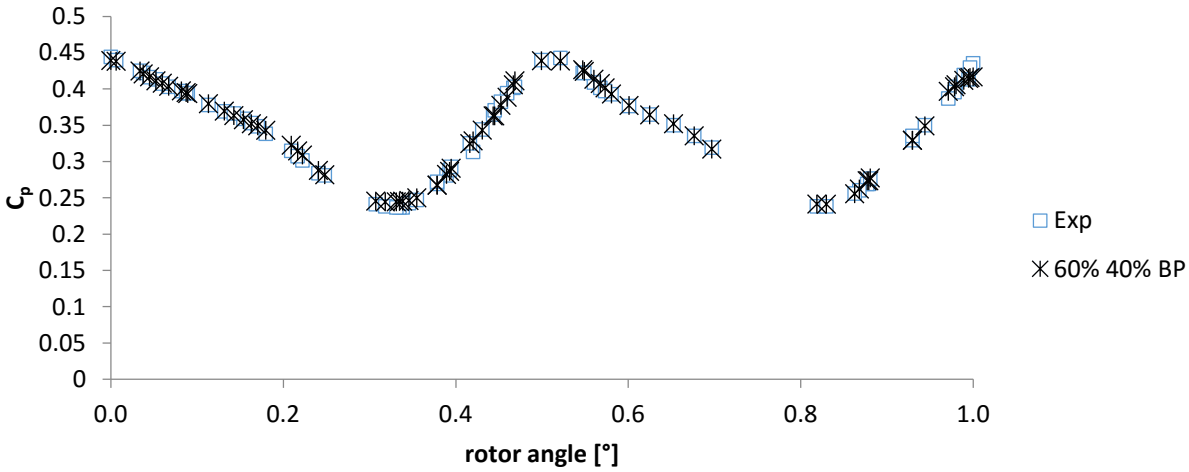

Figure 6.17: Comparison of 40% simulated BPNN with experimental data

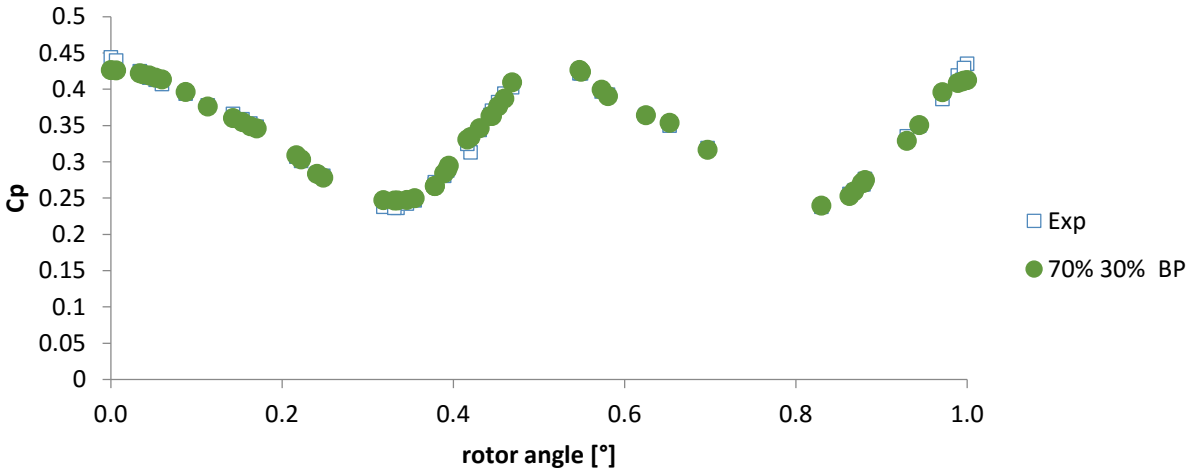

Figure 6.18: 30% simulated BPNN with experimental data

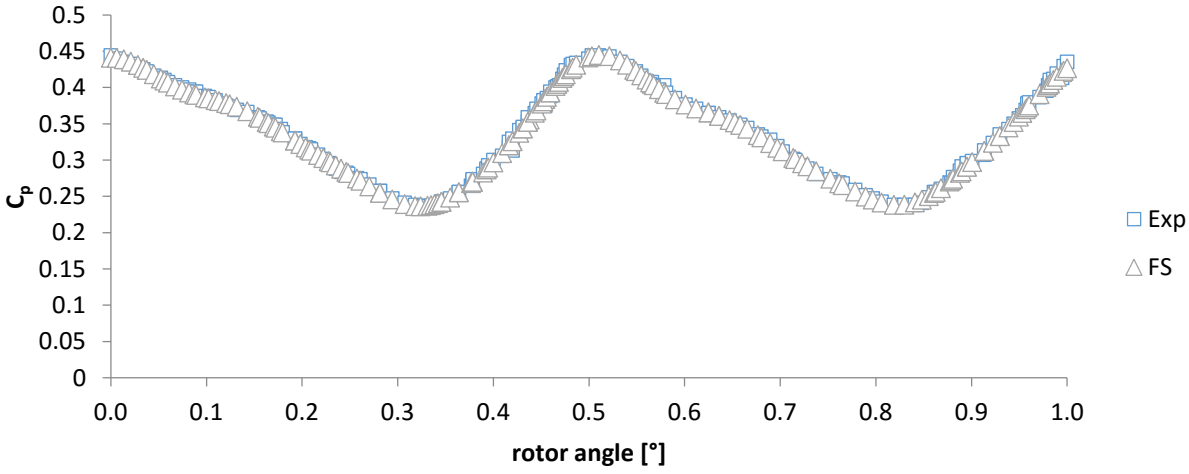

Figure 6.19: Comparison of FS with experimental data

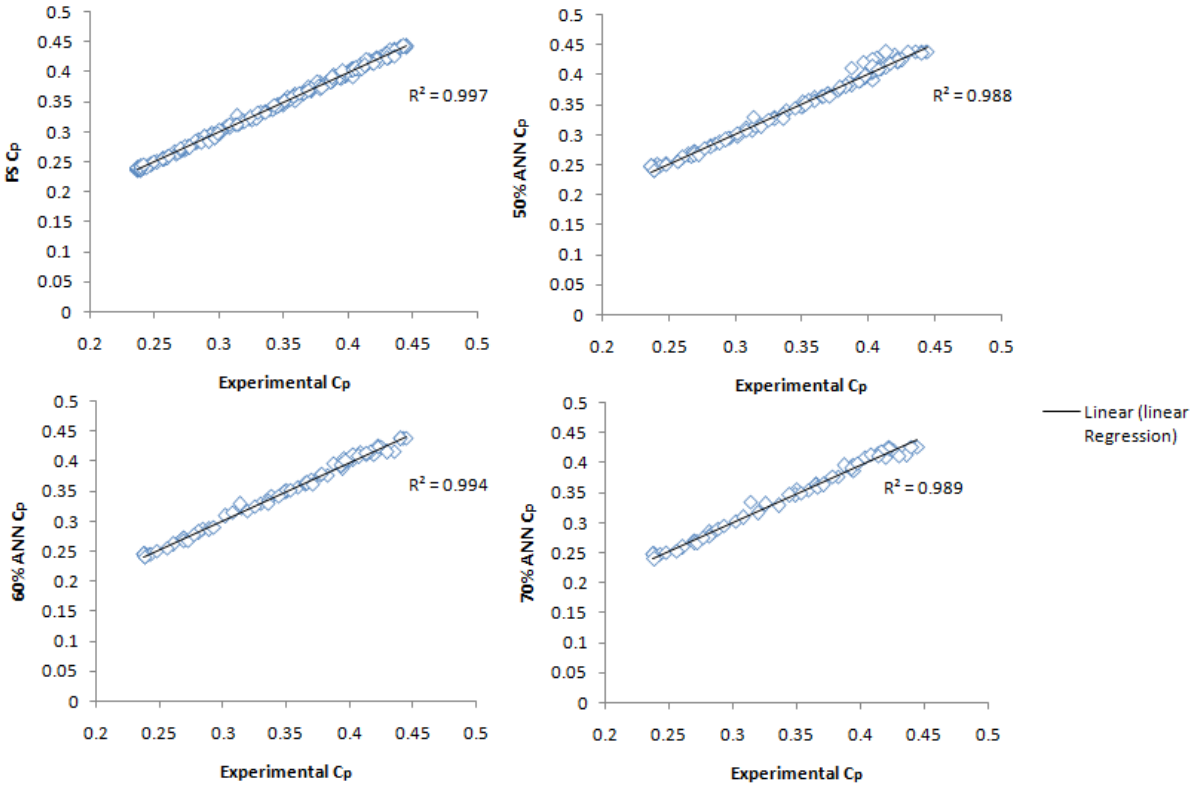

Figure 6.20: Simulated C_P vs. experimental C_P for all models

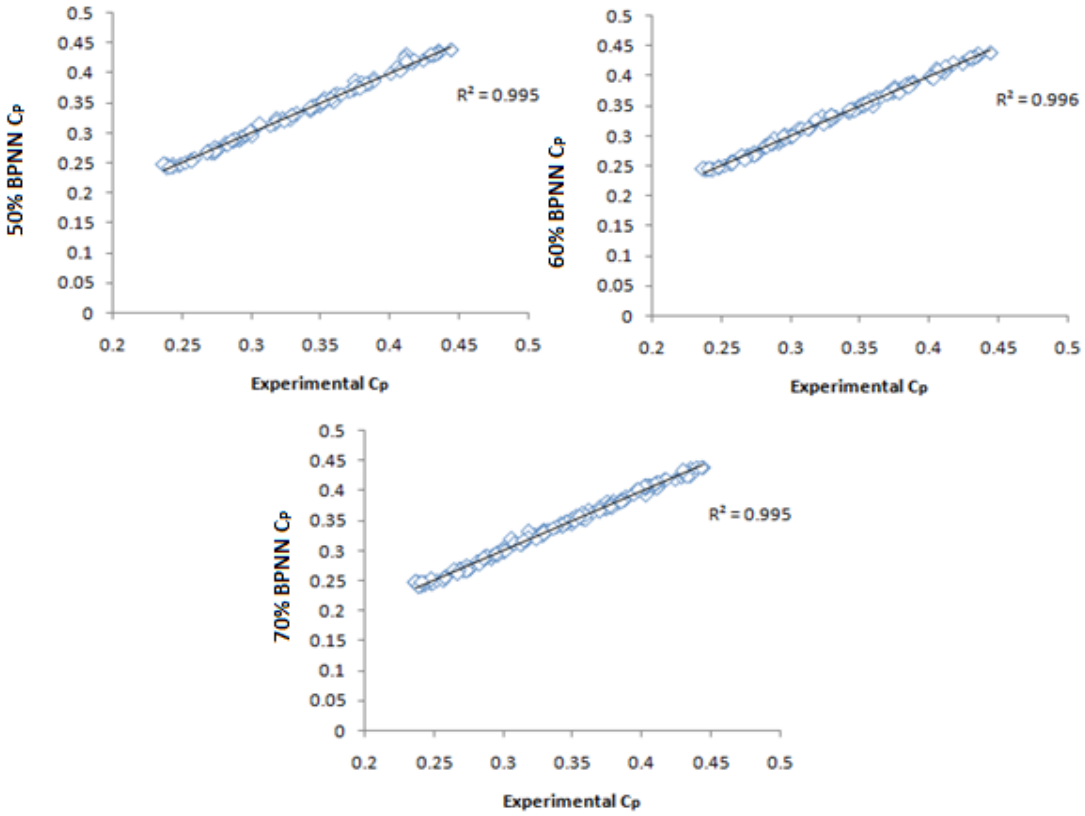

Figure 6.21: Trained C_P vs. experimental C_P for all models

6.3.2 C_t for two blades

Also, the predicted results of the models for torque coefficent of helix wind turbine are shown in Figures 6.22 to 6.26. The R^2 values of simulated and trained BPNN models show that these parameters can be accurately predicted from experimental results of turbine using these models as shown in Table 6.5 (Trained) and Figures 6.27 and 6.28. Hence, BPNN models are the best model for predicting the torque coefficent of helix turbine compared to FS model.

Table 6.5: Percentage division of experimental data for BPNN (C_t for two blade of helix Savonius turbine)

Group 1					
Training		50%			
Simulation		50%			
Epoch		4			
MSE		4.76E-4			
Equations of Training					
$Output = A\,Target + B$					
Training		R^2	**Test**		R^2
A	0.94	0.98	A	0.65	0.556
B	0.012		B	0.064	
Validation		R^2	**All**		R^2
A	0.63	0.625	A	0.84	0.844
B	0.066		B	0.03	
Group 2					
Training		60%			
Simulation		40%			
Epoch		7			
MSE		2.03E-5			
Equations of Training					
$Output = A\,Target + B$					
Training		R^2	**Test**		R^2
A	0.97	0.996	A	0.95	0.996
B	0.0049		B	0.01	
Validation		R^2	**All**		R^2
A	0.96	0.97	A	0.97	0.994
B	0.0059		B	0.0059	
Group 3					
Training		70%			
Simulation		30%			
Epoch		10			
MSE		4.787E-6			
Equations of Training					
$Output = A\,Target + B$					
Training		R^2	**Test**		R^2
A	0.99	4.787E-6	A	1	0.996
B	0.0026		B	0.0012	
Validation		R^2	**All**		R^2
A	1	0.994	A	0.99	0.994
B	0.002		B	0.0018	

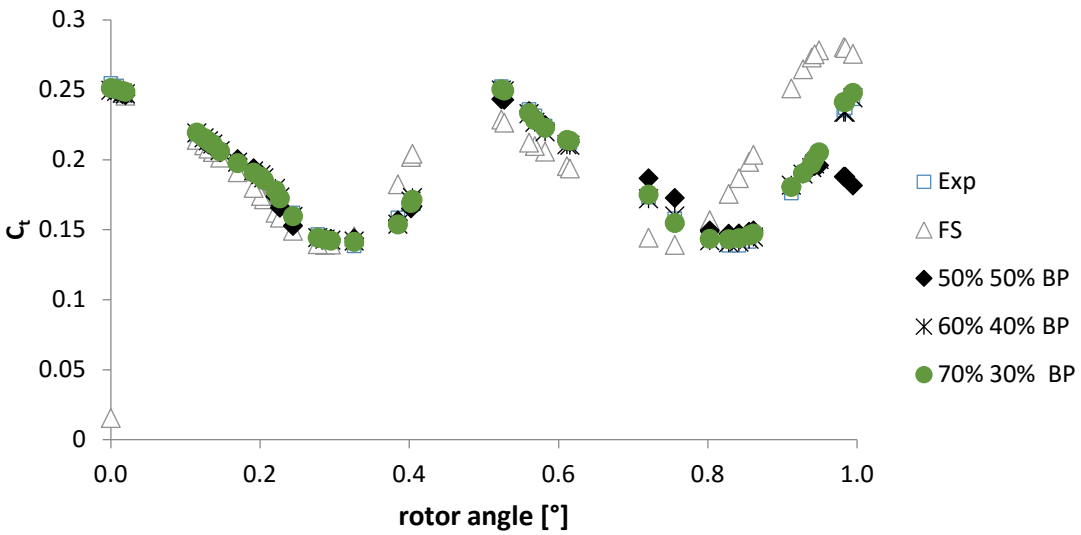

Figure 6.22: Comparison of all models with experimental data

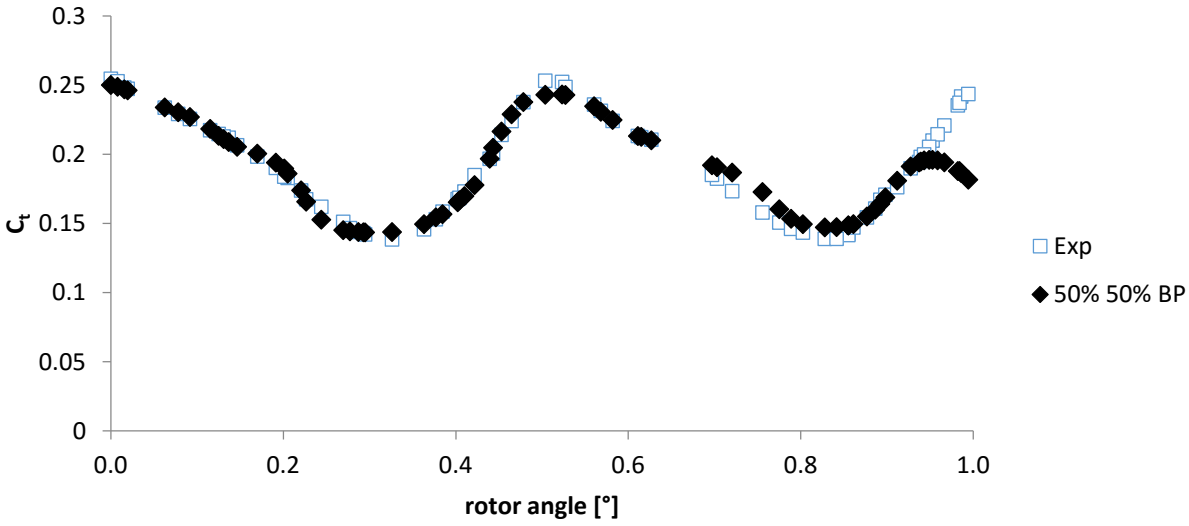

Figure 6.23: 50% simulated BPNN with experimental data

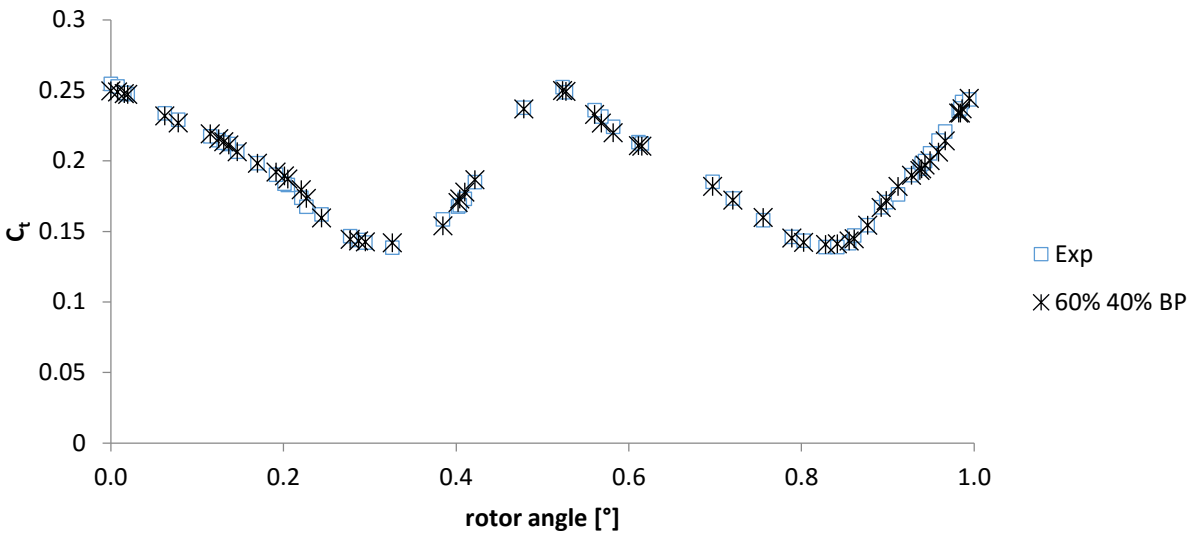

Figure 6.24: 40% simulated BPNN with experimental data

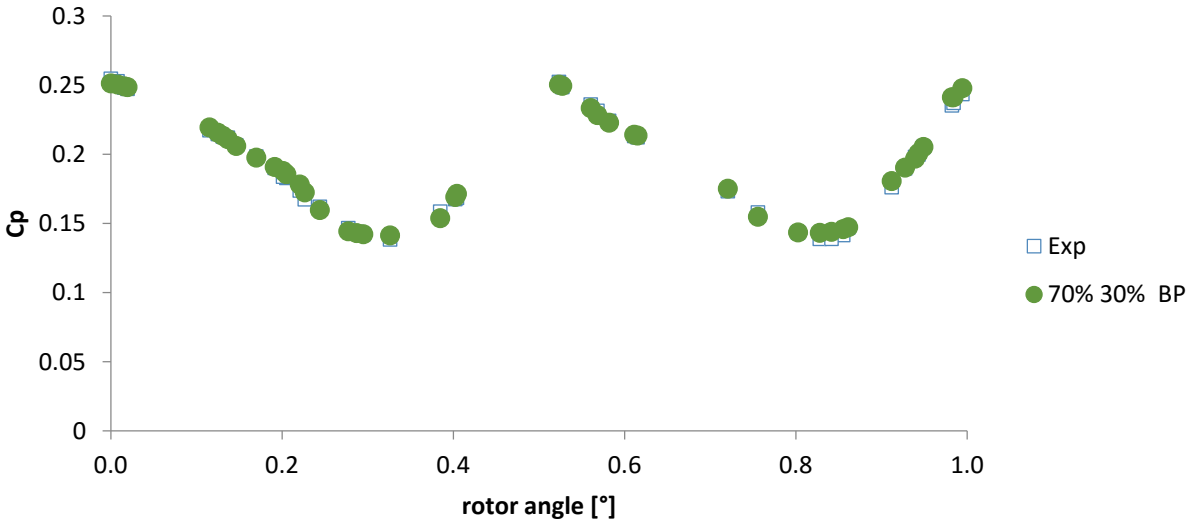

Figure 6.25: 30% BPNN with experimental data

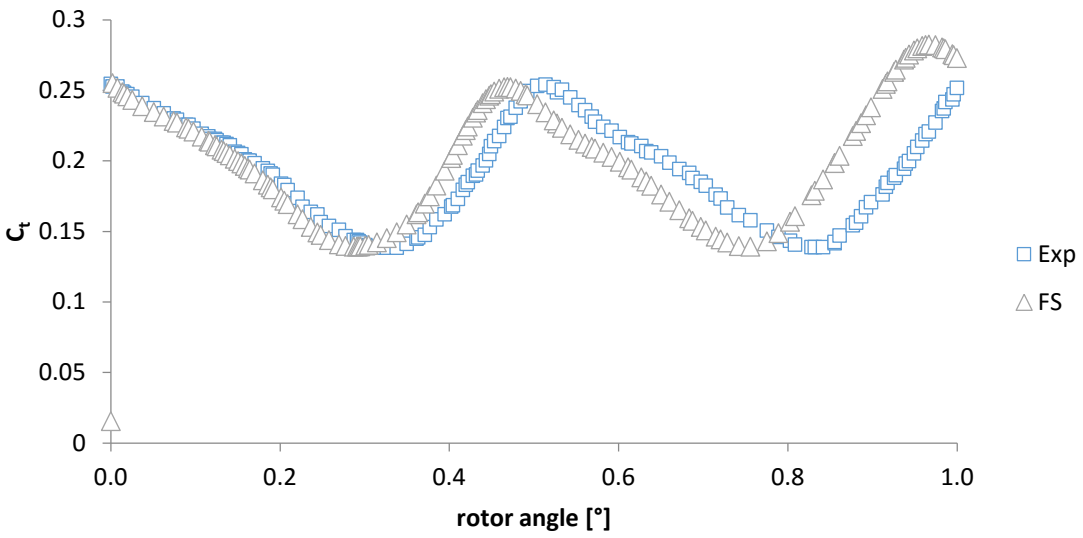

Figure 6.26: FS with experimental data

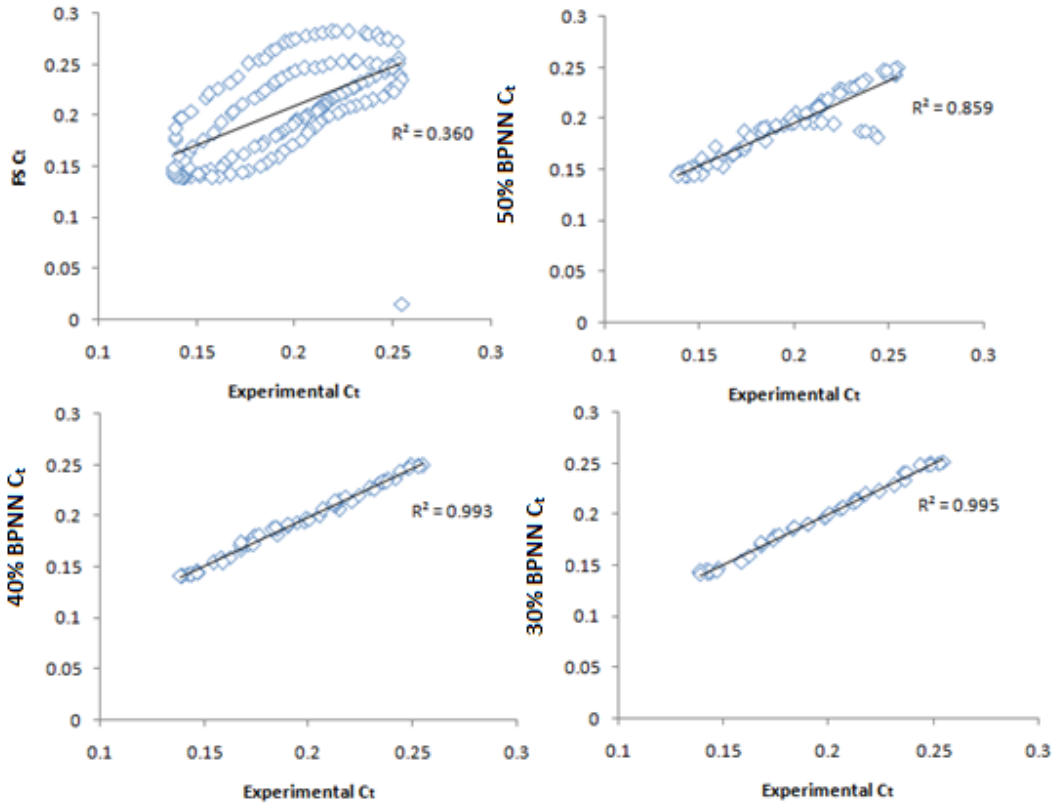

Figure 6.27: Simulated torque vs. experimental torque for all models

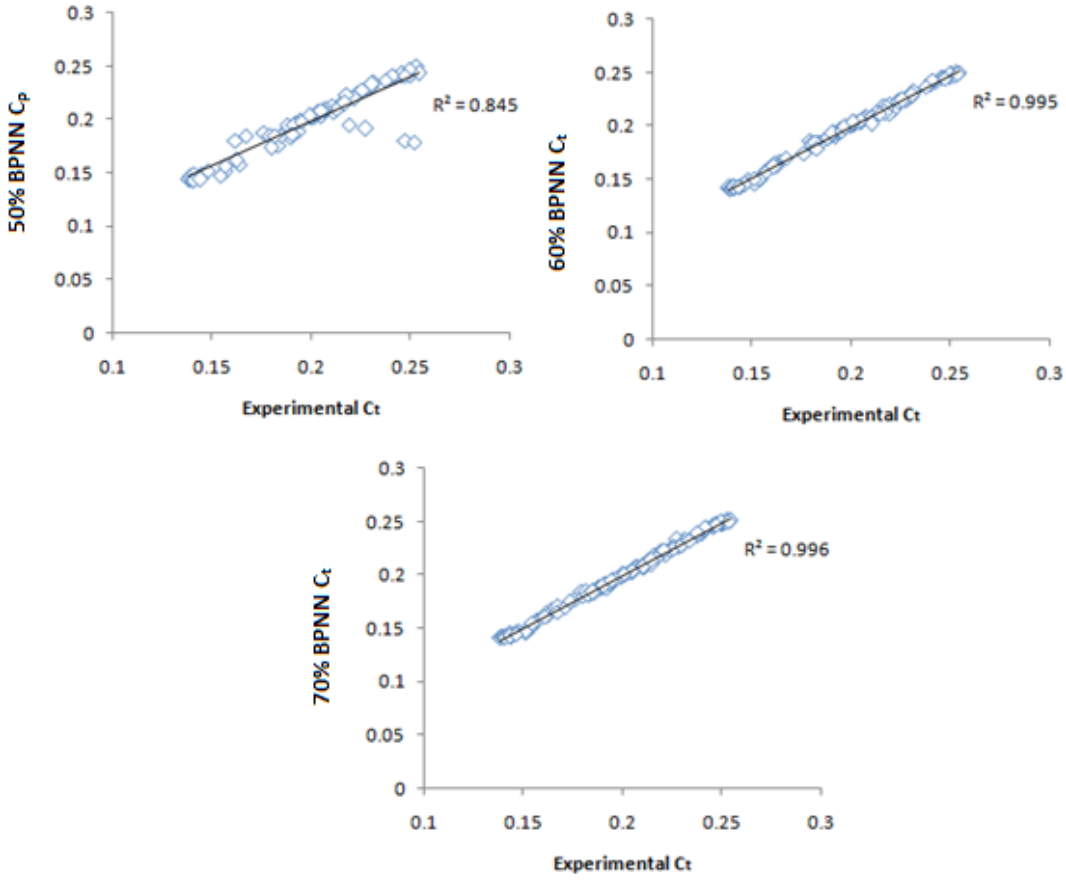

Figure 6.28: Trained torque vs. experimental torque for all models

6.3.3 C_p for three blades

Table 6.6 shows R^2 values of three groups of BPNN models. Additionally, graphical representations of the BPNN models and FS model for power coefficient of three blades helix wind turbine are shown in Figures 6.29 to 6.33. The R^2 value for simulated and trained BPNN models are also shown in Figure 6.34 and 6.35, respectively and for FS model is shown in Figure 6.33 as well. And they show very high values which attest to the statistical strength of the models for power coefficient of three blades helix wind turbine.

Table 6.6: Percentage division of experimental data for BPNN (C_p for three blade of helix Savonius turbine)

Group 1					
Training		50%			
Simulation		50%			
Epoch		8			
MSE		1.663E-6			
Equations of Training					
$Output = A\,Target + B$					
Training		R^2	**Test**		R^2
A	0.97	0.994	A	0.8	0.876
B	0.0081		B	0.056	
Validation		R^2	**All**		R^2
A	0.93	0.019	A	0.95	0.984
B	0.019		B	0.013	
Group 2					
Training		60%			
Simulation		40%			
Epoch		5			
MSE		1.627E-6			
Equations of Training					
$Output = A\,Target + B$					
Training		R^2	**Test**		R^2
A	0.94	0.984	A	0.83	0.98
B	0.018		B	0.05	
Validation		R^2	**All**		R^2
A	1	0.96	A	0.94	0.98
B	0.004		B	0.017	
Group 3					
Training		70%			
Simulation		30%			
Epoch		10			
MSE		1.455E-6			
Equations of Training					
$Output = A\,Target + B$					
Training		R^2	**Test**		R^2
A	0.96	0.984	A	0.89	0.986
B	0.0099		B	0.03	
Validation		R^2	**All**		R^2
A	0.97	0.986	A	0.95	0.982
B	0.0075		B	0.014	

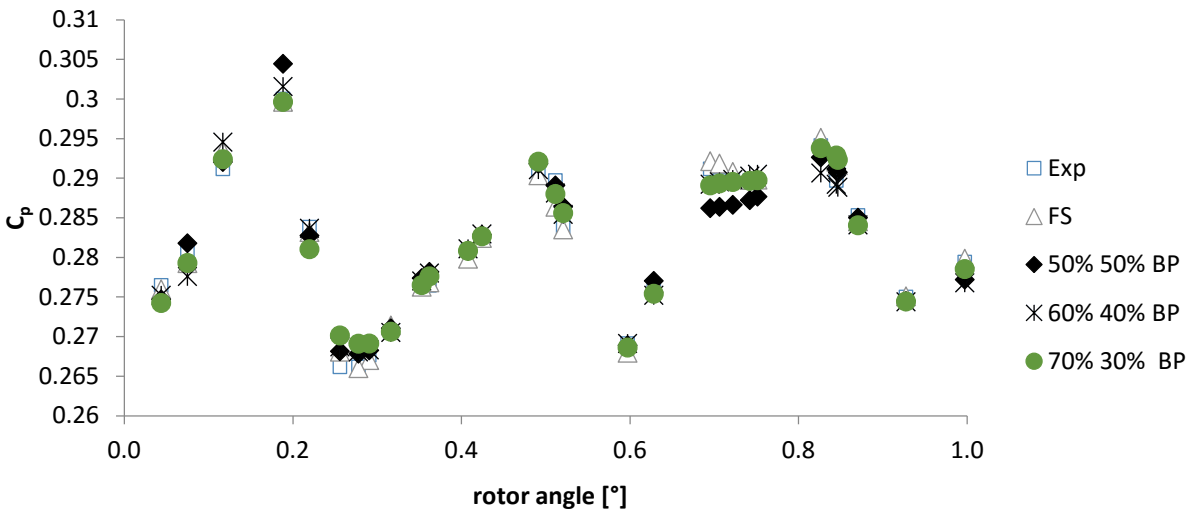

Figure 6.29: Comparison of all models with experimental data

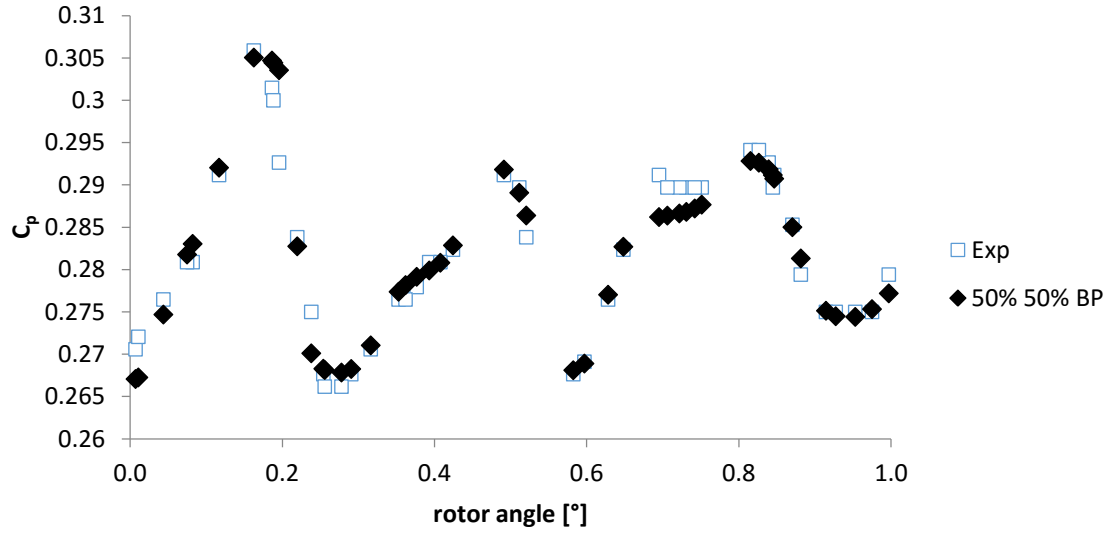

Figure 6.30: Comparison of 50% simulated BPNN with experimental data

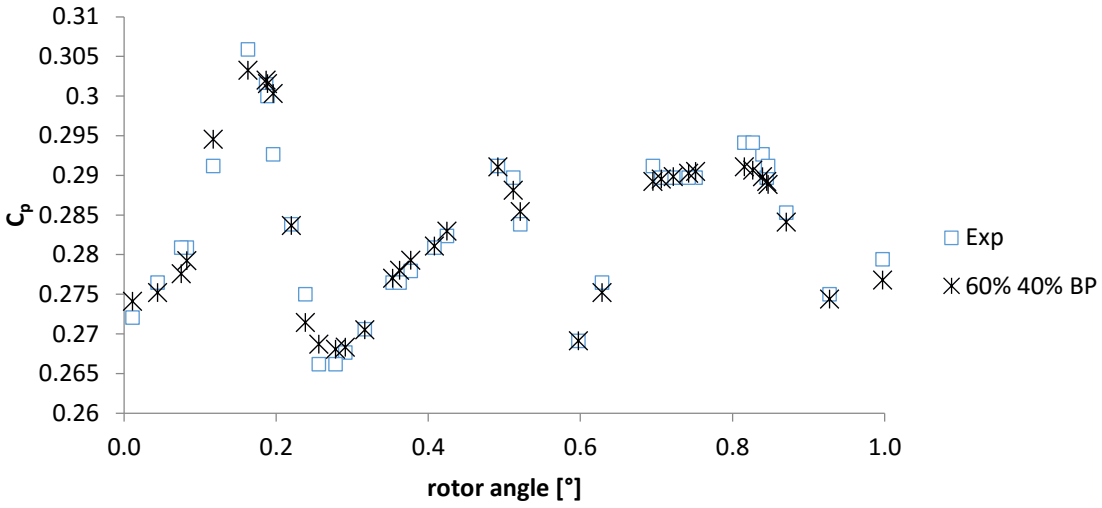

Figure 6.31: Comparison of 40% simulated BPNN with experimental data

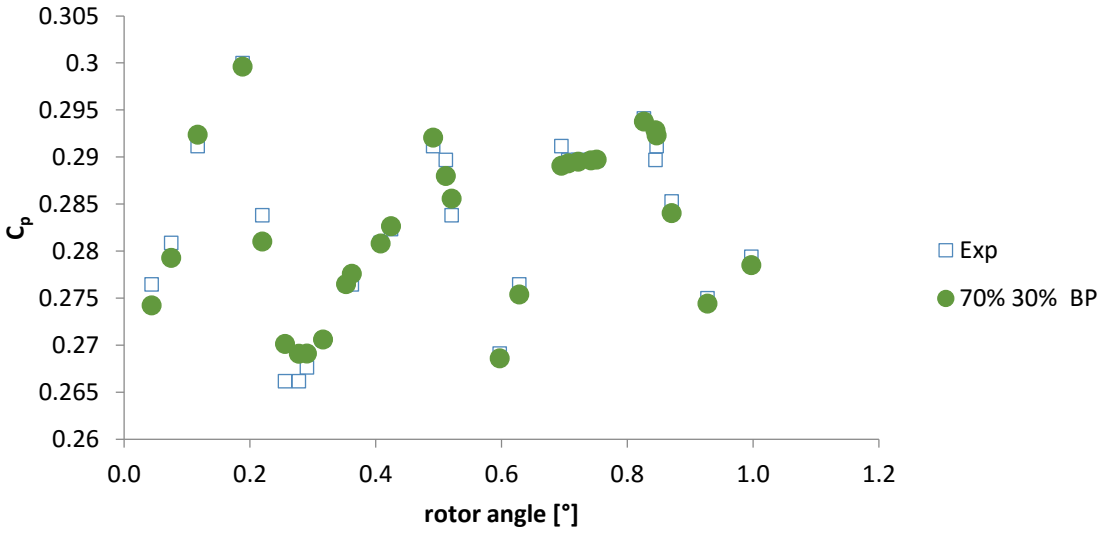

Figure 6.32: Comparison of 30% simulated BPNN with experimental data

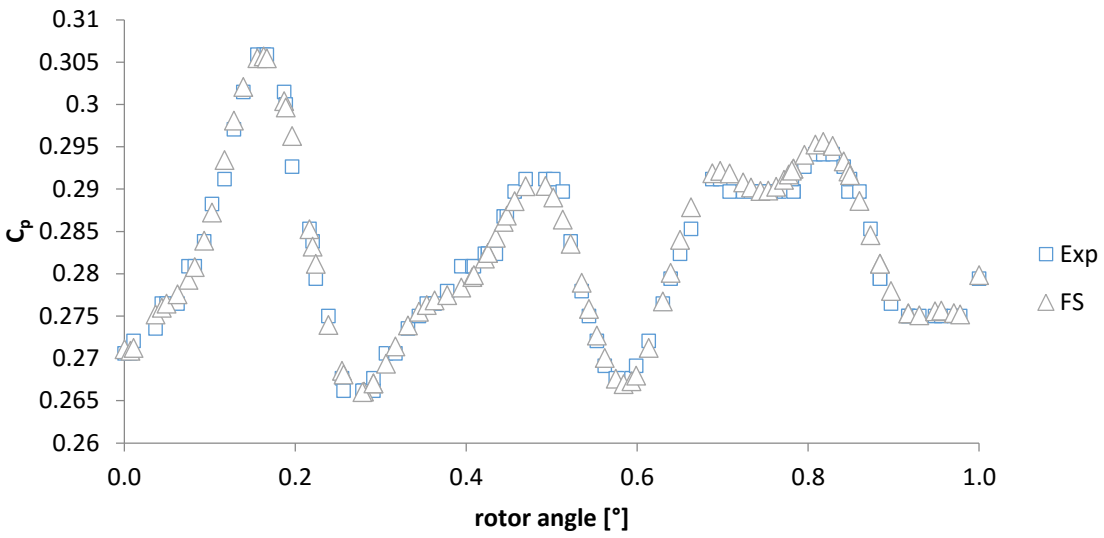

Figure 6.33: Comparison of FS with experimental data

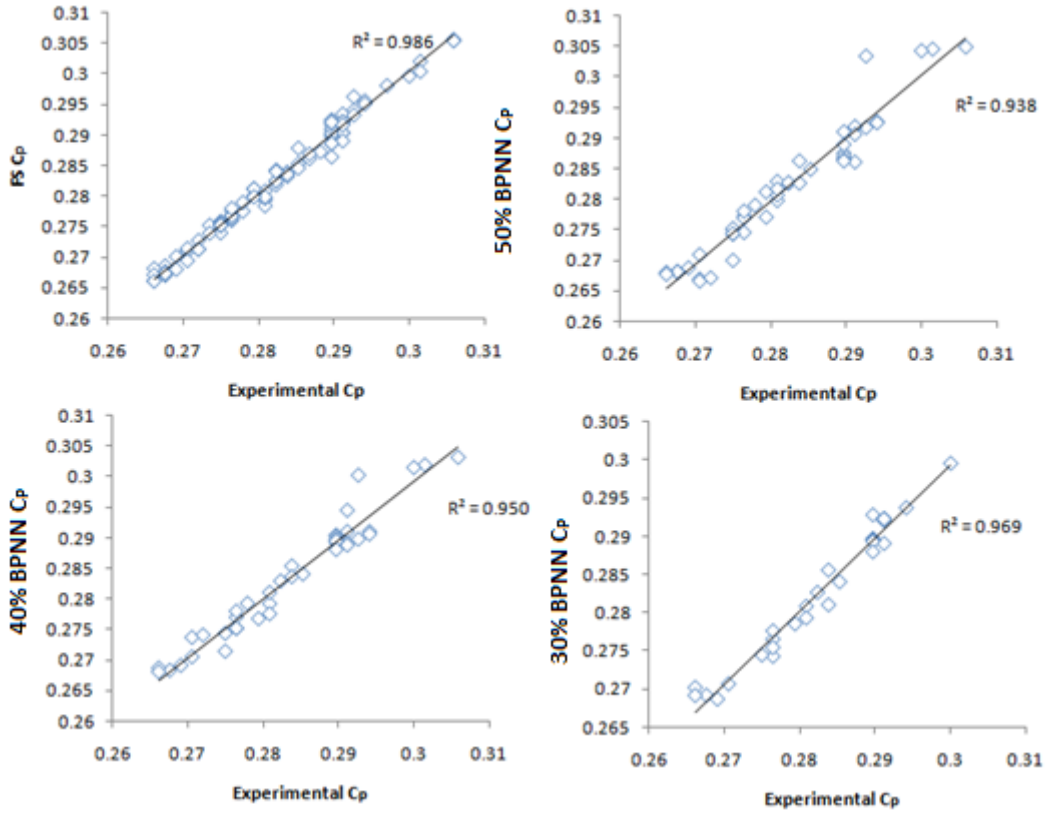

Figure 6.34: Simulated torque vs. experimental torque for all models

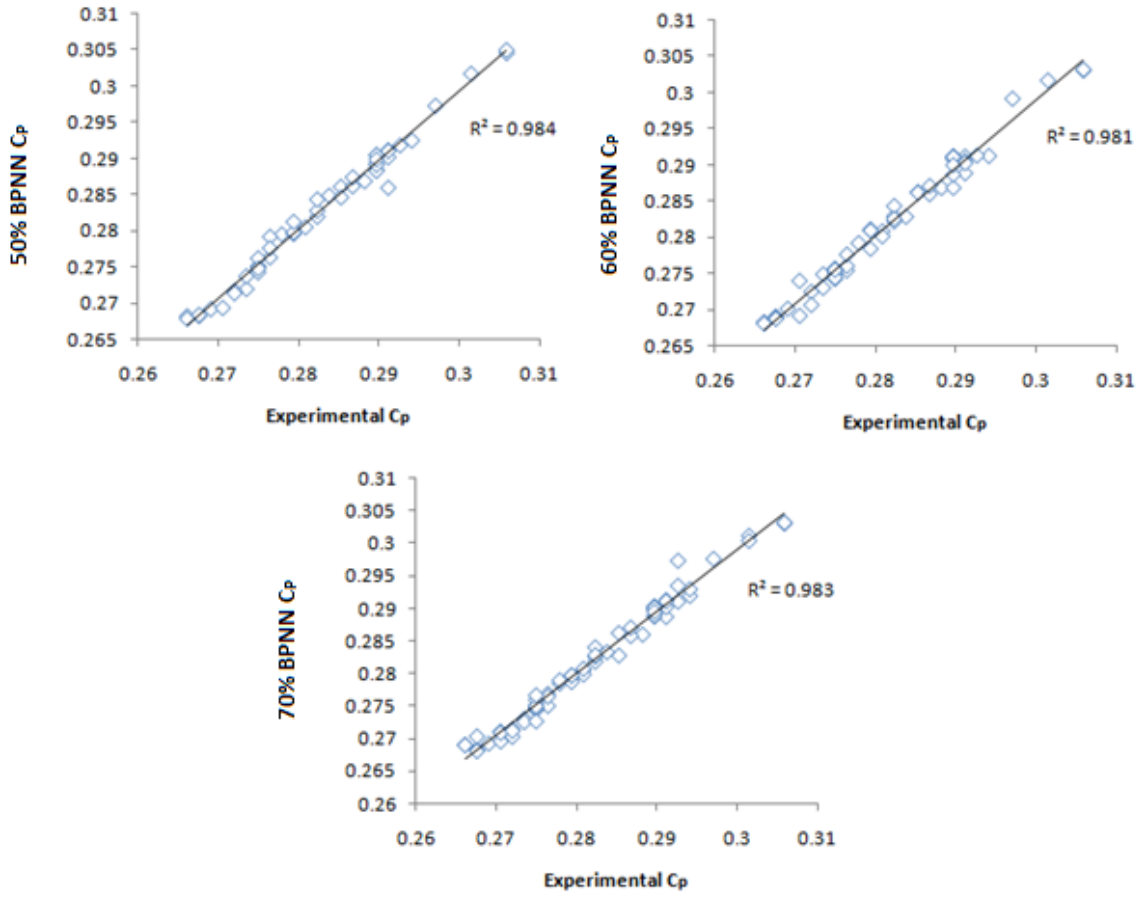

Figure 6.35: Trained torque vs. experimental torque for all models

6.3.4 C_t for three blades

Similarly, the comparison between the predicted results and experimental result for four models are shown in Figure 6.36 to 6.40. Table 6.7 and Figures 6.41 and 6.42 show the R^2 values for BPNN models and FS model. It observed that group 3 and FS are the best models used to estimate the C_t of three blades wind turbine.

Table 6.7: Percentage division of experimental data for BPNN (C_t for three blade of helix Savonius turbine)

Group 1					
Training		50%			
Simulation		50%			
Epoch		11			
MSE		5.548E-7			
Equations of Training					
$Output = A\,Target + B$					
Training		R^2	**Test**		R^2
A	0.95	0.988	A	0.85	0.603
B	0.0085		B	0.026	
Validation		R^2	**All**		R^2
A	1	0.972	A	0.97	0.923
B	0.0036		B	0.005	
Group 2					
Training		60%			
Simulation		40%			
Epoch		6			
MSE		2.414E-6			
Equations of Training					
$Output = A\,Target + B$					
Training		R^2	**Test**		R^2
A	0.9	0.95	A	0.024	0.986
B	0.017		B	0.85	
Validation		R^2	**All**		R^2
A	0.8	0.925	A	0.88	0.954
B	0.032		B	0.02	
Group 3					
Training		70%			
Simulation		30%			
Epoch		40			
MSE		4.838E-7			
Equations of Training					
$Output = A\,Target + B$					
Training		R^2	**Test**		R^2
A	0.98	0.986	A	0.89	0.958
B	0.0033		B	0.018	
Validation		R^2	**All**		R^2
A	0.97	0.99	A	0.97	0.986
B	0.0048		B	0.0044	

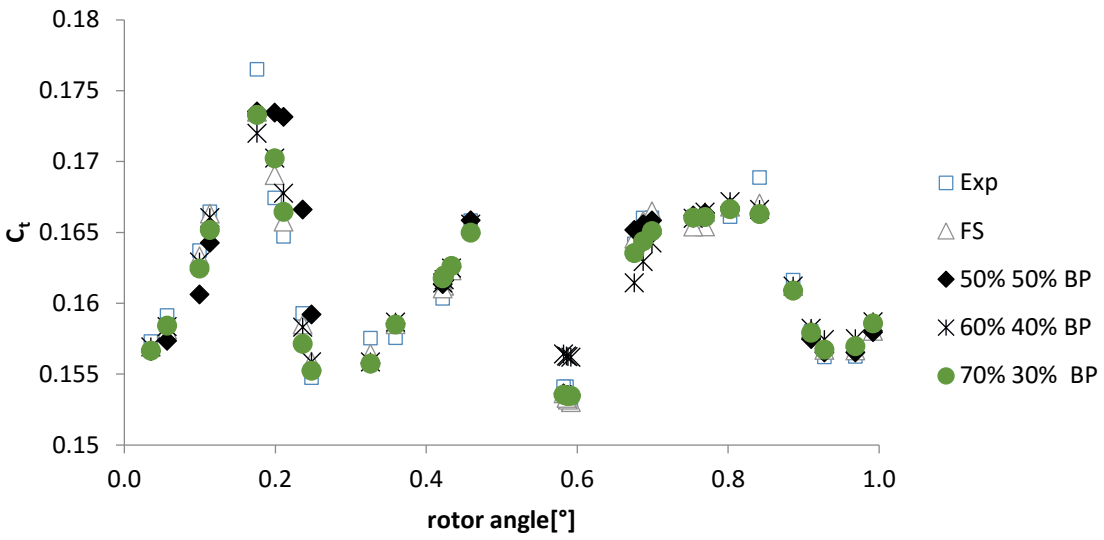

Figure 6.36: Comparison of all models with experimental data

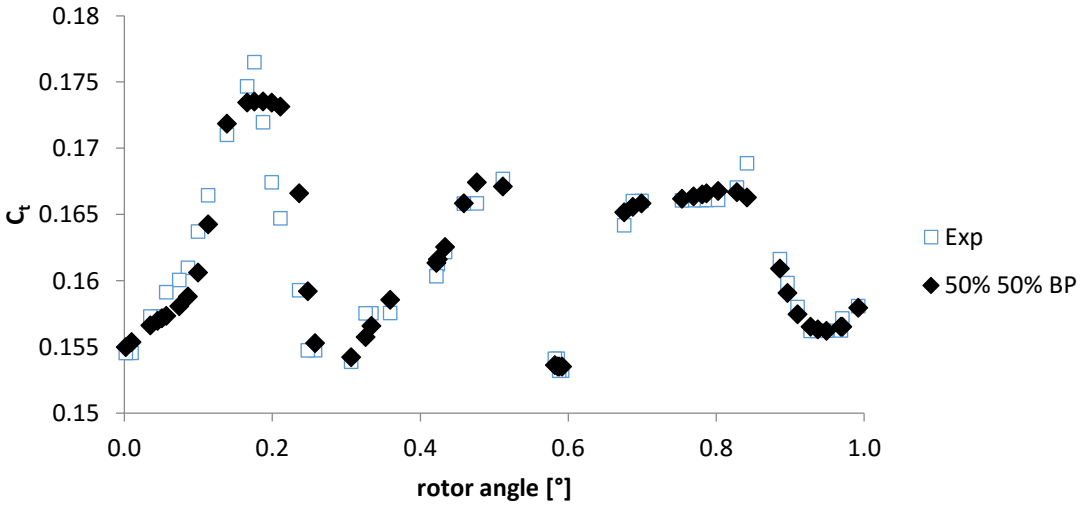

Figure 6.37: 50% simulated BPNN with experimental data

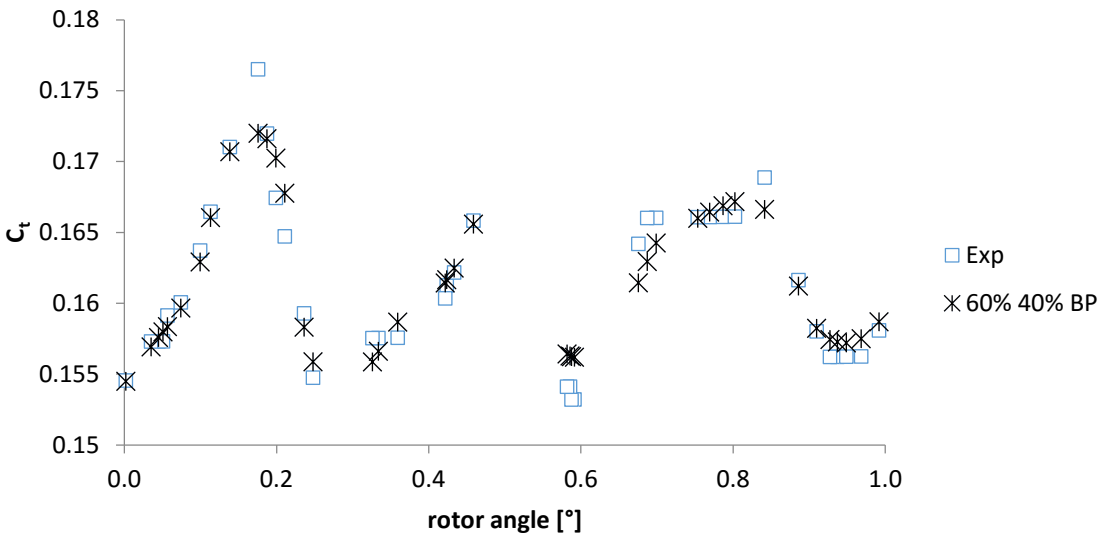

Figure 6.38: 40% simulated BPNN with experimental data

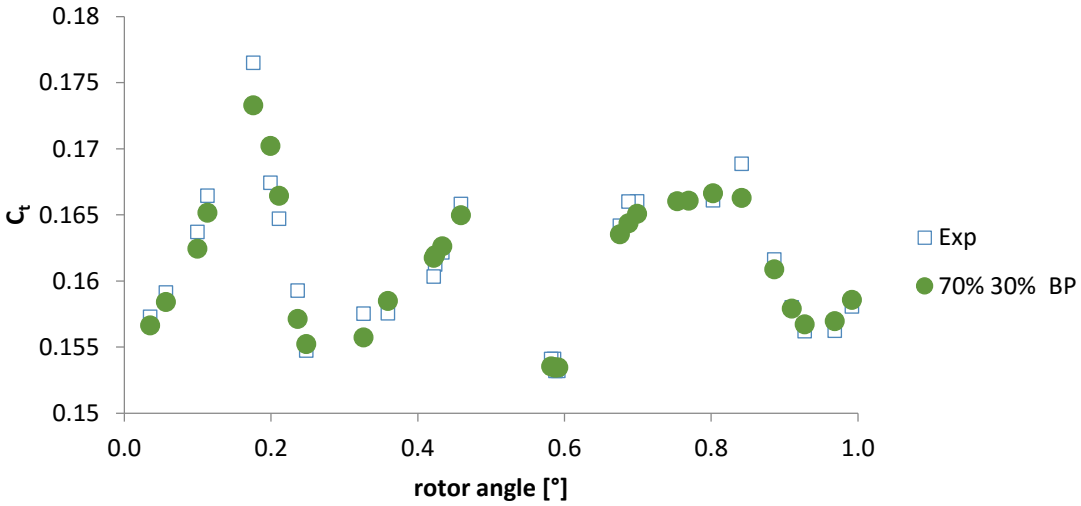

Figure 6.39: 30% BPNN simulated with experimental data

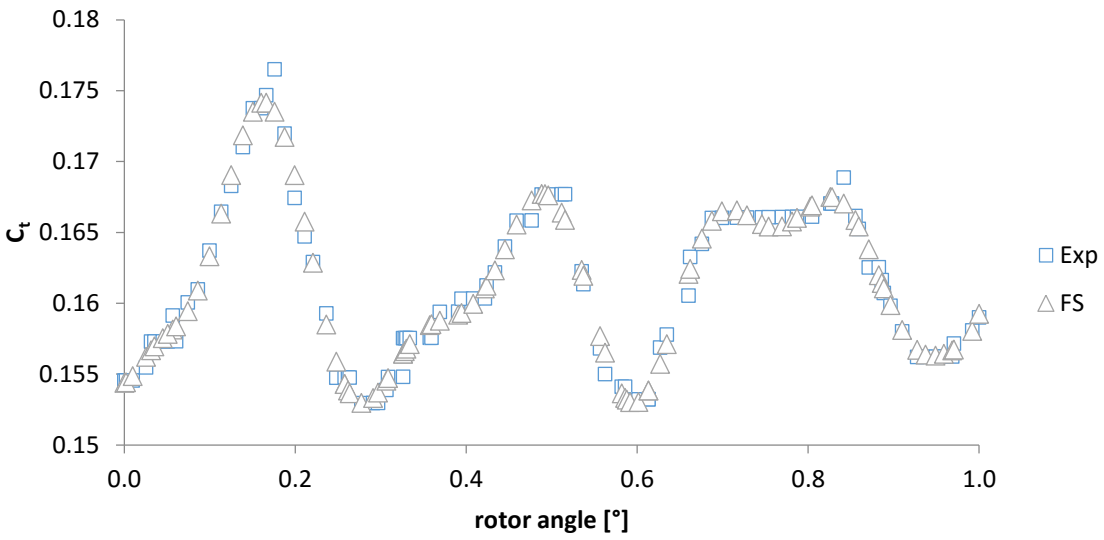

Figure 6.40: Comparison of FS with experimental data

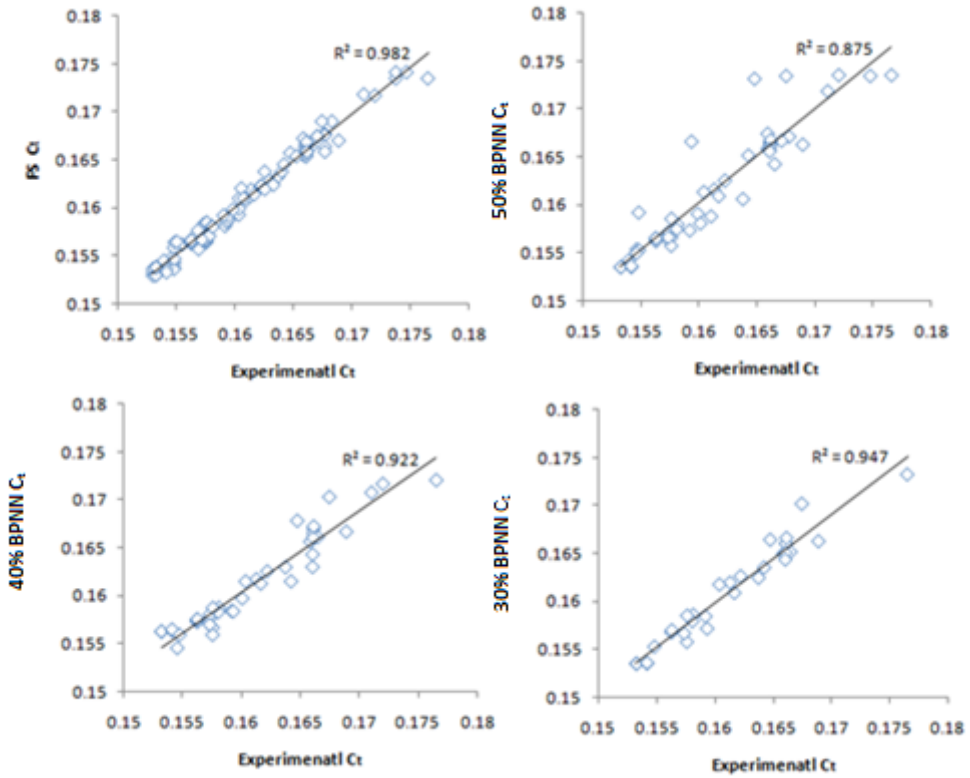

Figure 6.41: Simulated torque vs. experimental torque for all models

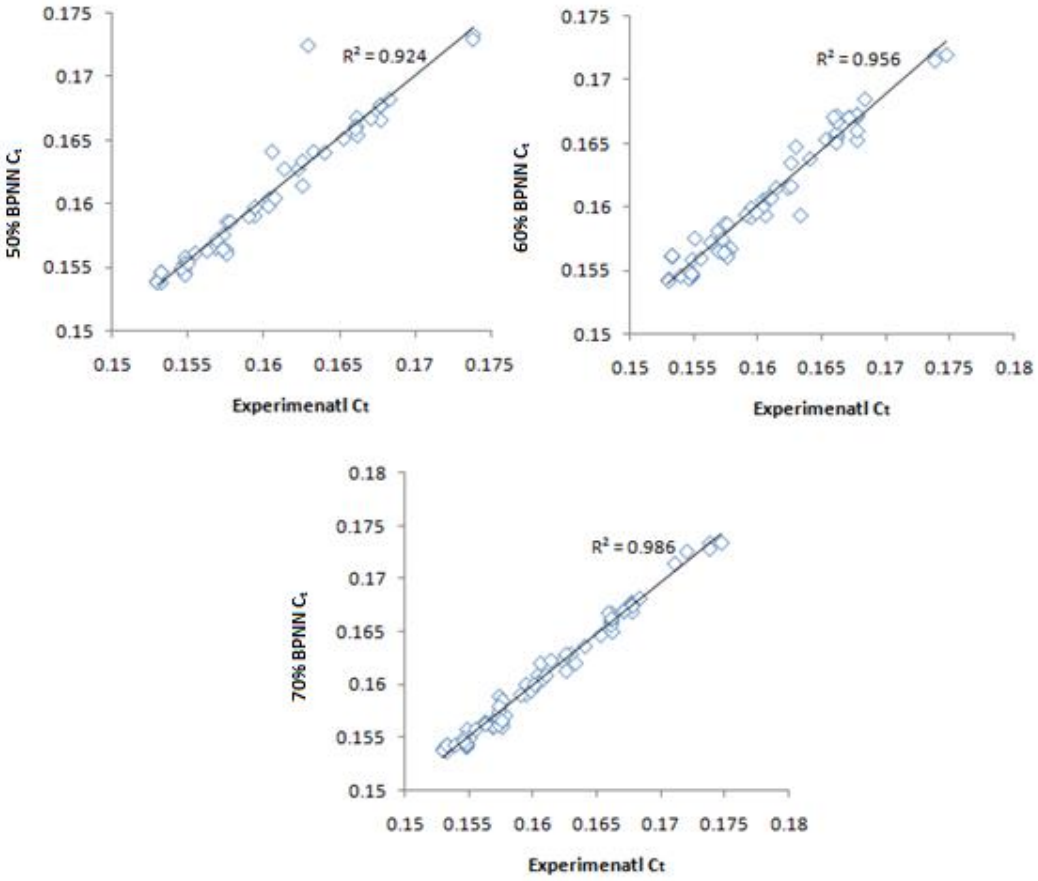

Figure 6.42: Trained torque vs. experimental torque for all models

6.4 Published Experimental Data (Sargolzaei and Kianifar, 2009)

6.4.1 Rotor I

Figures 6.43 to 6.47 depicts the output torque against the experimental torque for the four models. Table 6.8 and Figures 6.48 and 6.49 show the R^2 values of the models, it can be seen that the highest R^2 value is for group 3 (BPNN model) while the lowest R^2 value is 0.578 for FS model.

Table 6.8: Percentage division of experimental data for BPNN (Rotor I)

Group 1					
Training		50%			
Simulation		50%			
Epoch		9			
MSE		6.823E-6			
Equations of Training					
$Output = A\,Target + B$					
Training		R^2	**Test**		R^2
A	1	1	A	1.3	1
B	1.6E-7		B	0.032	
Validation		R^2	**All**		R^2
A	0.62	1	A	0.97	0.992
B	0.023		B	0.0018	
Group 2					
Training		60%			
Simulation		40%			
Epoch		4			
MSE		4.123E-7			
Equations of Training					
$Output = A\,Target + B$					
Training		R^2	**Test**		R^2
A	0.96	0.984	A	0.3	1
B	0.0025		B	0.066	
Validation		R^2	**All**		R^2
A	0.97	1	A	0.98	0.986
B	0.001		B	0.00072	
Group 3					
Training		70%			
Simulation		30%			
Epoch		10			
MSE		1.75E-6			
Equations of Training					
$Output = A\,Target + B$					
Training		R^2	**Test**		R^2
A	1	1	A	1	1
B	7.9E-5		B	0.0077	
Validation		R^2	**All**		R^2
A	1.2	0.99	A	1	0.991
B	0.0086		B	0.0016	

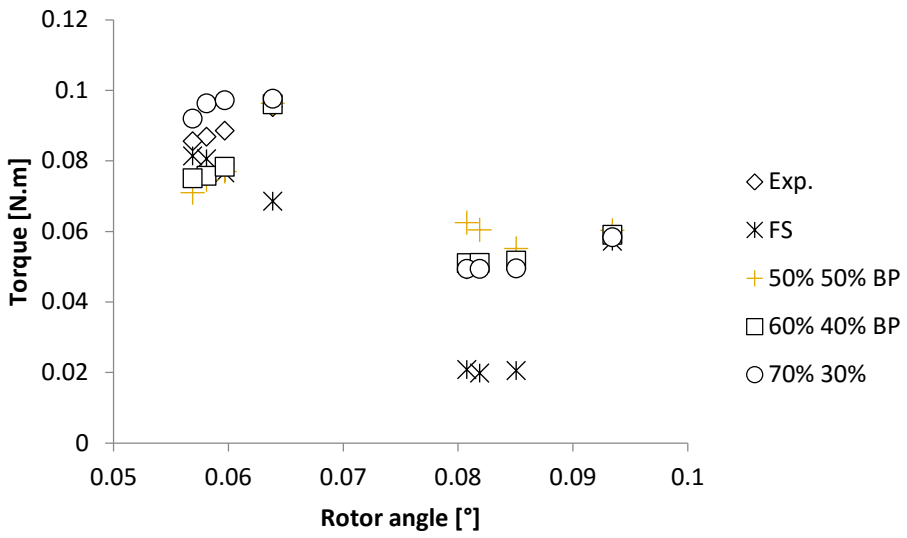

Figure 6.43: Comparison of all models with experimental data

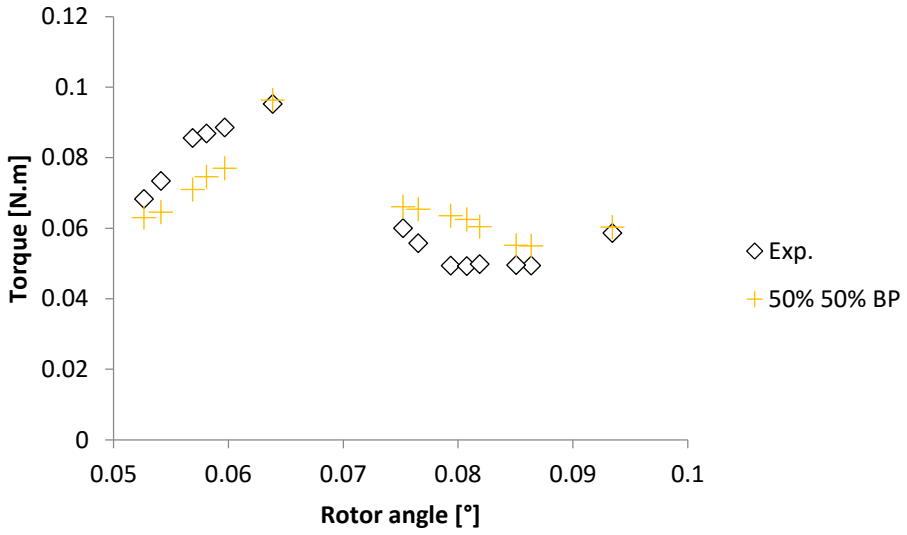

Figure 6.44: Comparison of 50% simulated BPNN with experimental data

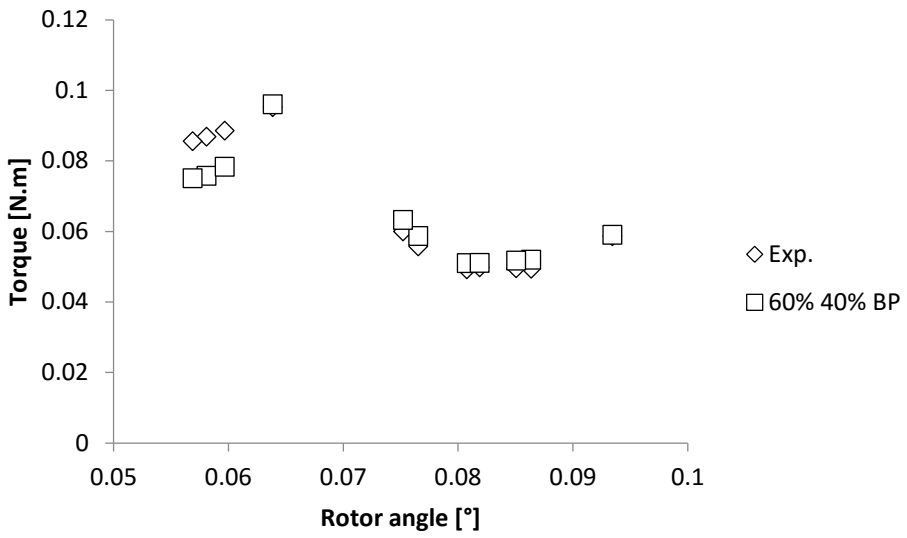

Figure 6.45: Comparison of 40% simulated BPNN with experimental data

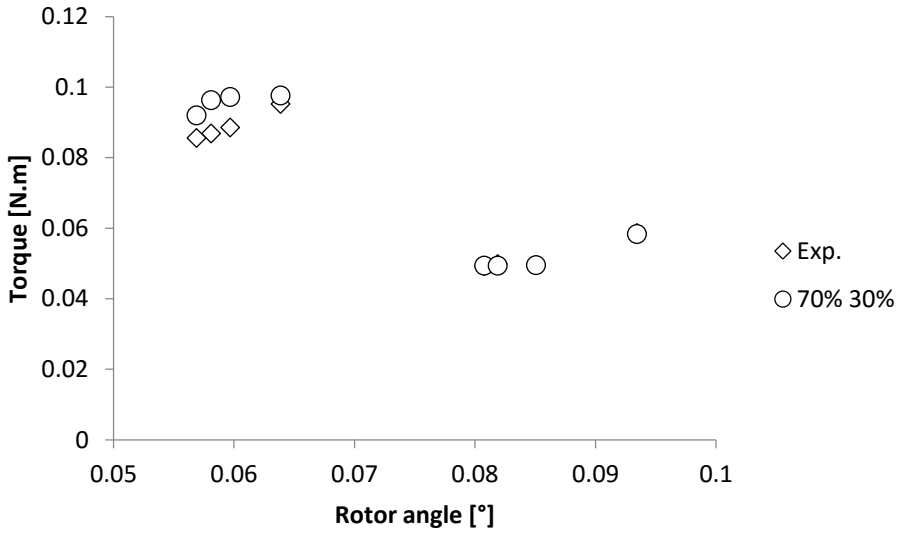

Figure 6.46: Comparison of 30% simulated BPNN with experimental data

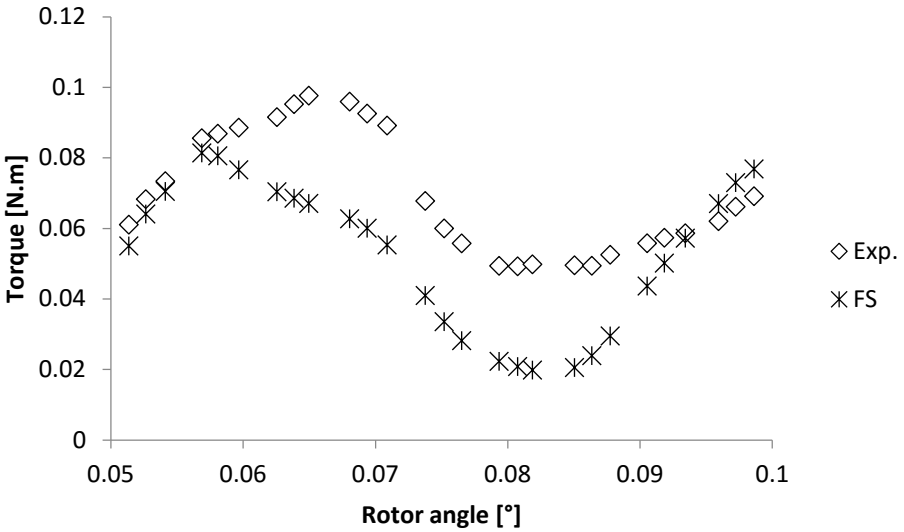

Figure 6.47: Comparison of FS with experimental data

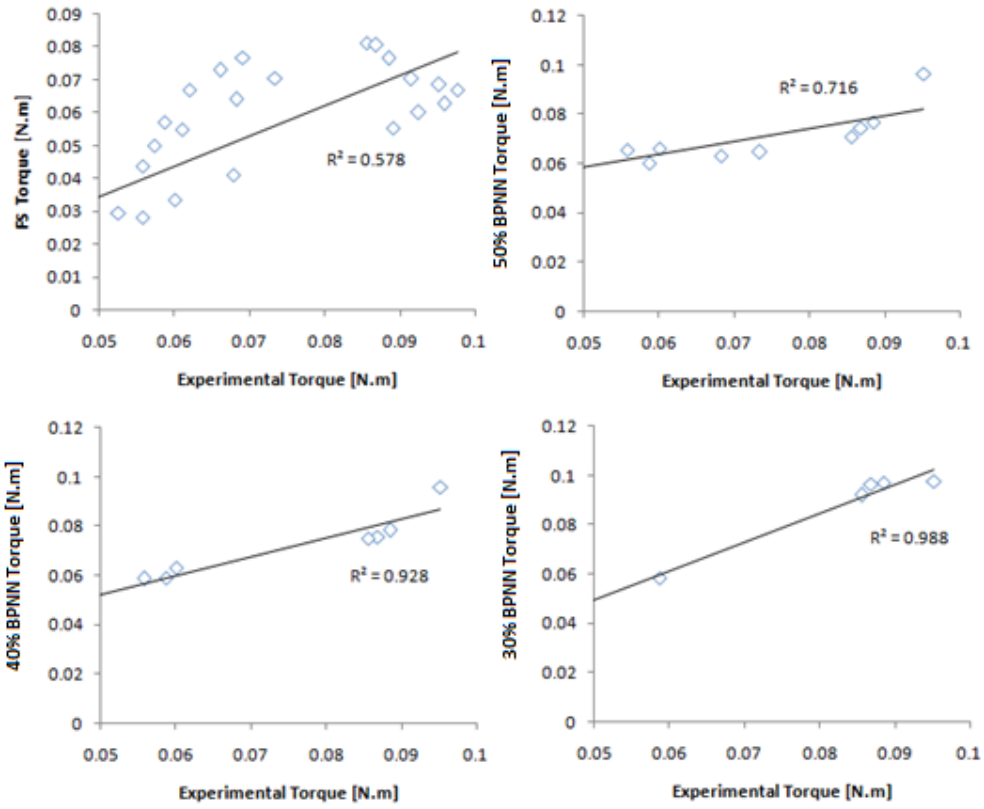

Figure 6.48: Simulated torque vs. experimental torque for all models

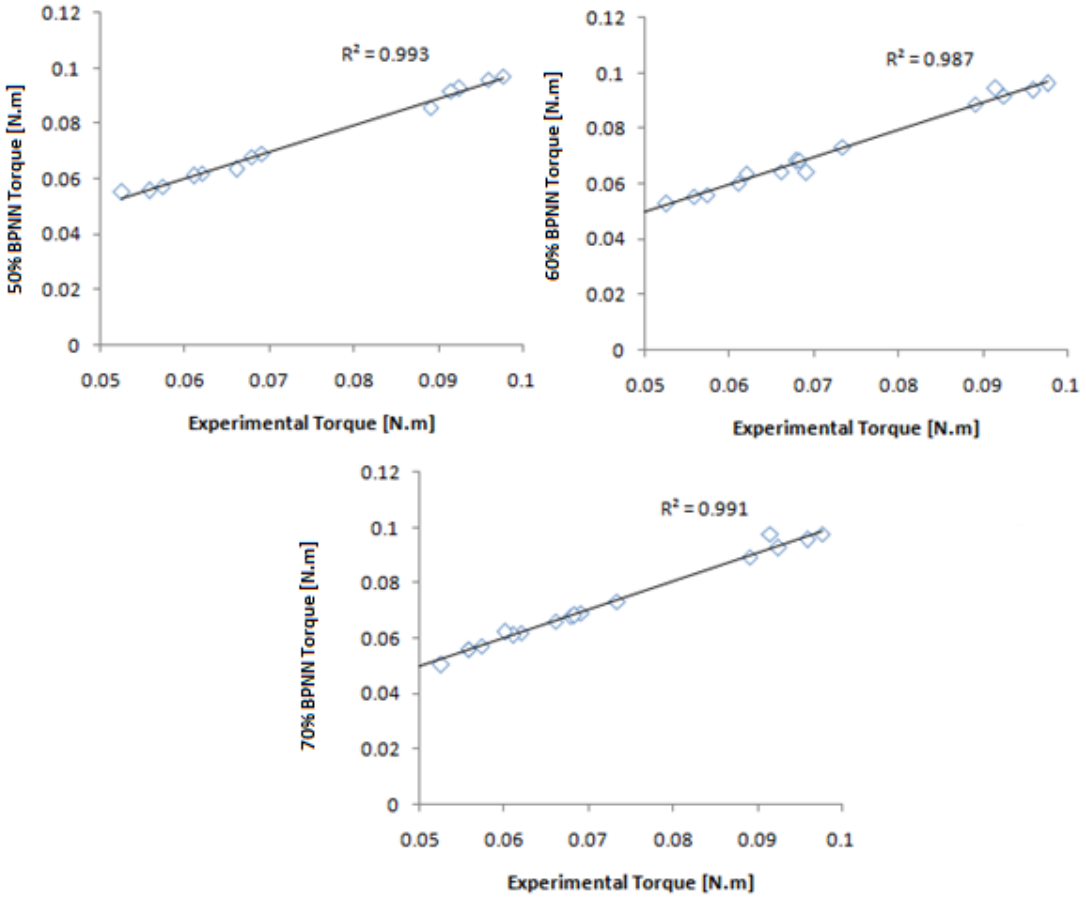

Figure 6.49: Trained torque vs. experimental torque for all models

6.4.2 Rotor II

Similarly, the comparison between the models results with experimental results of this rotor and the statistical strength of the models can be seen in Figure 6.50 to 6.54. In Figures 6.56, 6.57 and Table 6.9 (Training results), it was observed that the linear models (FS and group 3 BPNN) are acceptable since *R-squared* value is about 0.98.

Table 6.9: Percentage division of experimental data for BPNN (Rotor II)

Group 1					
Training		50%			
Simulation		50%			
Epoch		5			
MSE		1.059E-5			
Equations of Training					
$Output = A\,Target + B$					
Training		R^2	**Test**		R^2
A	0.95	0.998	A	0.3	1
B	0.0041		B	0.04	
Validation		R^2	**All**		R^2
A	1.1	1	A	0.9	0.974
B	0.014		B	0.00079	
Group 2					
Training		60%			
Simulation		40%			
Epoch		3			
MSE		9.134E-6			
Equations of Training					
$Output = A\,Target + B$					
Training		R^2	**Test**		R^2
A	0.85	0.913	A	4	1
B	0.01		B	3.8	
Validation		R^2	**All**		R^2
A	1	1	A	0.71	0.848
B	0.0018		B	0.02	
Group 3					
Training		70%			
Simulation		30%			
Epoch		5			
MSE		4.384E-5			
Equations of Training					
$Output = A\,Target + B$					
Training		R^2	**Test**		R^2
A	0.98	0.998	A	0.7	0.532
B	0.0015		B	0.017	
Validation		R^2	**All**		R^2
A	1	0.906	A	0.98	0.95
B	0.0083		B	0.0008	

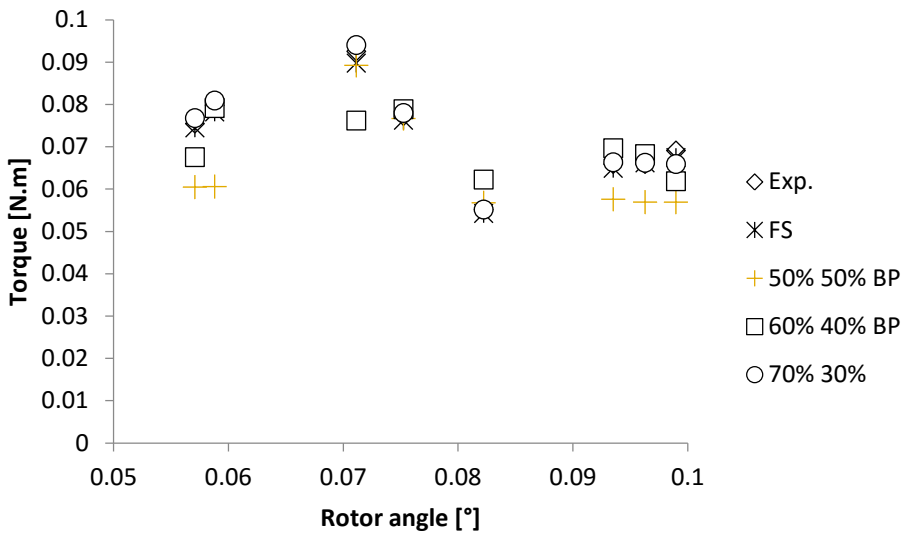

Figure 6.50: Comparison of all models with experimental data

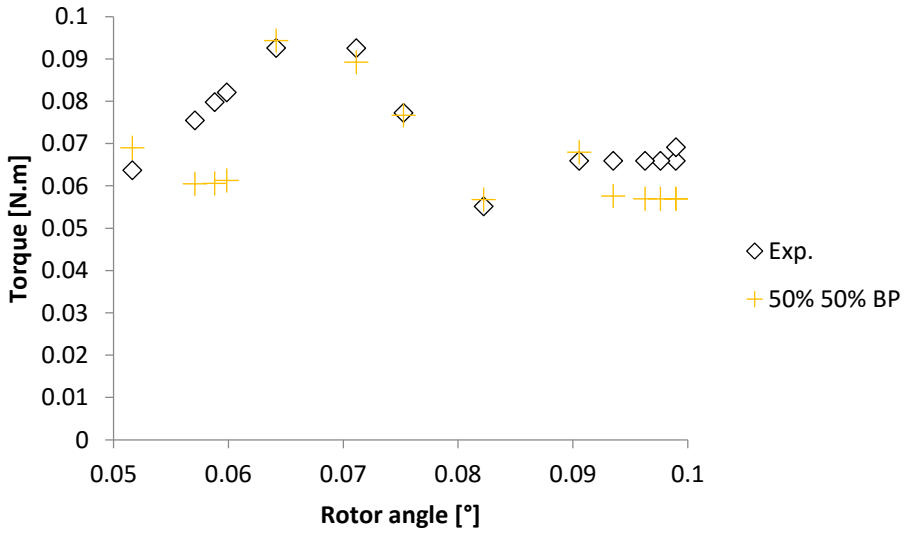

Figure 6.51: Comparison of 50% simulated BPNN with experimental data

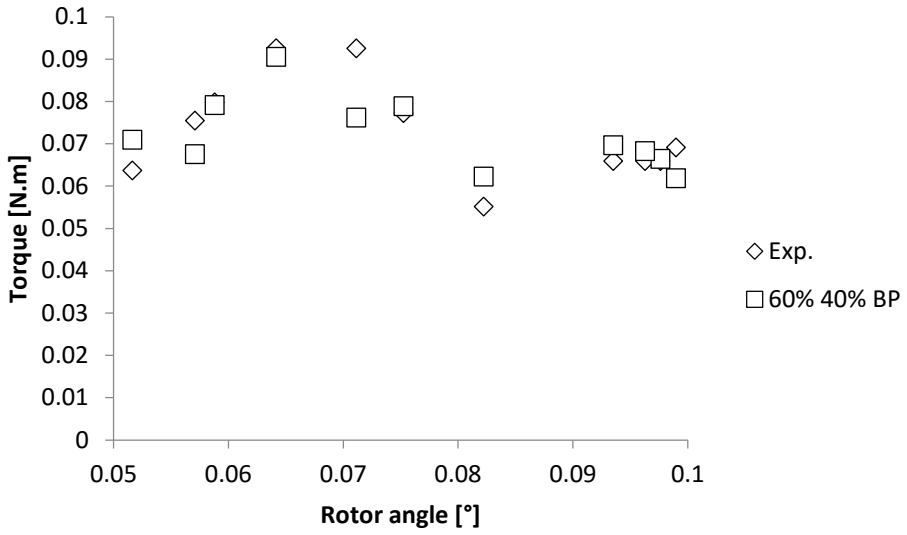

Figure 6.52: Comparison of 40% simulated BPNN with experimental data

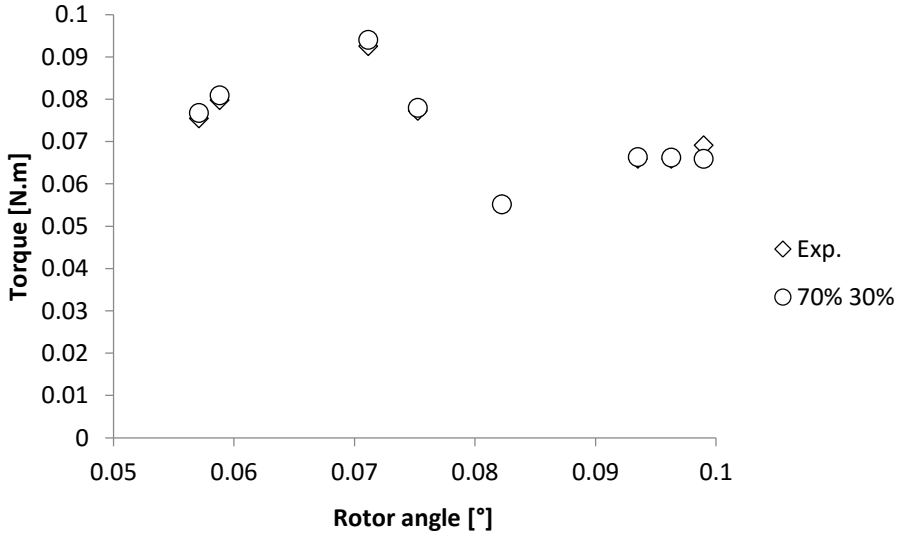

Figure 6.53: Comparison of 30% simulated BPNN with experimental data

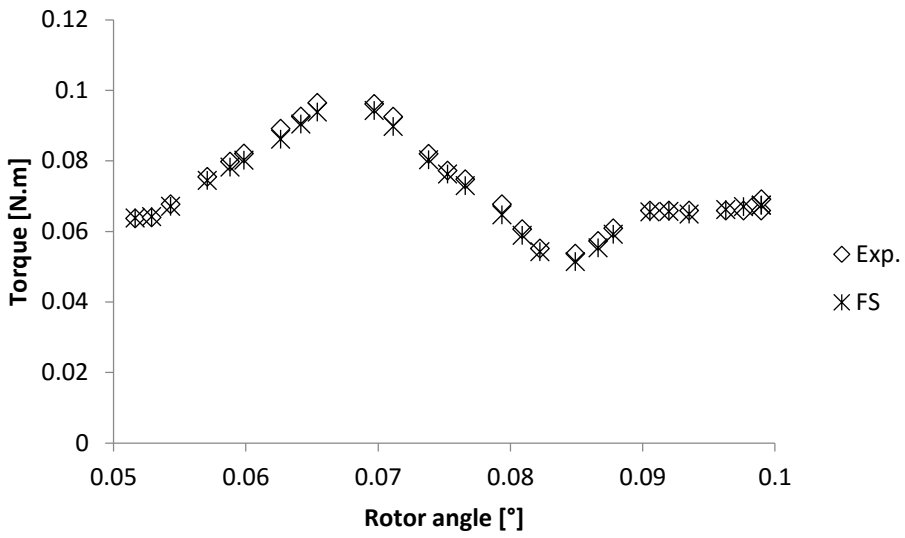

Figure 6.54: Comparison of FS with experimental data

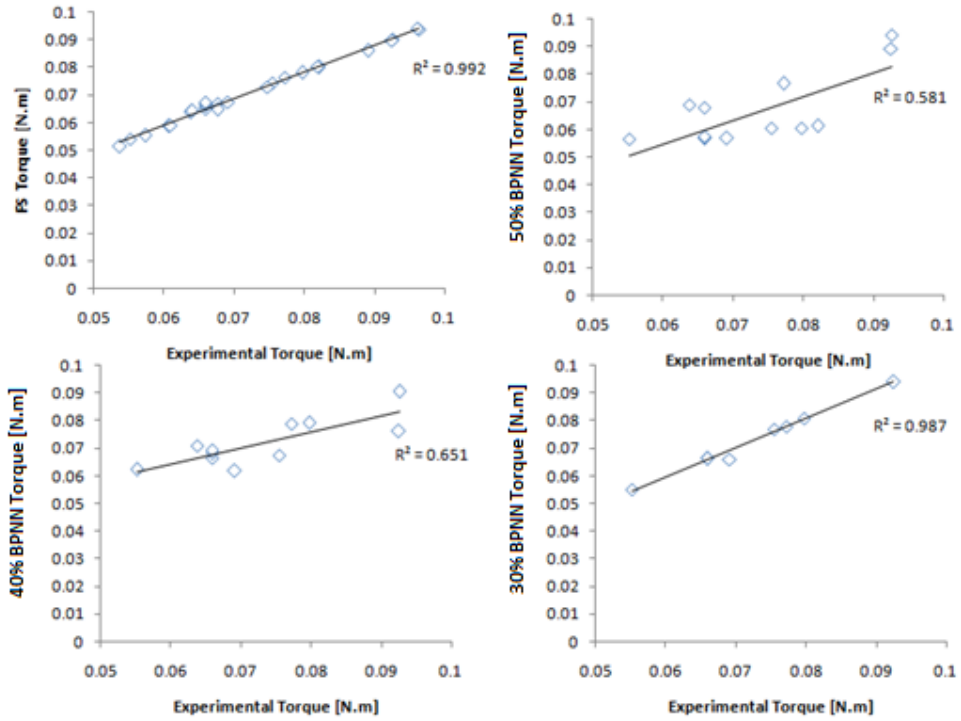

Figure 6.55: Simulated torque vs. experimental torque for all models

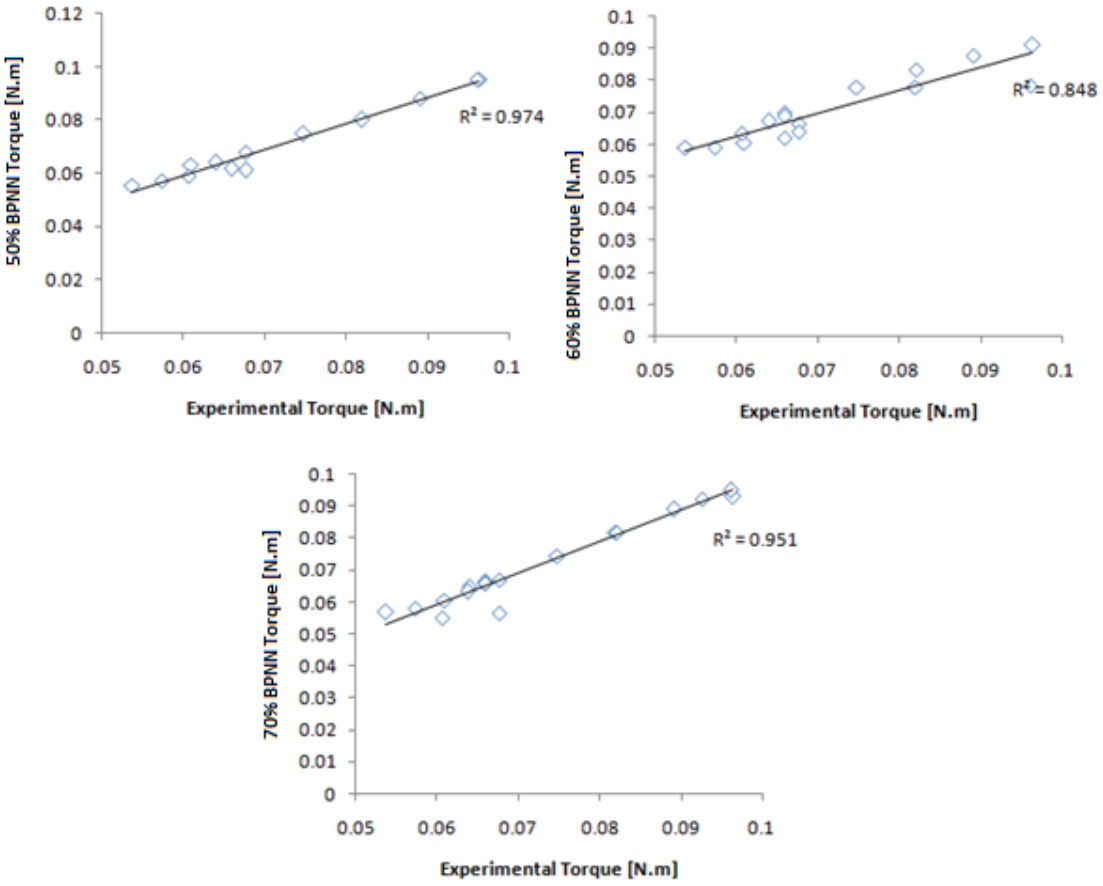

Figure 6.56: Trained torque vs. experimental torque for all models

6.4.3 Rotor III

The *mean squared error* and empirical equations of trained results for 3 groups of BPNN for torque of rotor III are shown in Table 6.10. Also, an *R-squared* value of trained results for 3 groups of BPNN is shown in Figure 6.60. A plot of the predicted and the measured torque is represented in Figures 6.57 to 6.61. As can be seen that the best empirical models for estimating the torque of rotor III from experimental results of torque of rotor III are FS and group 3 BPNN.

Table 6.10: Percentage division of experimental data for BPNN (Rotor III)

Group 1					
Training		50%			
Simulation		50%			
Epoch		11			
MSE		3.549E-05			
Equations of Training					
$Output = A\,Target + B$					
Training		R^2	**Test**		R^2
A	1	0.998	A	2.8	1
B	0.00019		B	0.23	
Validation		R^2	**All**		R^2
A	1.5	1	A	0.95	0.876
B	0.045		B	0.0035	
Group 2					
Training		60%			
Simulation		40%			
Epoch		11			
MSE		3.27E-07			
Equations of Training					
$Output = A\,Target + B$					
Training		R^2	**Test**		R^2
A	1	0.998	A	1	1
B	0.00013		B	0.0043	
Validation		R^2	**All**		R^2
A	1	1	A	1	0.996
B	0.0039		B	7.2E-05	
Group 3					
Training		70%			
Simulation		30%			
Epoch		8			
MSE		5.024E-07			
Equations of Training					
$Output = A\,Target + B$					
Training		R^2	**Test**		R^2
A	1	1	A	0.96	0.998
B	5.6E-05		B	0.028	
Validation		R^2	**All**		R^2
A	0.99	0.998	A	0.98	0.987
B	0.0011		B	0.0017	

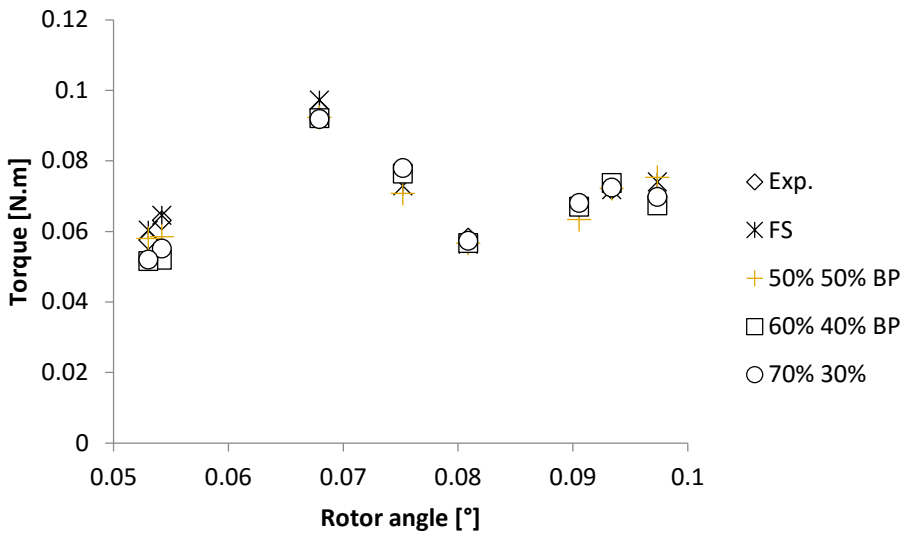

Figure 6.57: Comparison of all models with experimental data

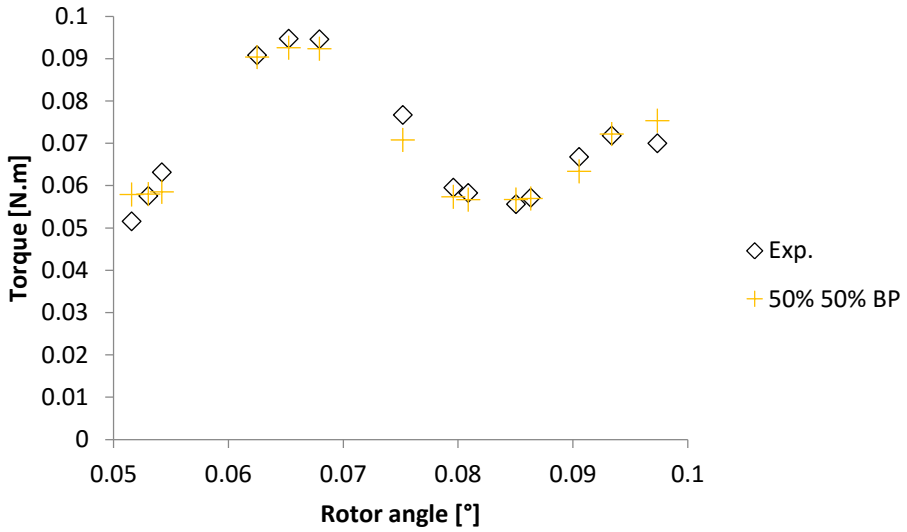

Figure 6.58: Comparison of 50% simulated BPNN with experimental data

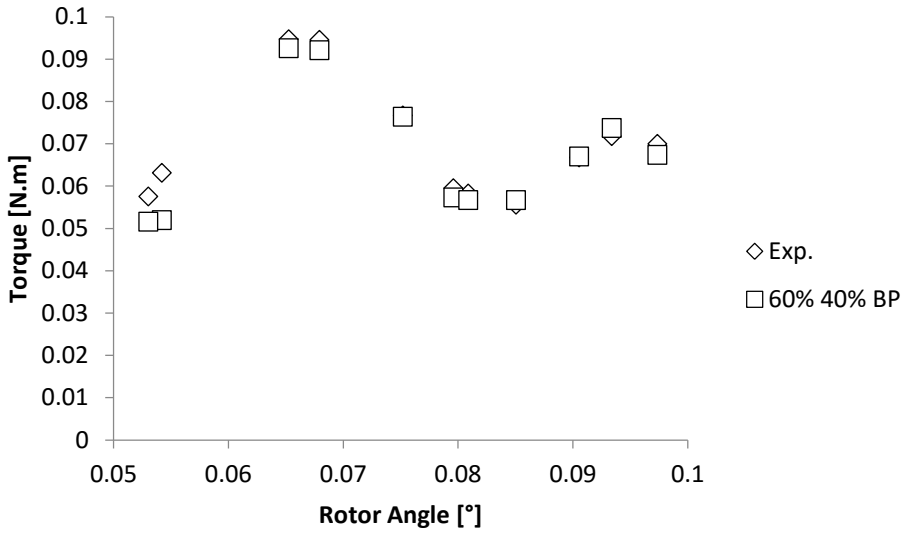

Figure 6.59: Comparison of 40% simulated BPNN with experimental data

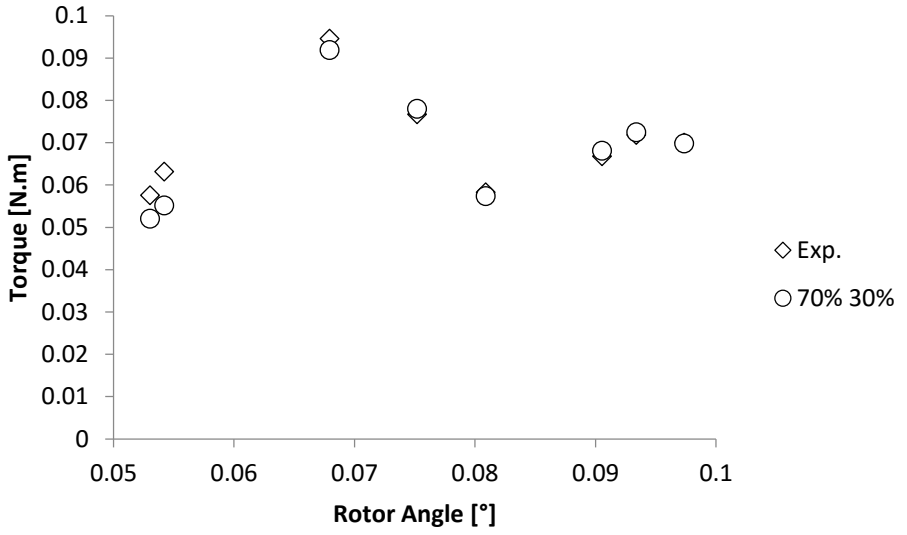

Figure 6.60: Comparison of 30% simulated BPNN with experimental data

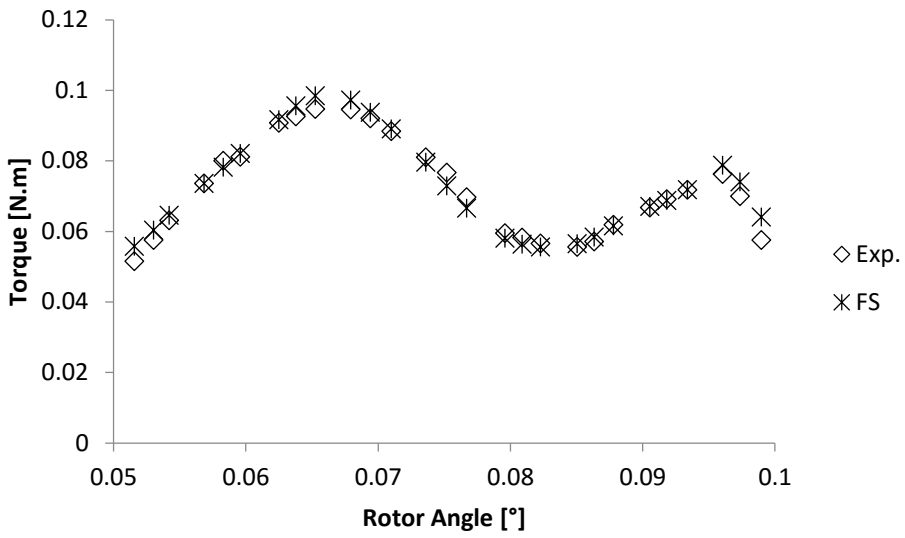

Figure 6.61: Comparison of FS with experimental data

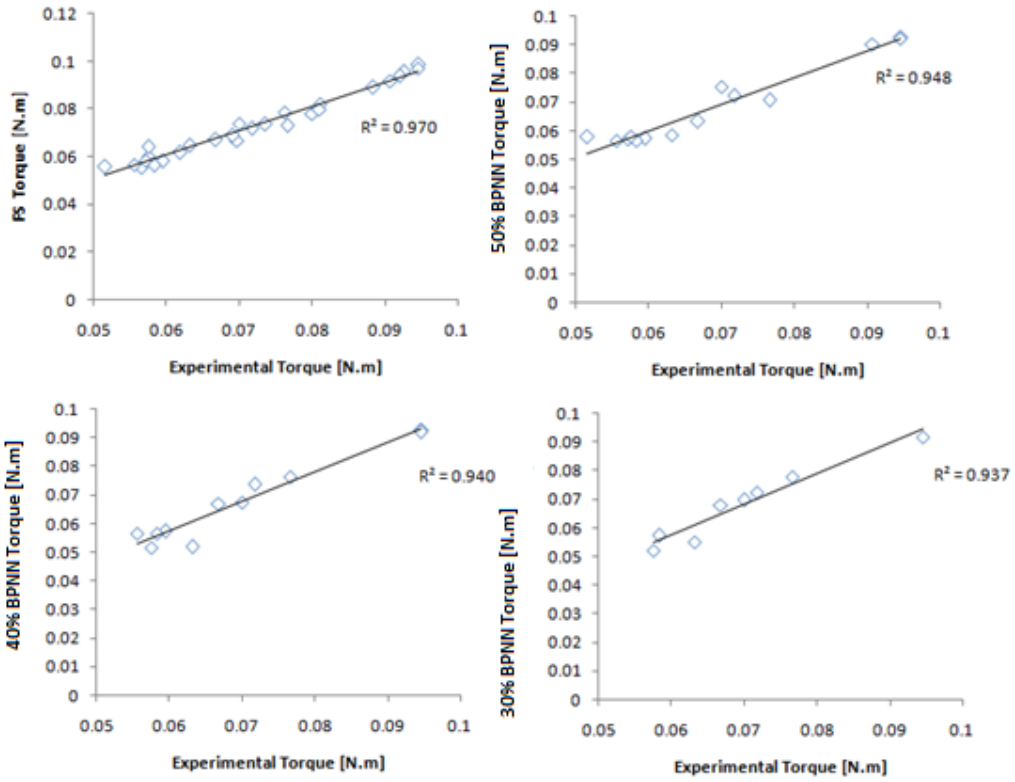

Figure 6.62 Simulated torque vs. experimental torque for all models

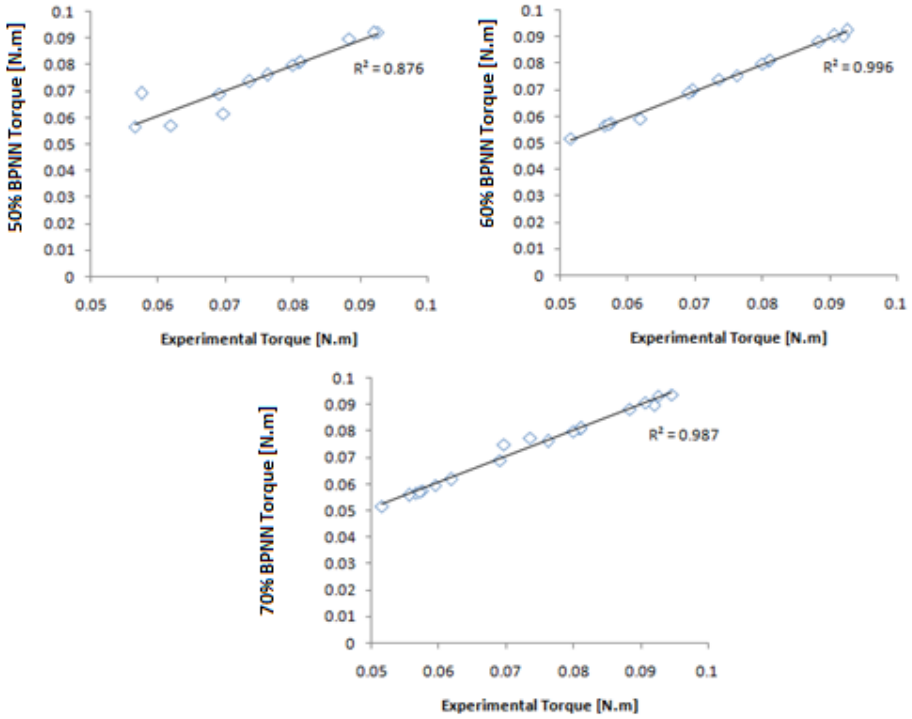

Figure 6.63: Trained torque vs. experimental torque for all models

6.5 Published Experimental Data (Kamoji et al., 2009)

6.5.1 Helix turbine without shaft and overlap ratio of 0.1

Table 6.11 and Figures 6.69 and 6.70 show the accuracy of the correlation measured by the *R-squared*, R^2. Consequently, the predicted plots becomes a significant method to predict the model. This can be noticed in Figures 6.64 to 6.68. Furthermore, this shows that the FS model can be used to predict torque coefficient of helix turbine without shaft.

Table 6.11: Percentage division of experimental data for BPNN (without shaft; Overlap ratio = 0.1)

Percentage of data of BPNN					
Training		50%			
Simulation		50%			
Epoch		4			
Best validation performance		2.14E-05			
Equations of Training					
$Output = A\,Target + B$					
Training		R^2	**Test**		R^2
A	1	0.891	A	0.94	1
B	0.0034		B	0.016	
Validation		R^2	**All**		R^2
A	1.1	1	A	1	0.923
B	0.032		B	0.0016	
Percentage of data of BPNN					
Training		60%			
Simulation		40%			
Epoch		7			
Best validation performance		7.1E-04			
Equations of Training					
$Output = A\,Target + B$					
Training		R^2	**Test**		R^2
A	1	1	A	0.91	1
B	7.9E-05		B	0.032	
Validation		R^2	**All**		R^2
A	5	1	A	0.99	0.859
B	1.1		B	0.0014	
Percentage of data of BPNN					
Training		70%			
Simulation		30%			
Epoch		52			
Best validation performance		1.08E-04			
Equations of Training					
$Output = A\,Target + B$					
Training		R^2	**Test**		R^2
A	1	1	A	0.64	0.938
B	2.7E-06		B	0.0072	
Validation		R^2	**All**		R^2
A	1.3	0.454	A	0.77	0.535
B	0.46		B	0.059	

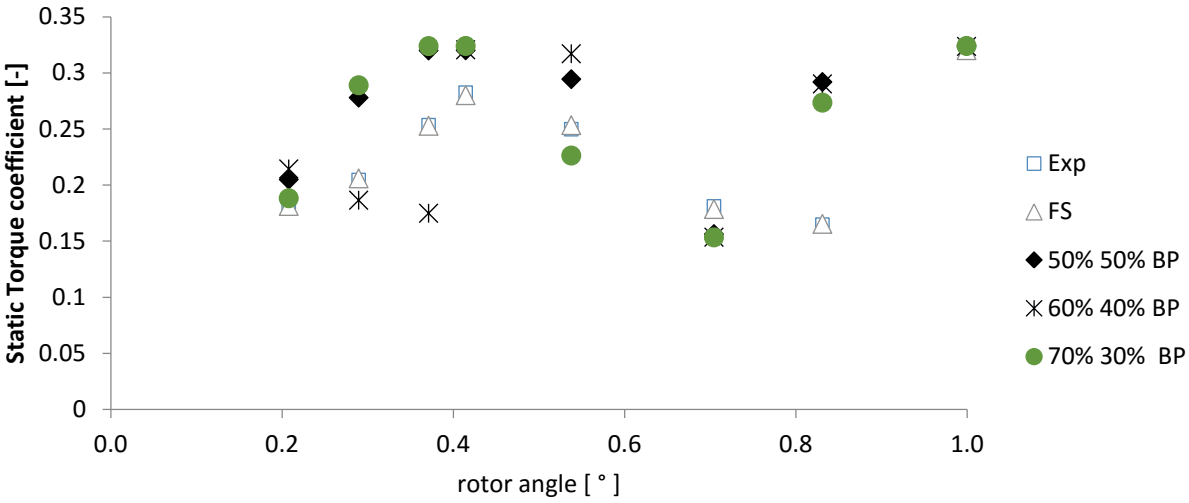

Figure 6.64: Comparison of all models with experimental data

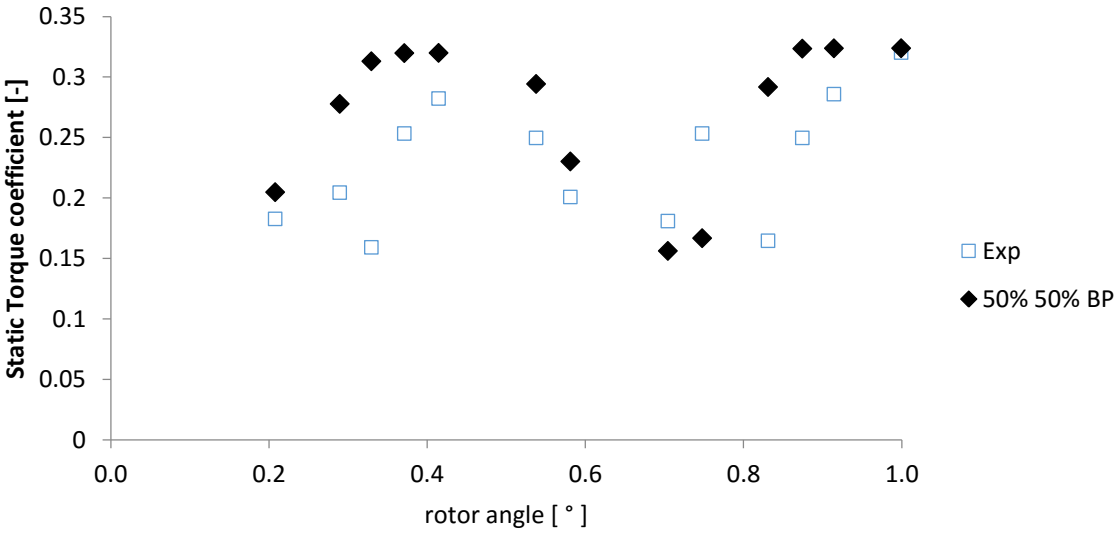

Figure 6.65: Comparison of 50% simulated BPNN with experimental data

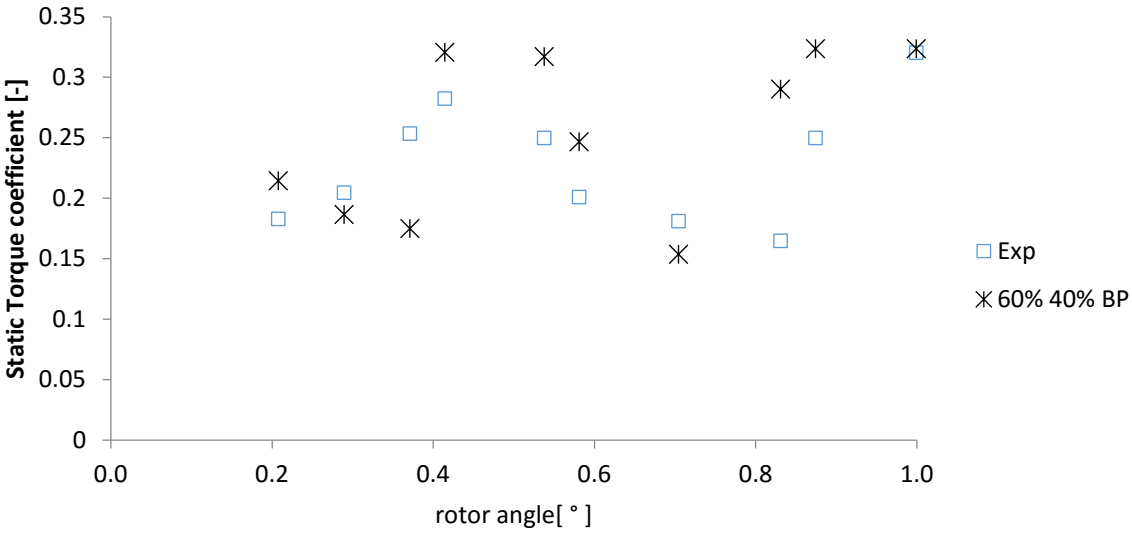

Figure 6.66: 40% simulated BPNN with experimental data

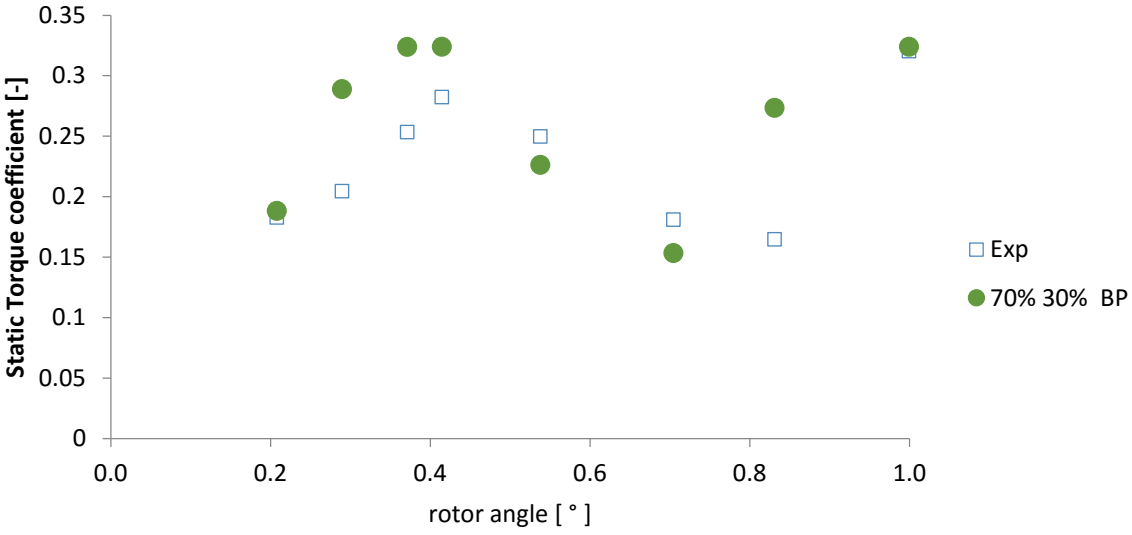

Figure 6.67: 30% simulated BPNN with experimental data

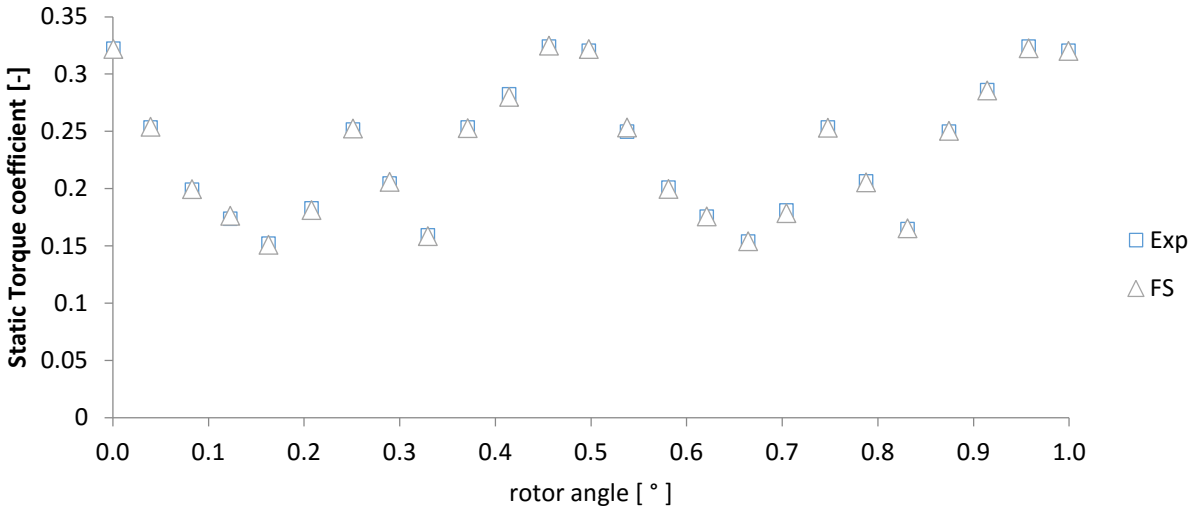

Figure 6.68: Comparison of FS with experimental data

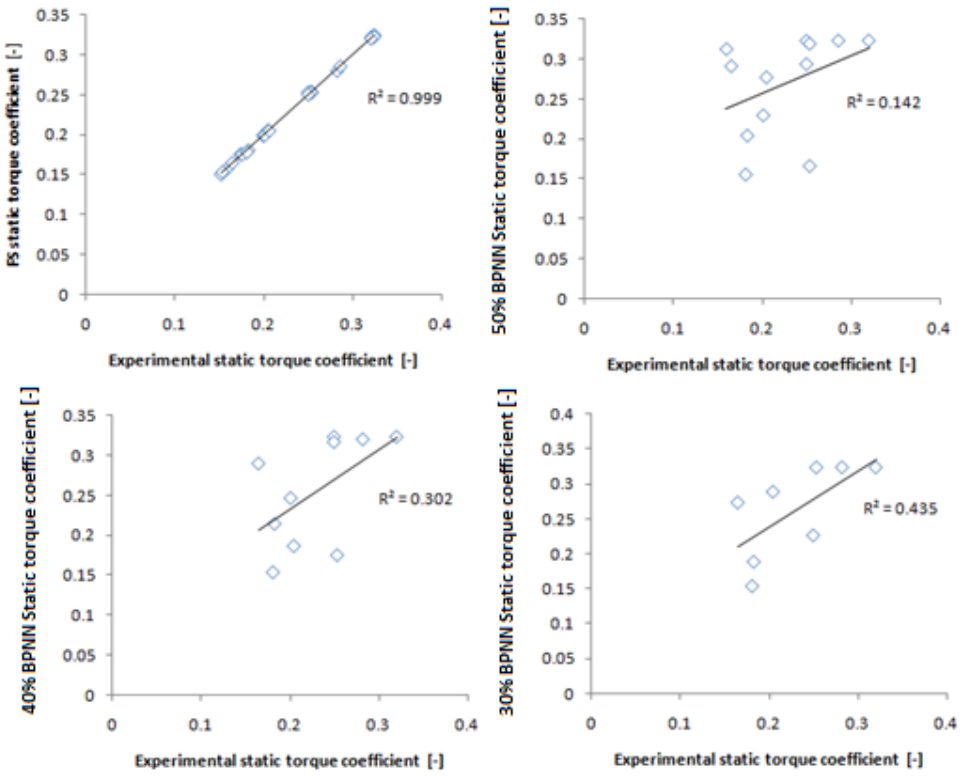

Figure 6.69: Simulated torque vs. experimental torque for all models

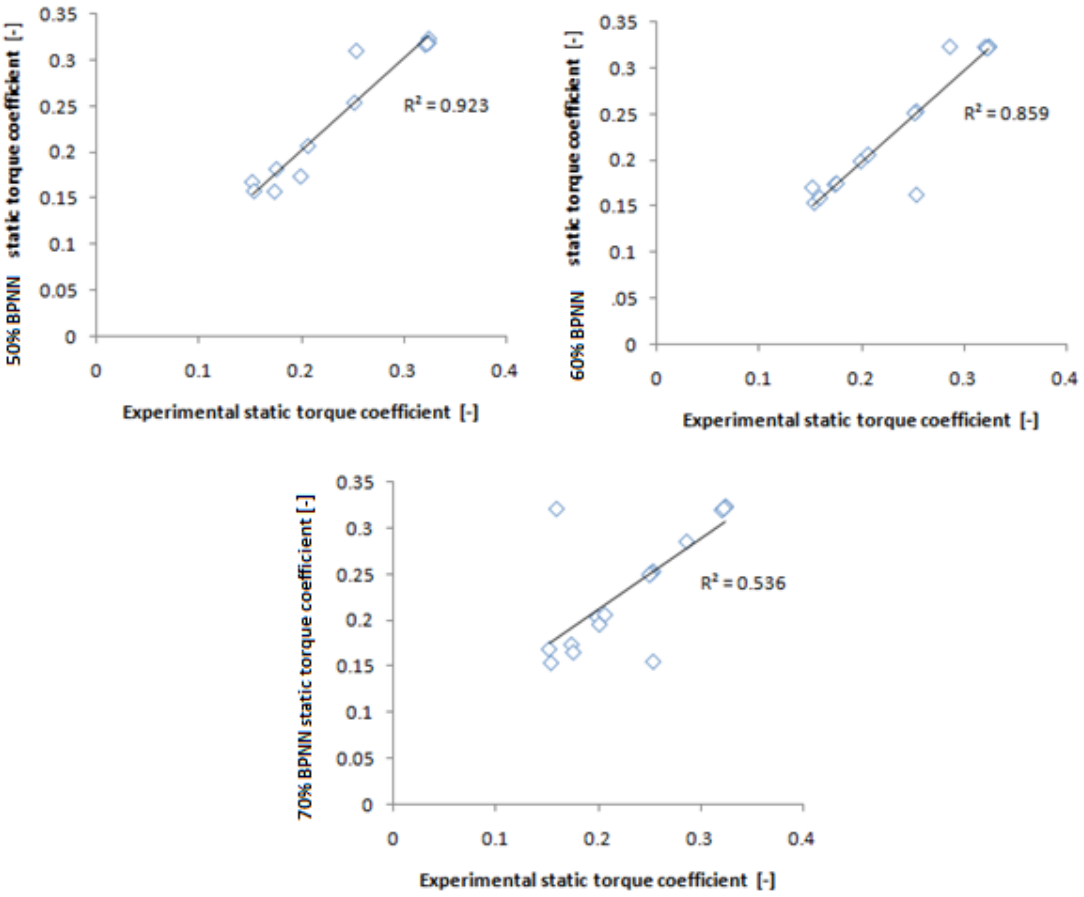

Figure 6.70: Trained torque vs. experimental torque for all models

6.5.2 Helix turbine with central shaft and overlap ratio of 0.0

The MSE, R^2 and empirical equations of the dependent and independent variables for calculating the torque of the turbine are shown in Table 6.12. Also, the comparison plots of the models are shown in Figures 6.71 to 6.75. Figures 6.76 and 6.77 shows the fitting result. It is observed from these figures that the Fourier series gives the best estimation of the torque coefficient of the turbine since R^2 of this model is 0.99 which is close to unity, as shown in Figure 6.75.

Table 6.12: Percentage division of experimental data for BPNN (with central shaft; Overlap ratio = 0.0)

Percentage of data of BPNN					
Training		50%			
Simulation		50%			
Epoch		0			
Best validation performance		2.58E-03			
Equations of Training					
$Output = A\,Target + B$					
Training		R^2	**Test**		R^2
A	0.074	0.0043	A	1.6	1
B	0.24		B	0.092	
Validation		R^2	**All**		R^2
A	-	0	A	0.032	0.001
B	-		B	0.23	
Percentage of data of BPNN					
Training		60%			
Simulation		40%			
Epoch		3			
Best validation performance		2.4E-03			
Equations of Training					
$Output = A\,Target + B$					
Training		R^2	**Test**		R^2
A	0.97	0.984	A	1.2	1
B	0.008		B	0.0092	
Validation		R^2	**All**		R^2
A	0.92	1	A	0.84	0.91
B	0.042		B	0.026	
Percentage of data of BPNN					
Training		70%			
Simulation		30%			
Epoch		7			
Best validation performance		2.84E-05			
Equations of Training					
$Output = A\,Target + B$					
Training		R^2	**Test**		R^2
A	0.99	0.998	A	1.1	0.992
B	0.0017		B	0.0054	
Validation		R^2	**All**		R^2
A	1	0.998	A	1	0.996
B	0.012		B	0.0013	

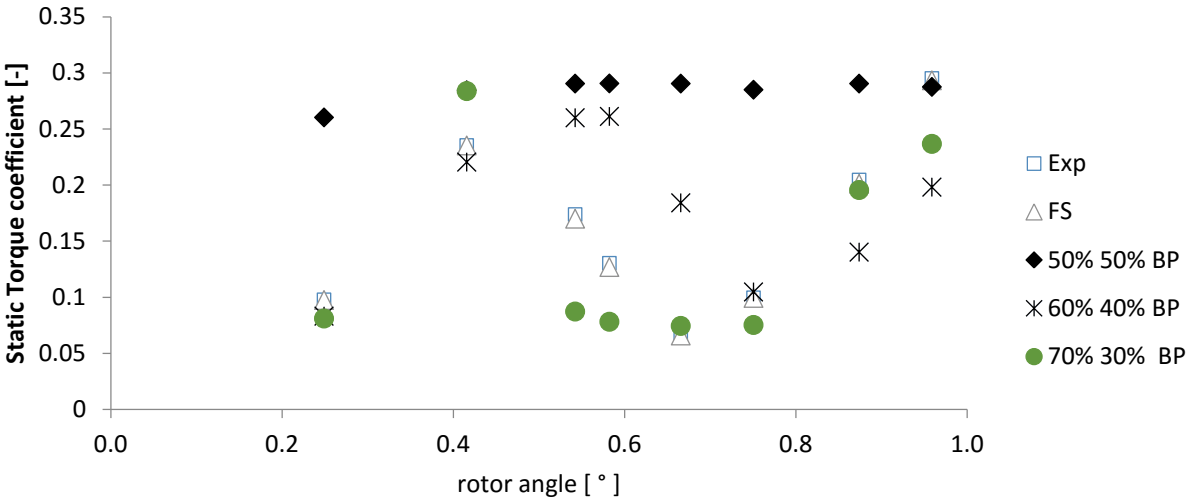

Figure 6.71: Comparison of all models with experimental data

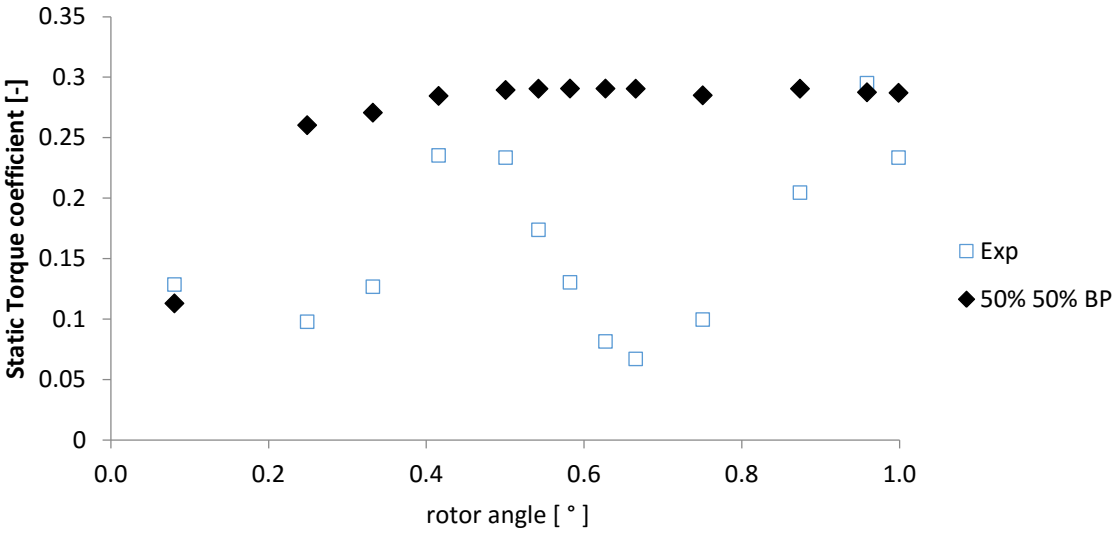

Figure 6.72: Comparison of 50% simulated BPNN with experimental data

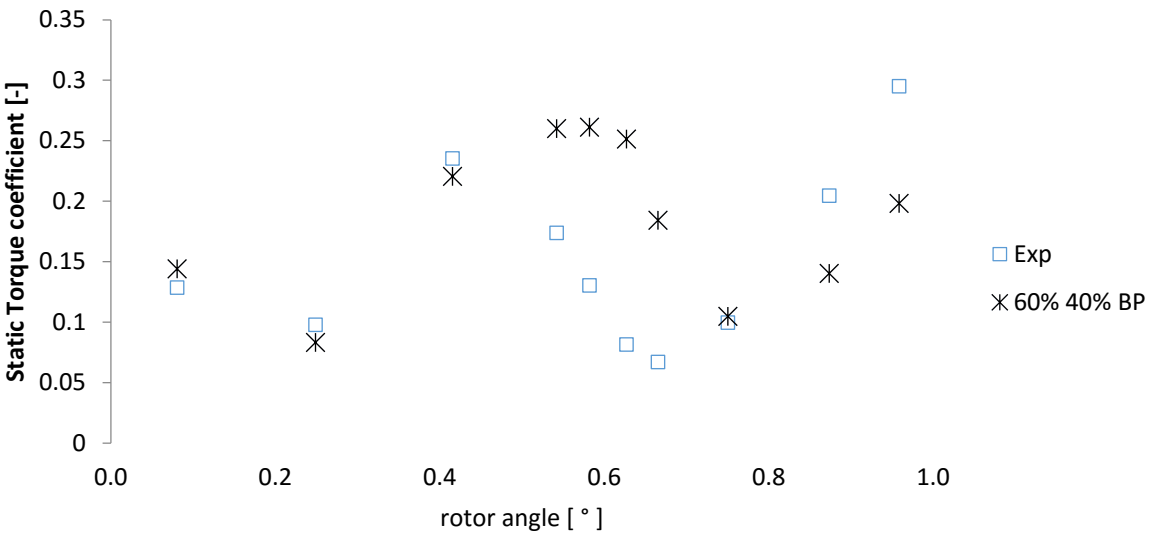

Figure 6.73: 40% simulated BPNN with experimental data

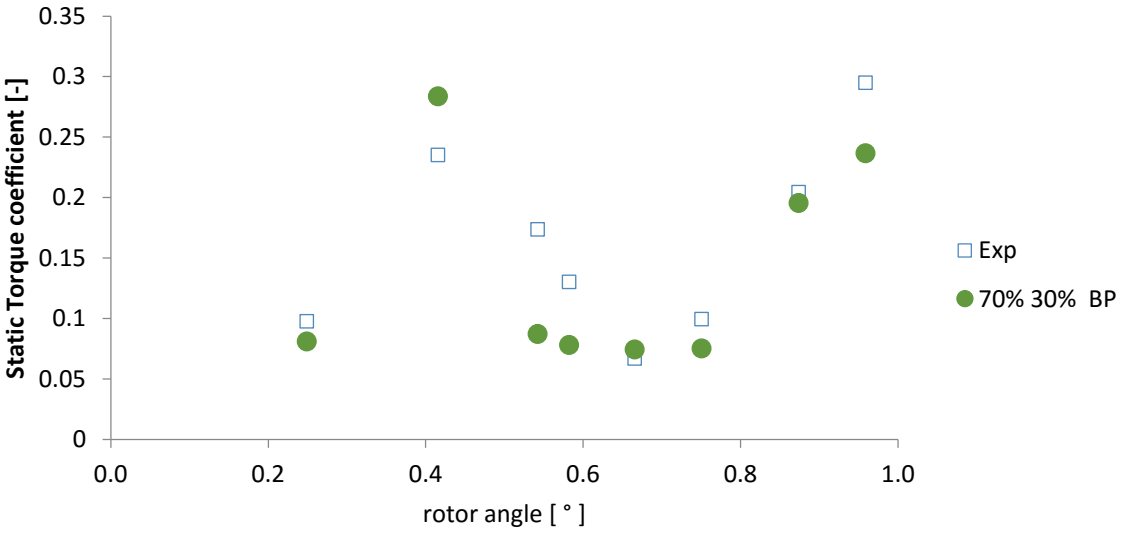

Figure 6.74: 30% simulated BPNN with experimental data

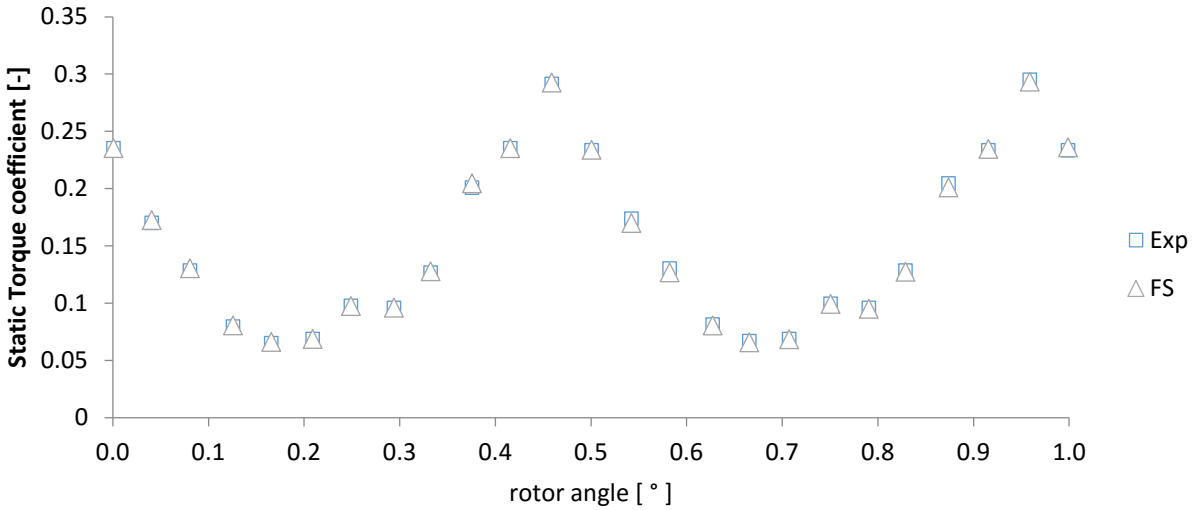

Figure 6.75: Comparison of FS with experimental data

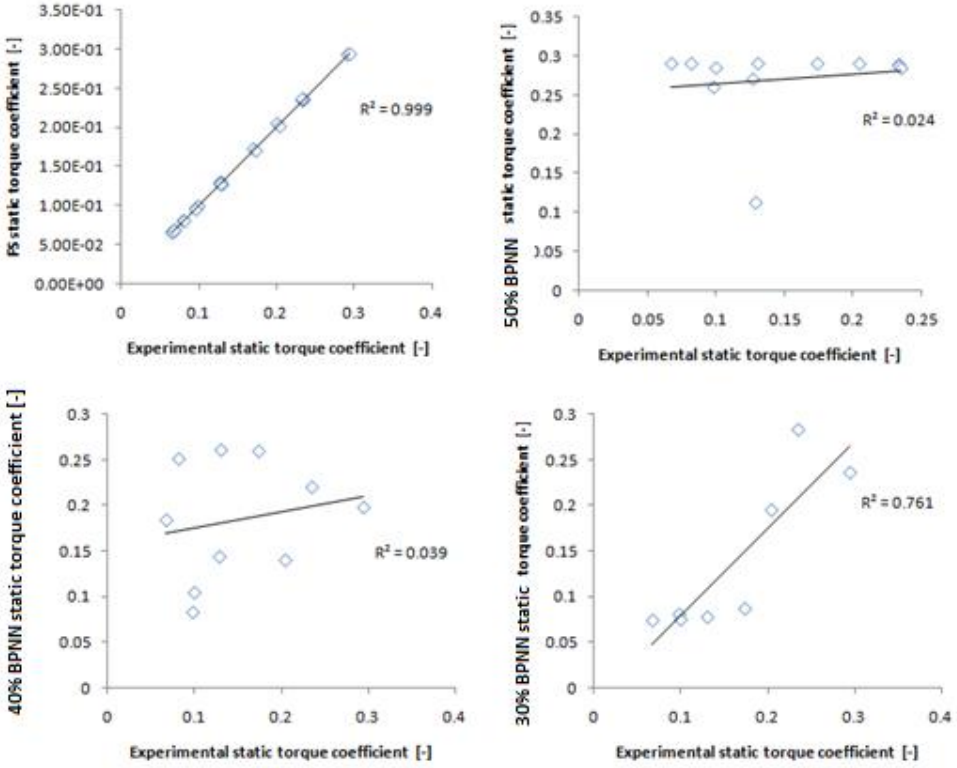

Figure 6.76: Simulated torque vs. experimental torque for all models

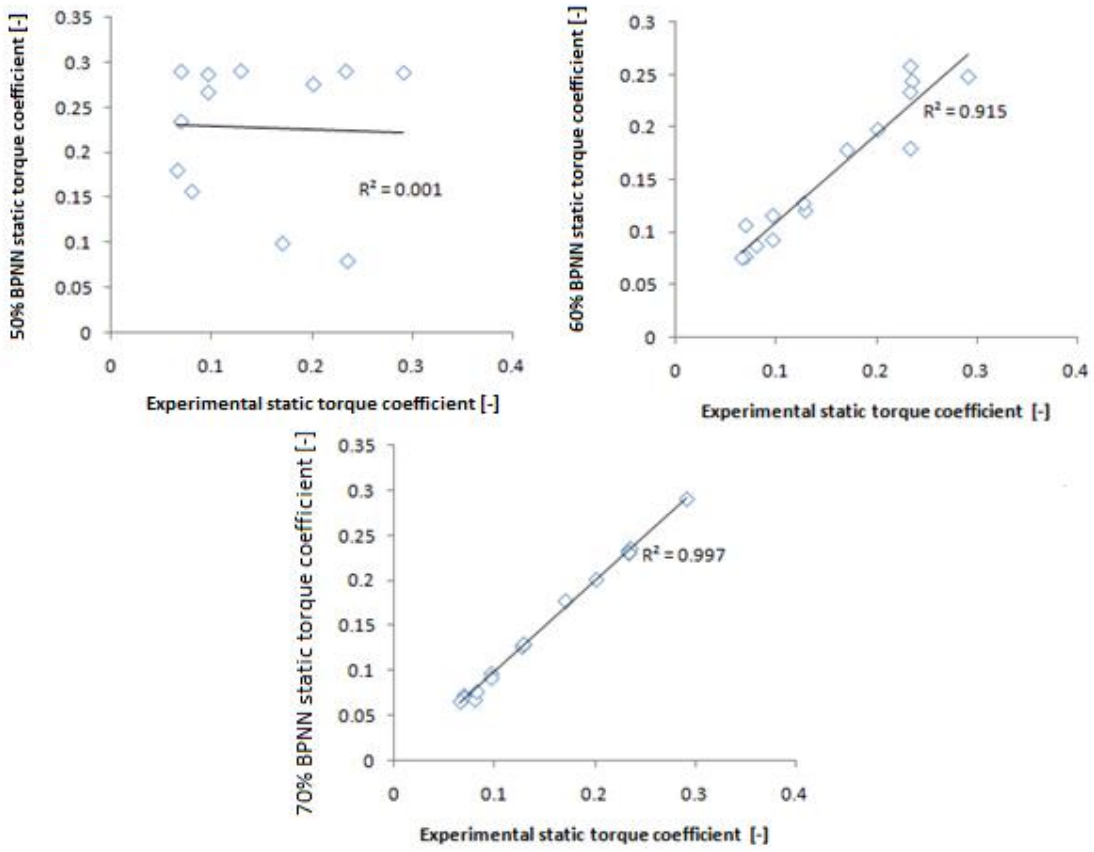

Figure 6.77: Trained torque vs. experimental torque for all models

6.6 Comparing FS and BPNN model with RBF model (Sargolzaei and Kianifar, 2009)

Table 6.13 shows *R-squared* values fitting line between predicted torque and experimental data. Figures 6.88, 6.89 and 6.80 compare the results of BPNN, FS, and RBF (Sargolzaei and Kianifar, 2009) models for measured torque of Rotor I, II and III. It is well illustrated in Table 6.13 and these figures shows that the BPNN and FS model have a high capability in predicting the performance parameters.

Table 6.13: *R-squared* value for FS, BPNN and RBF

Model	R^2		
	Rotor I	Rotor II	Rotor III
FS	0.845	0.9965	0.9375
BPNN	0.9885	0.9873	0.9565
RBF	0.9626	0.7833	0.9916

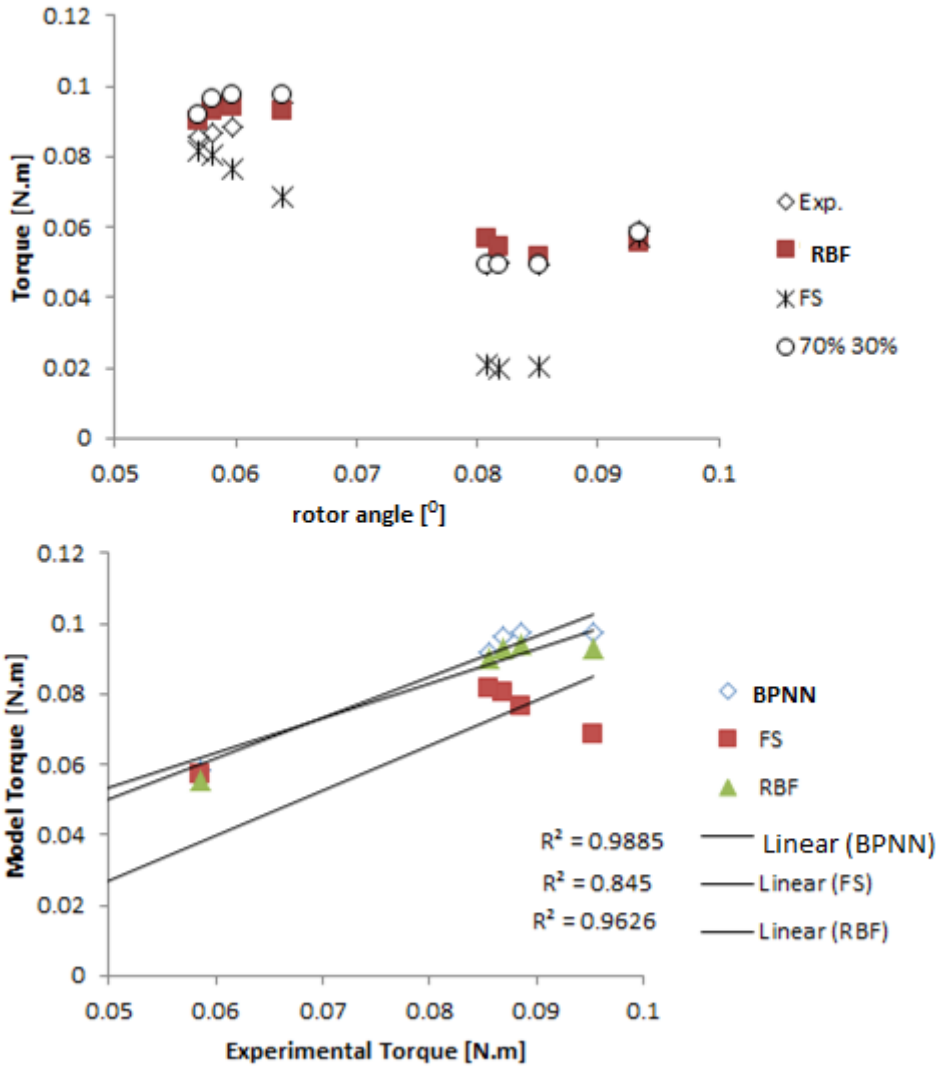

Figure 6.78: Plot of all three models with experimental torque of rotor I

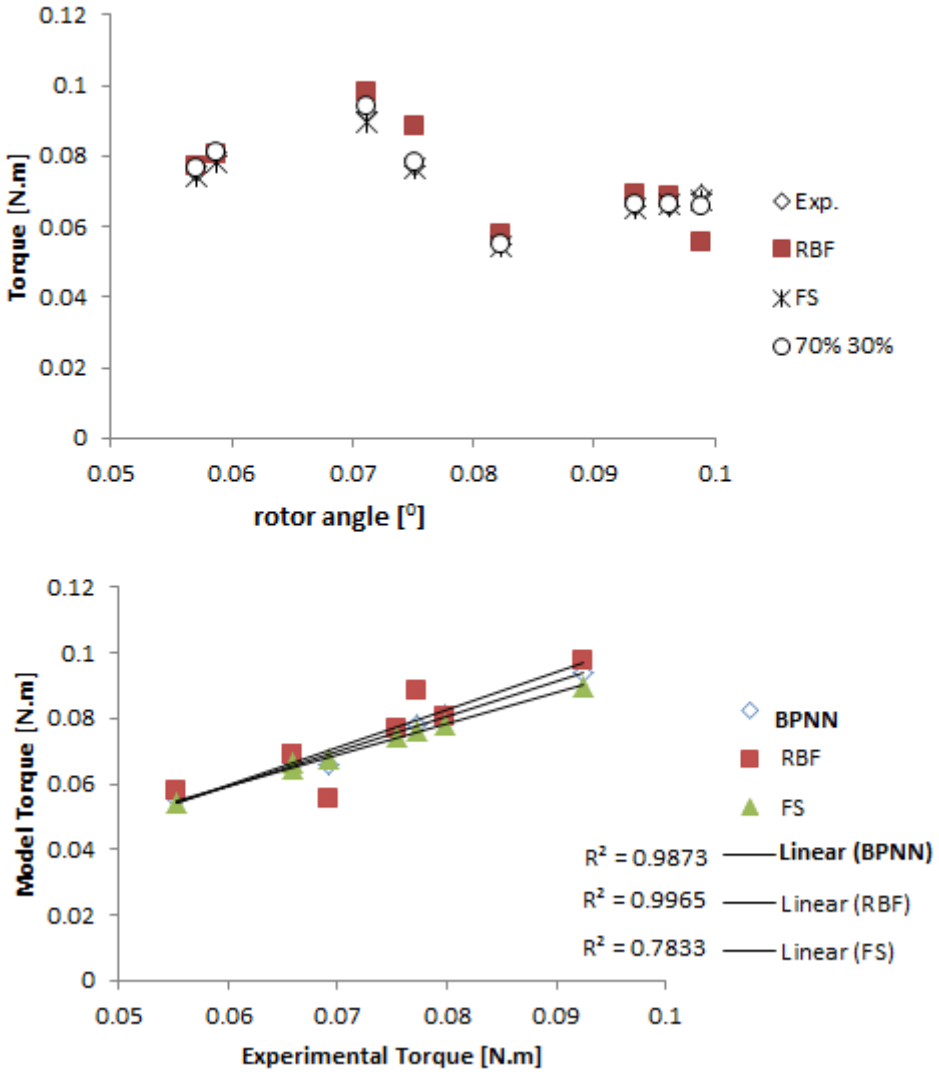

Figure 6.79: Plot of all three models with experimental torque of rotor II

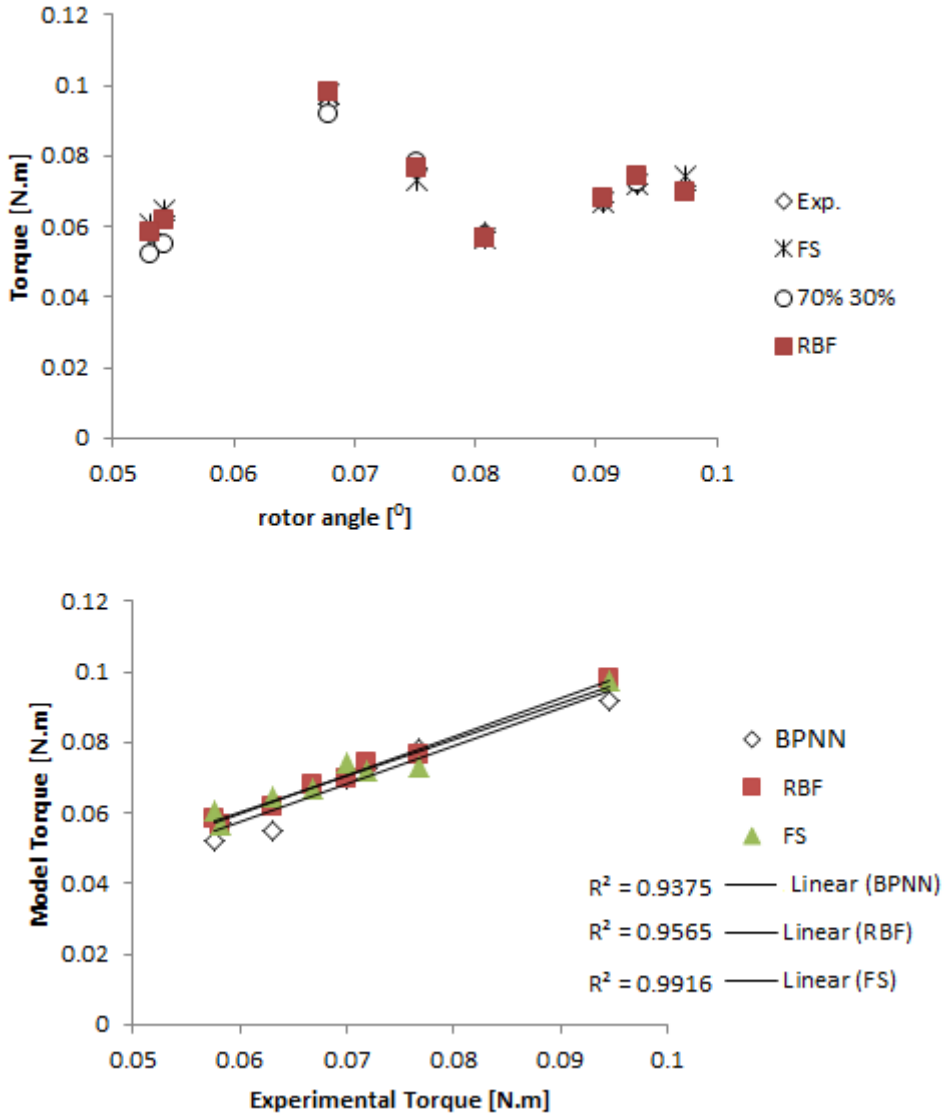

Figure 6.80: Plot of all three models with experimental torque of rotor III

CHAPTER 7
CONCLUSION

7.1. Conclusion

FS and BPNN modeling was carried out using trigonometric Fourier series and feedforward back propagation neural network architecture respectively to predict the aerodynamic characteristics of different Savonius wind turbine configurations and to compare the results with the main experimental datas collected. Based, on what is presented in this work, it can be concluded that the aims and objectives of the research is achieved. The following deductions can also be made:

i. The feedforward back propagation neural network and the Fourier series perfectly predict the mechanical torque of the two bladed Savonius wind turbine studied by Ali (2013). Both combination of training/testing data sets gives a reasonable prediction but the 70/30% provides better result in the back propagation neural network model. The MSE is extremely small and the R^2 is close to unity.

ii. The same applies to the second experimental data of helical Savonius rotors with two and three blades at 90^0 angle of twist studied by Debnath et al, (2014). Both models gives a good prediction of C_p and C_t.

iii. The back propagation gives a good prediction with extremely small MSE and R^2 close to unity for the three rotors of Sargolzaei and Kianifar (2009). Howecer, the Fourier series model only works with the datas for rotor II and III. Poor performance was obtained for rotor I with different input/output training and testing data sets.

iv. Lastly, a comparison was made between the two models in this study with RBF model carried out by Sargolzaei and Kianifar (2009). The BPNN shows a good prediction for rotor I compared to other two models while FS works perfecly for rotor II and RBF for rotor III.

7.2. Future Work

Another artificial neural network model such as the FIS, ANFIS, GRNN etc. should be used in the future and their performance be evaluated.

REFERENCES

Adaramola, M. (2014). Wind Turbine Technology Principles and Design, 2nd Edition. Toronto: Apple Academic Press.

Akwa, J. V., Vielmo, H. A., & Petry, A. P. (2012). A review on the performance of Savonius wind turbines. *Journal of Renewable and Sustainable Energy Reviews, 16,* 3054-3064.

Aldoss, T. K., & Obeidat, K. M. (1987). Performance analysis of two Savonius rotors running side by side using discrete vortex method. *Journal of Wind Engineering, 20,* 79-89.

Ali, M. H. (2013). Experimental comparison study for Savonius wind turbine of two and three blades at low wind speed. *International Journal of Modern Engineering Research, 68,* 2978-2986.

Al-Shemmeri, T. (2010). Wind Turbines. Staffordshire: T. Al-Shemmeri and Ventus Publishing ApS.

Altan, B. D., Atılgana, M., & Özdamar, A. (2008). An experimental study on improvement of a Savonius rotor performance with curtaining. *Journal of Experimental Thermal and Fluid Science , 32,* 1673-1678.

Anderson, D., & McNeill, G. (1992). Artificial Neural Networks Technology. New York: Kaman Sciences Corporation.

Bai, C. J., & Wang, W. C. (2016). Review of computational and experimental approaches to analysis of aerodynamic performance in horizontal-axis wind turbines (HAWTs). *Journal of Renewable and Sustainable Energy Reviews, 63,* 506-519.

Chapra, S. C., & Canale, R. P. (1990). Numerical Methods for Engineers, Third edition. New York: McGraw-Hill Book Company.

Debnath, P., Gupta, R., & Pandey, K. M. (2014). Performance Analysis of the Helical Savonius Rotor Using Computational Fluid Dynamics. *ISESCO Journal of Science and Technology, 3,* 17-28.

Fujisawa, N., & Gotoh, F. (1994). Experimental study on the aerodynamic performance of Savonius rotor. *ASME Journal of Solar Energy Engineering, 116,* 148-152.

Gupta, R., Biswas, A., & Sharma, K. K. (2008). Comparative study of a three bucket Savonius rotor with a combined three-bucket Savonius–three-bladed Darrieus rotor. *Journal of Renewable Energy, 33,* 1974-1981.

Hristov, H. N. (2008). Wind Turbines Introduction. Gabrovo: Technical University of Gabrovo Publishing Company.

Jin, X., Zhao, G., Gao, K., & Ju, W. (2016). Darrieus vertical axis wind turbine: Basic research methods. *Journal of Renewable and Sustainable Energy Reviews, 42,* 212-225.

Kamoji, M. A., Kedare, S. B., & Prabhu, S. V. (2009). Performance tests on helical Savonius rotors. *Journal of Renewable Energy, 34*, 521-529.

Kustrin, S. A., & Beresford, R. (2000). Basic concepts of artificial neural network (ANN) modeling and its application in pharmaceutical research. *Journal of Pharmaceutical and Biomedical Analysis, 22*, 717-727.

Menet, J. L. (2004). A double-step Savonius rotor for local production of electricity: a design study. *Journal of Renewable Energy, 29*, 1843-1862.

Modelling and simulation of wind turbine Savonius rotors using artificial neural networks for estimation of power ratio and torque. (2009). *Journal of Simulation Modelling Practice and Theory, 17*, 1920-1928.

Negnevitsky, M. (2005). Artificial Intelligence, A Guide to Intelligent Systems. London: Person Education Limited.

Rahman, M., Morshed, K. N., Lewis, J., & Fuller, M. (2009). Experimental and numerical investigations on drag and torque characteristics of three-bladed Savonius wind turbine. *In Proceedings of ASME International Mechanical Engineering Conference and Exposition (IMECE 2009)* (pp. 85-94). Orlando: The American Society of Mechanical Engineers (ASME).

Roshmin, N., Jauhari, A. S., Mustaamal, A. H., Husin, F., & Hassan, M. Y. (2015). Experimental study for the single-stage and double-stage two-bladed Savonius micro-sized turbine for rain water harvesting (RWH) system. *Journal of Energy Procedia, 68*, 274-281.

Roy, S., & Saha, U. K. (2013). Review on the numerical investigations into the design and development of Savonius wind rotors. *Journal of Renewable and Sustainable Energy Reviews, 24*, 73-83.

Saha, U. K., & Rajkumar, M. J. (2006). On the performance analysis of Savonius rotor with twisted blades. *Journal of Renewable Energy, 31*, 1776-1788.

Sargolzaei, J., & Kianifar, A. (2010). Neuro-fuzzy modelling tools for estimation of torque in Savonius wind rotor machine. *Journal of Advances in Engineering Software, 41*, 619-626.

Sawada, T., Nakamura, M., & Kamada, S. (1986). Blade force measurement and flow visualisation of Savonius rotors. *Journal of Japan Society of Mechanical Engineers, 29*, 2095-2100.

Singh, G. (2008). Exploit Nature-Renewable Energy Technologies. New Delhi: Aditya Books Pvt. Ltd.

Sivanandam, S. N., Sumathi, S., & Deepa, S. N. (2006). Introduction to Neural Networks using Matlab 6.0. New Delhi: Tata Mc-Graw Hill.

Sun, Y., Peng, Y., Chen, Y., & Shukla, A. J. (2003). Application of artificial neural networks in the design of controlled release drug delivery systems. *Journal of Advanced Drug Delivery Reviews, 55*, 1201-1215.

Tummala, A., Velamati, R. K., Sinha, D. K., Indraja, V., & Krishnad, V. H. (2016). A review on small scale wind turbines. *Journal of Renewable and Sustainable Energy Reviews, 56*, 1351-1371.

Wenehenubun, F., Saputra, A., & Sutanto, H. (2015). An experimental study on the performance of Savonius wind turbines related with the number of blades. *Journal of Energy Procedia, 68*, 297-304.